



Michigan Technological University  
Create the Future Digital Commons @ Michigan Tech

---

Dissertations, Master's Theses and Master's Reports - Open

Dissertations, Master's Theses and Master's Reports


---

2014

## OUT-OF-STEP DETECTION BASED ON ZUBOV'S APPROXIMATION BOUNDARY METHOD

Yawei Wei  
*Michigan Technological University*

Follow this and additional works at: <https://digitalcommons.mtu.edu/etds>

 Part of the [Power and Energy Commons](#)


Copyright 2014 Yawei Wei

---

### Recommended Citation

Wei, Yawei, "OUT-OF-STEP DETECTION BASED ON ZUBOV'S APPROXIMATION BOUNDARY METHOD", Master's Thesis, Michigan Technological University, 2014.  
<https://digitalcommons.mtu.edu/etds/899>

Follow this and additional works at: <https://digitalcommons.mtu.edu/etds>

 Part of the [Power and Energy Commons](#)

**OUT-OF-STEP DETECTION BASED ON ZUBOV'S APPROXIMATION BOUNDARY  
METHOD**

By

Yawei Wei

A THESIS

submitted in partial fulfillment of the requirements for the degree of  
Master of Science  
In Electrical Engineering

MICHIGAN TECHNOLOGICAL UNIVERSITY

2014

© Yawei Wei, 2014.

This thesis has been approved in partial fulfillment of the requirements for the Degree of MASTER OF SCIENCE in Electrical Engineering.

Department of Electrical and Computer Engineering

Thesis Co-advisor: *Dr. Sumit Paudyal*

Thesis Co-advisor: *Dr. Bruce A. Mork*

Committee Member: *Dr. Leonard J. Bohmann*

Committee Member: *Dr. Laura E. Brown*

Department Chair: *Dr. Daniel R. Fuhrmann*

## TABLE OF CONTENTS

<b>LIST OF TABLES</b> . . . . .	iv
<b>LIST OF FIGURES</b> . . . . .	v
<b>ACKNOWLEDGEMENTS</b> . . . . .	vi
<b>ABSTRACT</b> . . . . .	vii
<b>CHAPTER 1. Introduction</b> . . . . .	1
1.1 Motivation . . . . .	1
1.2 Literature Review . . . . .	5
1.2.1 Out-of-step Protections Based on Rate of Change of Parameters . . . . .	5
1.2.2 Computer Intelligence Based Methods . . . . .	7
1.2.3 Equal Area Criterion (EAC) based Methods . . . . .	7
1.2.4 Lyapunov Theory Based Approaches . . . . .	8
1.3 Thesis Overview . . . . .	9
1.4 Thesis Outline . . . . .	10
<b>CHAPTER 2. Background</b> . . . . .	12
2.1 Introduction . . . . .	12
2.2 Phasor Measurement Unit . . . . .	12
2.3 Power Swing Fundamentals . . . . .	16
2.4 Out-of-Step Detection Techniques . . . . .	19
2.4.1 Rate of Change of Impedance Based Method (Blinder Technique) . . . . .	20

2.4.2	Swing Center Voltage Technique . . . . .	22
2.4.3	Techniques Based on Fuzzy Logic and Neural Network . . . . .	25
2.4.4	Techniques Based on EAC and Its Modification . . . . .	26
2.4.5	Lyapunov's Theory Based Techniques . . . . .	28
2.5	Summary . . . . .	34
<b>CHAPTER 3. Proposed Out-of-step Algorithm Applied to SMIB System . . . . .</b>		<b>35</b>
3.1	Introduction . . . . .	35
3.2	Zubov's Stability Boundaries for Power Systems . . . . .	35
3.3	Proposed Out-of-step Detection Algorithm . . . . .	39
3.4	SMIB Case Studies . . . . .	40
3.4.1	Stable Swing Simulations . . . . .	42
3.4.2	Out-of-step Cases . . . . .	48
3.5	Summary . . . . .	53
<b>CHAPTER 4. Proposed Out-of-step Algorithm Applied to Multi-machine Systems</b>		<b>54</b>
4.1	Introduction . . . . .	54
4.2	Proposed Out-of-step Detection Algorithm for Multi-machine Systems . . . . .	54
4.3	IEEE 3-machine 9-bus System Case Studies . . . . .	56
4.4	IEEE 10-machine 39-bus Case Studies . . . . .	75
4.5	Summary . . . . .	85
<b>CHAPTER 5. Hardware Implementation and Testing . . . . .</b>		<b>86</b>
5.1	Introduction . . . . .	86
5.2	Hardware/Software . . . . .	86
5.2.1	Phasor Measurement Unit . . . . .	86
5.2.2	System Computing Platform . . . . .	88
5.2.3	Doble Power Simulator . . . . .	88
5.3	System Configuration . . . . .	88

5.4 Summary . . . . .	92
<b>CHAPTER 6. Summary and Conclusions . . . . .</b>	<b>93</b>
6.1 Summary . . . . .	93
6.2 Conclusions . . . . .	94
6.3 Thesis Contributions . . . . .	95
6.4 Future Plans . . . . .	95
<b>APPENDIX A. SMIB System Parameters . . . . .</b>	<b>96</b>
<b>APPENDIX B. IEEE 3-machine 9-bus Parameters . . . . .</b>	<b>97</b>
<b>APPENDIX C. IEEE 10-machine 39-bus Parameters . . . . .</b>	<b>99</b>
<b>APPENDIX D. Zubov's Boundary Parameters for SMIB Case . . . . .</b>	<b>103</b>
<b>REFERENCES . . . . .</b>	<b>105</b>

## LIST OF TABLES

Table 3.1	Performance of the Proposed Method in Stable Swing Detection in SMIB. . . . .	48
Table 3.2	Performance of the Proposed Method in Out-of-step Detection in SMIB. . . . .	53
Table 4.1	Summary of Case Studies in IEEE 3-machine 9-bus System. . . . .	62
Table 4.2	Summary of Case Studies for Cascading Failures in IEEE 3-machine 9-bus System . . . . .	74
Table 4.3	Out-of-step Condition for Line-between Cases Machine Coherent Results. . . . .	77
Table 4.4	Out-of-step Condition for Line-between Cases Machine Coherent Results. . . . .	78
Table 4.5	Performance of the Proposed Method in Stable Swing Cases Detection for G38 with Fault at Nodes 25-26. . . . .	84
Table 4.6	Performance of the Proposed Method in Out-of-step Cases Detection for G38 with Fault at Nodes 25-26. . . . .	84
Table 5.1	SMIB Comparisons for Different Fault Duration Time. . . . .	91
Table B.1	Generators Parameters in p.u. . . . .	97
Table B.2	Transformer Parameter in p.u. . . . .	97
Table B.3	Lines Parameters in p.u. . . . .	97

Table B.4	Load Parameters in p.u. . . . .	98
Table C.1	Generators Parameters in p.u. . . . .	99
Table C.2	Lines Parameters in p.u. . . . .	100
Table C.3	Lines Parameters in p.u. . . . .	101
Table C.4	Power Parameters . . . . .	102



## LIST OF FIGURES

Figure 1.1	Typical Components and Functionality of Power Systems, adapted from [1]. . . . .	2
Figure 1.2	Location of Synchrophasors in the U.S. and Canada in 2013 [9]. . . . .	5
Figure 1.3	Overview of the Proposed Work. . . . .	10
Figure 2.1	A Sinusoidal Waveform Illustrating Synchrophasors, adapted from [44]. . . . .	13
Figure 2.2	Block Diagram of Phasor Measurement Unit, adapted from [43]. . . . .	14
Figure 2.3	Power System Synchrophasor Network, adapted from [45]. . . . .	15
Figure 2.4	Current Waveform in Stable and Out-of-step Situation. . . . .	16
Figure 2.5	Two-machine Network to Illustrate Power Swing Loci. . . . .	17
Figure 2.6	Impedance Loci at Relay Location O for $E_g = E_m$ , adapted from [16]. . . . .	18
Figure 2.7	Impedance Loci at Relay Location O for $E_g \neq E_m$ . . . . .	19
Figure 2.8	Relay Development Timeline, adapted from [48] . . . . .	20
Figure 2.9	Blinder Scheme for Out-of-step Protection, adapted from [16]. . . . .	21
Figure 2.10	Two Machine Example for SCV. . . . .	22
Figure 2.11	SCV in Phasor Diagram, adapted from [16]. . . . .	24
Figure 2.12	Fuzzy Algorithm for Out-of-Step Detection, adapted from [23]. . . . .	25
Figure 2.13	ANN Data Training Diagram for Out-of-step Detection. . . . .	26
Figure 2.14	P- $\delta$ Curves for EAC Method, adapted from [30]. . . . .	27

Figure 2.15	P- <i>t</i> Curve for Modified EAC Method in Time Domain, adapted from [49]. . . . .	28
Figure 2.16	Energy Based Approach for Stability Detection, adapted from [41]. . . . .	30
Figure 2.17	Solution of Van Der Pol's Equation in Time Domain. . . . .	33
Figure 2.18	Van Der Pol Equation' Stability Boundary in State Plane. . . . .	33
Figure 2.19	Approximation Boundary for Van Der Pol Equation. . . . .	34
Figure 3.1	Single Machine Infinite Bus System. . . . .	36
Figure 3.2	SMIB System Set-up for Out-of-step Detection. . . . .	40
Figure 3.3	Flowchart of Zubov's Approximation Method for Out-of-step Detection. . . . .	41
Figure 3.4	Zobuv's Boundaries at Original Reference (0, 0). . . . .	43
Figure 3.5	Zobuv's Boundaries Shifted to a New Reference ( $\delta_o, \omega_o$ ) . . . . .	43
Figure 3.6	Stable Swing Case for Pre-fault Angle of 20°, Fault Duration Time 0.048 s. . . . .	45
Figure 3.7	Stable Swing Case for Pre-fault Angle of 20°, Fault Duration Time 0.096 s. . . . .	45
Figure 3.8	Stable Swing Case for Pre-fault Angle of 20°, Fault Duration Time 0.144 s. . . . .	46
Figure 3.9	Stable Swing Case for Pre-fault Angle of 20°, Fault Duration Time 0.328 s. . . . .	46
Figure 3.10	Stable Swing Case for Pre-fault Angle of 30°, Fault Duration Time 0.192 s. . . . .	47
Figure 3.11	Stable Swing Case for Pre-fault Angle of 30°, Fault Duration Time 0.288 s. . . . .	47

Figure 3.12	Out-of-step Case for Pre-fault Angle of $20^0$ , Fault Duration Time of 0.336 s. . . . .	50
Figure 3.13	Out-of-step Case for Pre-fault Angle of $20^0$ , Fault Duration Time of 0.352 s. . . . .	50
Figure 3.14	Out-of-step Case for Pre-fault Angle of $20^0$ , Fault Duration Time of 0.384 s. . . . .	51
Figure 3.15	Out-of-step Case for Pre-fault Angle of $30^0$ , Fault Duration Time of 0.480 s. . . . .	51
Figure 3.16	Out-of-step Case for Pre-fault Angle of $30^0$ , Fault Duration Time of 0.576 s. . . . .	52
Figure 3.17	Out-of-step Case for Sensitivity Analysis with Fault Duration Time 0.576 s. . . . .	52
Figure 4.1	Flowchart of the Proposed Out-of-step Detection Algorithm in Multi-machine Power Systems. . . . .	55
Figure 4.2	IEEE 3-machine 9-bus System. . . . .	57
Figure 4.3	$\delta$ -t and $\omega$ -t Curves for Stable Swing Fault Duration Time of 0.1 s Between Nodes 6-9. . . . .	58
Figure 4.4	$\delta$ - $\omega$ Curves for Stable Swing Fault Duration Time of 0.1 s Between Nodes 6-9. . . . .	58
Figure 4.5	$\delta$ -t and $\omega$ -t Curves for Out-of-step Fault Duration Time of 0.45 s Between Nodes 6-9. . . . .	60
Figure 4.6	$\delta$ - $\omega$ Curves for Out-of-step Fault Duration Time of 0.45 s Between Nodes 6-9. . . . .	60
Figure 4.7	$\delta$ -t and $\omega$ -t Curves for Stable Swing Fault Duration Time of 0.1 s Between Nodes 5-7. . . . .	61

Figure 4.8	$\delta$ - $\omega$ Curves for Stable Swing Fault Duration Time of 0.1 s Between Nodes 5-7. . . . .	61
Figure 4.9	$\delta$ -t and $\omega$ -t Curves for Out-of-step Fault Duration Time of 0.45 s Between Nodes 5-7. . . . .	63
Figure 4.10	$\delta$ - $\omega$ Curves for Out-of-step Fault Duration Time of 0.45 s Between Nodes 5-7. . . . .	63
Figure 4.11	$\delta$ -t and $\omega$ -t Curves for Stable Swing Fault Duration Time of 0.1 s Between Nodes 7-8. . . . .	64
Figure 4.12	$\delta$ - $\omega$ Curves for Stable Swing Fault Duration Time of 0.1 s Between Nodes 7-8. . . . .	64
Figure 4.13	$\delta$ -t and $\omega$ -t Curves for Out-of-step Fault Duration Time of 0.45 s Between Nodes 7-8. . . . .	65
Figure 4.14	$\delta$ - $\omega$ Curves for Out-of-step Fault Duration Time of 0.45 s Between Nodes 7-8. . . . .	65
Figure 4.15	$\delta$ -t and $\omega$ -t Curves for Stable Swing Fault Duration Time of 0.1 s Between Nodes 8-9. . . . .	66
Figure 4.16	$\delta$ - $\omega$ Curves for Stable Swing Fault Duration Time of 0.1 s Between Nodes 8-9. . . . .	66
Figure 4.17	$\delta$ -t and $\omega$ -t Curves for Out-of-step Fault Duration Time of 0.45 s Between Nodes 8-9. . . . .	67
Figure 4.18	$\delta$ - $\omega$ Curves for Out-of-step Fault Duration Time of 0.45 s Between Nodes 8-9. . . . .	67
Figure 4.19	$\delta$ -t and $\omega$ -t Curves for Stable Swing Fault Duration Time of 0.1 s Between Nodes 4-5. . . . .	68
Figure 4.20	$\delta$ - $\omega$ Curves for Stable Swing Fault Duration Time of 0.1 s Between Nodes 4-5. . . . .	68

Figure 4.21	$\delta$ -t and $\omega$ -t Curves for Out-of-step Fault Duration Time of 0.45 s Between Nodes 4-5. . . . .	69
Figure 4.22	$\delta$ - $\omega$ Curves for Out-of-step Fault Duration Time of 0.45 s Between Nodes 4-5. . . . .	69
Figure 4.23	$\delta$ -t and $\omega$ -t Curves for Stable Swing Fault Duration Time of 0.1 s Between Nodes 4-6. . . . .	70
Figure 4.24	$\delta$ - $\omega$ Curves for Stable Swing Fault Duration Time of 0.1 s Between Nodes 4-6. . . . .	70
Figure 4.25	$\delta$ -t and $\omega$ -t Curves for Out-of-step Fault Duration Time of 0.45 s Between Nodes 4-6. . . . .	71
Figure 4.26	$\delta$ - $\omega$ Curves for Out-of-step Fault Duration Time of 0.45 s Between Nodes 4-6. . . . .	71
Figure 4.27	$\delta$ -t and $\omega$ -t Curves for Stable Swing with Cascading Faults Between Nodes 5-7. . . . .	72
Figure 4.28	$\delta$ - $\omega$ Curves for Stable Swing with Cascading Faults Between Nodes 5-7. . . . .	72
Figure 4.29	$\delta$ -t and $\omega$ -t Curves for Out-of-step with Cascading Faults Between Nodes 5-7 and 6-9. . . . .	73
Figure 4.30	$\delta$ - $\omega$ Curves for Out-of-step with Cascading Faults Between Nodes 5-7 and 6-9. . . . .	73
Figure 4.31	IEEE 10-machine 39-bus System. . . . .	75
Figure 4.32	$\delta$ - $\omega$ Curve with Fault Duration 0.3 s, Fault at 25-26. . . . .	79
Figure 4.33	$\delta$ - $\omega$ Curve with Fault Duration 0.3 s, Fault at 2-3. . . . .	80
Figure 4.34	$\delta$ - $\omega$ Curve with Fault Duration 0.3 s, Fault at 10-11. . . . .	81
Figure 4.35	Stable Swing Trajectory for Cascading Faults. . . . .	82
Figure 4.36	Out-of-step Trajectory for Cascading Faults. . . . .	83

Figure 5.1	Michigan Tech Smart Grid Lab Relay Testbed. . . . .	87
Figure 5.2	PMU Testbed-1. . . . .	89
Figure 5.3	PMU(SEL-421) and GPS Clock. . . . .	89
Figure 5.4	ATP-EMTP Model of SMIB System. . . . .	91
Figure 5.5	SEL-421 Protection Event History Report. . . . .	91

## **ACKNOWLEDGEMENTS**

First I would like to express my thanks to my advisor Dr. Sumit Paudyal for his guidance on my research work. His encouraging words have inspired me to continue and complete my graduate education. I would like to thank Dr. Bruce Mork for his guidance and support, not only on my thesis, but also on my entire academic path.

I would also like to thank my colleagues, Elizaveta Egorova, and Zagros Shahooei, Amol Kathe for their help during my stay at Michigan Tech.

I would like to thank my committee members, Dr. Laura Brown and Dr. Leonard Bohmann for their suggestions to improve the quality of my thesis.

I would like to thank Prof. John Lukowski, for his guidance on power system laboratories, which gave me inspirations to build relay test bed.

I would like to thank Pacific Northwest National Laboratory for providing me the detailed Phasor Measurement Unit deployment map for using. I appreciate the great support from my family during the entire graduate study period.

## ABSTRACT

Disturbances in power systems may lead to electromagnetic transient oscillations due to mismatch of mechanical input power and electrical output power. Out-of-step conditions in power system are common after the disturbances where the continuous oscillations do not damp out and the system becomes unstable. Existing out-of-step detection methods are system specific as extensive off-line studies are required for setting of relays. Most of the existing algorithms also require network reduction techniques to apply in multi-machine power systems. To overcome these issues, this research applies Phasor Measurement Unit (PMU) data and Zubov's approximation stability boundary method, which is a modification of Lyapunov's direct method, to develop a novel out-of-step detection algorithm.

The proposed out-of-step detection algorithm is tested in a Single Machine Infinite Bus system, IEEE 3-machine 9-bus, and IEEE 10-machine 39-bus systems. Simulation results show that the proposed algorithm is capable of detecting out-of-step conditions in multi-machine power systems without using network reduction techniques and a comparative study with an existing blinder method demonstrate that the decision times are faster. The simulation case studies also demonstrate that the proposed algorithm does not depend on power system parameters, hence it avoids the need of extensive off-line system studies as needed in other algorithms.



## **CHAPTER 1. Introduction**

### **1.1 Motivation**

Power systems are complex, non-linear and highly interconnected networks which aim at supplying high quality and reliable electrical energy to customers at reasonable prices [1]. Typical physical and functional components of power systems include generation, transmission, distribution, operation, electricity market, and utilization [2], as shown in Figure 1.1. The operation of power system includes power generation, delivery, and utilization at the end users. Generations comprise of a variety of resources including traditional fossil-fuel as well as renewable energy. Power delivery comprises of energy highway to distribute electrical energy from sources to consumers, which include transmission and distribution lines, along with their operations. Power market manages all financial and energy transactions. Power utilization is the final destination of the power system energy loop, which involves customers.

Like other non-linear physical systems, power systems are prone to stability issues [3]. To maintain reliability and the power quality [4]-[7], the operators of power systems are required to satisfy a set of steady state and transient indices, which include electrical parameters of power systems such as voltage, current, frequency, etc.

Disturbances in power systems are common and unavoidable. Such disturbances include line faults caused by falling trees, broken conductor caused by thunderstorms etc, change in load demands, loss of lines, loss of generation or similar events [8]. These disturbances cause transients in the non-linear power systems and some of the

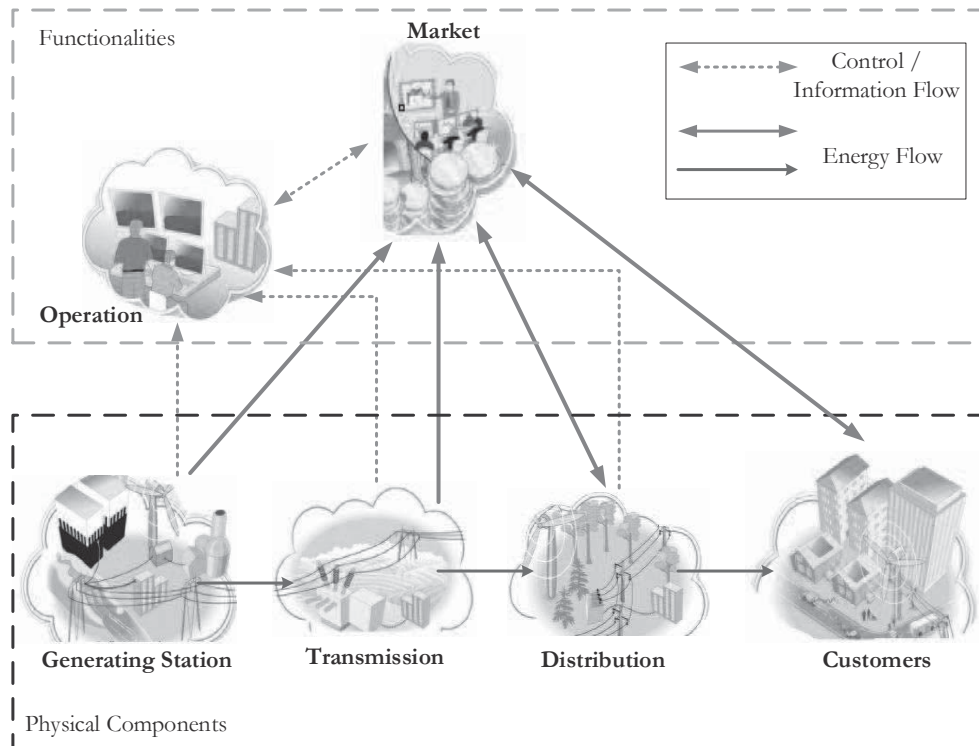


Figure 1.1 Typical Components and Functionality of Power Systems, adapted from [1].

disturbances may impact system stability and lead to the blackout or brownout of the systems [3], [6], [8]. Thus, power systems are equipped with protective devices, such as protection relays and circuit breakers to detect and prevent these incidents. Stability analysis of any physical system refers to system's ability to settle to a steady-state condition after disturbances. Power system stability analysis is similar to the generic stability concept, where steady-state in power systems refer to constant voltage, current, frequency, etc. observed throughout the system. After the disturbances, the electrical parameters of power system (voltage, current, frequency) fluctuate. The disturbance would be severe that the continuous oscillations do not damp out and the system becomes unstable, which is commonly referred as out-of-step condition. However, the

oscillations may damp out and the power system achieves a new steady state operating conditions, which is referred as stable swing.

Statistics from the Department of Energy (DOE) shows that at least 5 major incidents have occurred in North American power grid from various disturbances since 1960. It is worthwhile to mention here that 3 of the 5 incidents were due to the out-of-step condition, which impacted large number of customers leading to huge economic losses [2]-[11]. In the event of 1996, the cascading disturbances in the West Coast Transmission System lead to blackout impacting power supply of 12 million households for 8 hours; the estimated loss of which is \$2 billion [1]. In the event 1998, thunderstorm caused a single line to ground fault that lead to tripping of a 345 kV transmission line from Minnesota to Wisconsin. This disturbance further lead to an out-of-step condition and power flow in second 345 kV line crossed the limit. The second line was also disconnected in short time, which triggered cascading outages and caused more lines from Minnesota to Wisconsin to disconnect [1]. This disturbance leads the Northern Mid-American Power Pool (MAPP)'s electricity price increased to \$10,000 from a regular price of \$30 per MWh. The worst power disturbance occurred in Northeast America-Canada system in 2003, commonly called "2003 blackout". The 2003 blackout lead to 2,400 square kilometers area without electricity, which is about 50 million customers, and lead to economic loss of nearly \$6 billion [10]. This 2003 blackout disconnected 61,800 MW of power due to the cascading event which made it the largest power system incident in the world [10]. Based on the report by North American Electric Reliability Corporations (NERC), this blackout is a consequence started with a common three-phase line-to-ground fault leading to out-of-step due to lack of appropriate protections. Based on the above observations, out-of-step condition is one of the major cause of blackout and may impact reliability, economic, and quality of power system. The estimated loss is nearly \$188 billion worldwide due to blackouts arising from the out-of-step incidents.

Most of the existing out-of-step protection devices are based on blinder scheme [6], which use local measurements. The issue with such schemes in a large interconnected power system is to find appropriate settings of the blinders. With the availability of Phasor Measurement Units (PMUs), the protection system can utilize the benefits of wide-area measurements and novel out-of-step protection algorithms can be developed [11]. PMUs; which are also called synchrophasors; measure, communicate, and analyze the time-tagged real-time measurements, for example, voltage, current, and frequency in the power grid [12]. Commercial products such as SEL-421, GE N60, and ABB RES521 are some of the examples of such PMU devices [12]. The use of PMUs has been increased since NERC recommended in 2008 that real-time operational tools require high-speed sampling capabilities for accessing and processing the data, which is possibly driven by the 2003 blackout. Based on the DOE's smart grid statistics in 2009 [9], the North America, power systems in total have deployed 50 PMUs. After the the American Recovery and Reinvestment Act of 2009, the entire U. S. power systems will spend about \$4.5 billion in building smart grid infrastructure including installation of PMUs [9]. North American Synchrophasor Initiative (NASIP) map in Figure 1.2 showed that in total 2,000 PMUs have been deployed until 2013 [9], [12]. The number of PMUs are also increased worldwide: China deployed more than 800 PMUs in the state grid until 2009 [13], and about 1,500 PMUs until 2013 [13]-[14]; Japan installed around 50 PMUs nationwide until 2007 [15].

Since power system is highly interconnected and prone to stability issues, keeping the grid in steady-state condition is always of priority. Based on aforementioned discussion, out-of-step protection is a crucial functionality in power systems. Also, the PMUs are becoming key equipment for operation and protection. The conventional out-of-step protection relied on local measurements and had various issues including dependency on the network topology and system parameters. Thus, this work

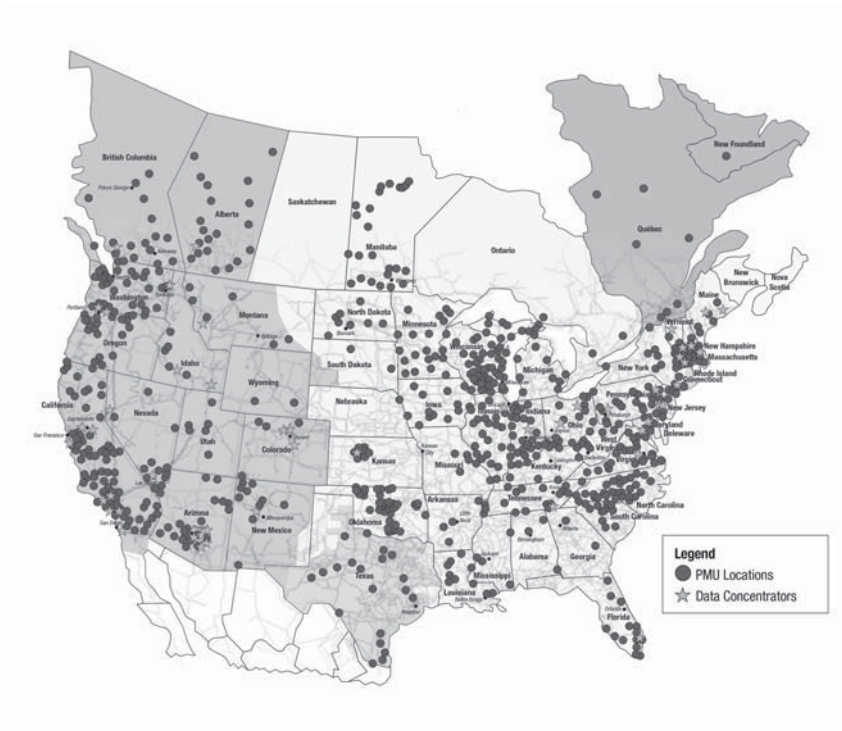


Figure 1.2 Location of Synchrophasors in the U.S. and Canada in 2013 [9].

concentrates on developing a novel out-of-step protection algorithm for interconnected power system which makes use of wide-area measurements available from the PMUs.

## 1.2 Literature Review

A brief literature survey of various out-of-step protection algorithms are discussed next, which are mainly grouped into 4 categories.

### 1.2.1 Out-of-step Protections Based on Rate of Change of Parameters

Most of the existing out-of-step protection requires measurement of one or more electrical parameters in power system, and based on rate of change of these parameters decision regarding out-of-step conditions are made. One of the conventional techniques

reported in [16], [17] requires the rate of change of impedance at relay location, called blinder technique. The blinder method needs two rectangular protection zones, inner and outer blinders; setting these blinders' threshold and finding a proper time delay are two major tasks in this technique. The details to set these blinders are explained in reference [17], [18], which are system specific, depended on system loading conditions, and are only applicable for two-machine systems. Therefore, settings of the blinder require extensive off-line stability simulations for different swing conditions, and thus designing a relay for all possible system conditions is usually an involving task. Many modifications of the rate of change of impedance methods have been tried, such as the rate of change of apparent resistance [19]. However, the modifications only change the study domain, but do not bring any advantages and still possess the same shortcomings as the case of rate of change of impedance method.

Swing Center Voltage (SCV) technique discussed in [20] computes voltage at a virtual center in the power system. Then, SCV method uses the changing rate of voltage at the swing center to make a decision about out-of-step condition [16], [21], [22]. However, the estimation of voltage at the virtual center is accurate only when voltage at two ends of the power system are close to  $180^\circ$ . Also, the SCV methods are clearly defined only for a two-machine system; applying SCV to multi-machine systems require cumbersome network reduction techniques.

All of the methods discussed above, that depend on the rate of change of parameters, require extensive off-line simulation of stability studies, and are clearly defined only for 2-machine system. Besides these, the blinder schemes do not perform well for fast power swings and the SCV techniques do not perform well if the system impedance is not close to  $90^\circ$  [17].

### 1.2.2 Computer Intelligence Based Methods

Intelligence based methods have been extensively used in power system protection applications including the out-of-step protection [23]-[26]. In [23], a fuzzy logic based approach is used where pre-fault and post-fault currents, voltages and angular speeds of the generators are used as inputs to the fuzzy inference blocks. The results reported in [23] are promising, however, the authors only demonstrated fuzzy logic application in 2-machine systems. In [24] -[26], Artificial Neural Network (ANN) based approach has been used for out-of-step protection; which has been tested up to 3-machine system. The main issue with fuzzy logic based methods applied for multi-machine system is to identify input variables, which are infact measurements throughout the system. Fuzzy-logic based approach require to construct right membership functions and well designed “if-then” decision rules. The ANN based approach require extensive off-line simulations.

### 1.2.3 Equal Area Criterion (EAC) based Methods

The Equal Area Criterion (EAC) is a famous tool in power systems for transient stability studies. EAC describes the system stability based on the area under the  $P-\delta$  curve. This approach is applicable directly to single machine infinite bus (SMIB) systems [27] - [31]. The out-of-step detection method based on EAC algorithm in  $P-\delta$  domain compares power angle with critical angle. In [30], based on EAC, critical clearing angle ( $\delta_{cr}$ ) is computed and compared with the power-angle of SMIB system to make a decision on out-of-step condition. The main drawback of EAC method is that it can not be directly applied to multi-machine systems. Moreover, the EAC based method in  $P-\delta$  domain requires power angle information from two areas, which means requirement of additional communication devices.

In [31], EAC method is modified to time domain, which eliminates the need of power-angle information from two-area. However, the method proposed and results

provided in [31] are not promising for multi-machine systems.

The Extended EAC (EEAC) is introduced in [32], which could be applied directly to multi-machine system. An equivalent two-area system is created using the EEAC method and based on it an out-of-step algorithm is proposed in [33]. Since network reduction is used in the EEAC method, the settings of the out-of-step relays are system specific. This approach was used in out-of-step protection in the inter-tie transmission line between the states of Georgia and Florida's power system in 1993 and was operational until 1995 [33]. Since EEAC requires wide-area information, the use of PMU seems to be inevitable for out-of-step protection.

#### **1.2.4 Lyapunov Theory Based Approaches**

The Out-of-step decision, from control theory's viewpoint, is to find an analytical solution to the swing equations after disturbances. Instead of directly solving a system of partial differential equations (PDE), Lyapunov proposed a method that does not require numerical or analytical solutions, rather, it analyzes the eigenvalue distributions of the system to find out the stability region [34] - [41]. In power systems, many attempts [4], [7], [38] have been made to apply this theory for stability studies.

In [41], Lyapunov's method is combined with PMU data for state estimation and out-of-step detection. In [41], pre-fault, post-fault, and during-fault energy trajectories (kinetic and potential energy) are used for the out-of-step detection. The results are promising, however, this method is only demonstrated for SMIB system.

The Lyapunov's theory is great for stability analysis, however, in some critical cases, even eigenvalues distributions are not easy to calculate. Hence, V. I. Zubov, first proposed an modified method to achieve the similar stability region as Lyapunov's direct method but with approximations [39]. Later on, it was proved to be suitable for numerical computing [36], [40]. Zubov's method have been used for power system stability studies,



but not applied for out-of-step detection yet. In this work, Zubov's method, which is a modified form of Lyapunov based method, is used for out-of-step detection in multi-machine power systems.

### **1.3 Thesis Overview**

The existing out-of-step algorithms have many shortcomings: methods based on "rate of change of parameters" require off-line studies for setting the thresholds, methods based on computer intelligence require extensive off-line studies for training the system, require properly structured "if-then" rules, and also the number of inputs required for such methods in multi-machine systems are large. Methods based on EAC and its modifications are applicable for 2-machine system while for multi-machine systems network reduction techniques are required. Since Lyapunov and its modifications have been extensively used for stability studies, this work attempts to use the method of Lyapunov theory for out-of-step protection, which do not require off-line simulation and is directly applicable to multi-machine system without network reductions. Thus, the objective of this thesis are:

- To use Zubov's method to develop an out-of-step detection algorithm applicable to multi-machine systems. The proposed Zubov's based method uses PMU data for pre-fault operating conditions and trajectories during transients.
- To Implement a blinder scheme on commercially available hardware and to compare the performance of proposed method with the blinder scheme.

A general overview of the proposed work is shown in Figure 1.3, the proposed Zubov's out-of-step detection algorithm analyzes the multi-machines' PMU data and detects swings either as stable swing or out-of-step conditions.

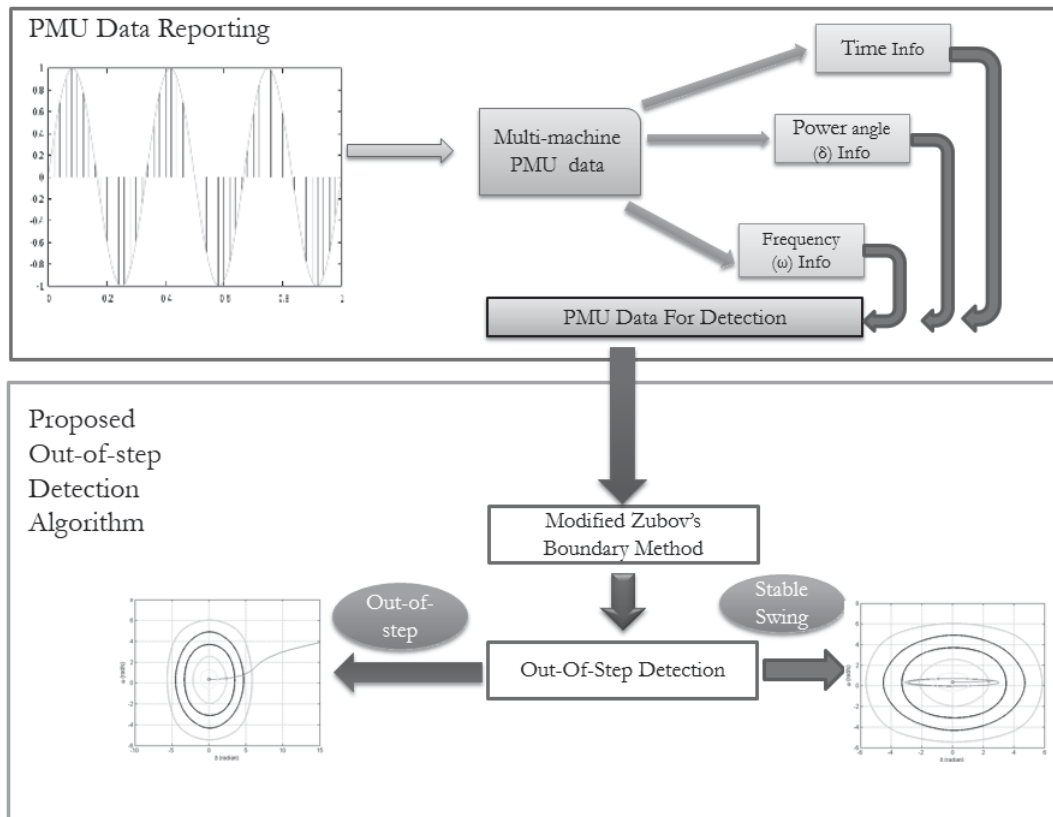


Figure 1.3 Overview of the Proposed Work.

## 1.4 Thesis Outline

The thesis has six chapters and five appendices, including this chapter (Chapter 1). Chapter 2 explains the background information on PMUs, power swing fundamentals and out-of-step protection techniques, and Zubov's approximation method with two numerical examples.

Chapter 3 contains explanations of Zubov's method in reference to power systems and its application in out-of-step protection of SMIB system.

Chapter 4 demonstrates more case studies in multi-machine system to show the application and robustness of the proposed method.

A hardware implementation of the blinder scheme is illustrated in Chapter 5. Using Schweitzer Engineering Laboratories (SEL)'s commercial out-of-step relay for comparison testing, the improvements of the proposed method over blinder scheme are elaborated based on the results.

Chapter 6 consists of summary, contribution, and future work for this research.

There are 5 appendices at the end. Appendix A lists parameters of SMIB system. Appendix B lists parameter of IEEE 3-machine 9-bus system. The parameters of IEEE 39-bus 10-machine system are listed in Appendix C. An example to calculate Zubov's boundaries for SMIB system is included in appendix D.

## CHAPTER 2. Background

### 2.1 Introduction

In this chapter, background information of PMU and out-of-step phenomena are elaborated. The power system impedance loci during out-of-step condition is analyzed in details. Then, out-of-step protection methods like blinder method, swing center voltage method, EAC and modified EAC method in time domain, Fuzzy Logic and Neural Network based methods, and Lyapunov energy function based method are discussed. Their advantages and disadvantages are discussed for improving the proposed algorithm in this thesis. Besides, Zubov's approximation boundary calculation procedures for general non-linear system stability analysis are illustrated.

### 2.2 Phasor Measurement Unit

A Phasor Measurement Unit (PMU) is a device for capturing phasors of Alternating Current (AC) signals. Phasors of AC waveform consists of RMS magnitude values and the phasor angles [42] - [45] . An AC waveform can be mathematically defined by the following equation:

$$x(t) = X_m \cos(2\pi ft + \phi) \quad (2.1)$$

where the  $X_m$  indicates the magnitude of the sinusoidal waveform,  $f$  is power system synchronous frequency, which is typically 50 Hz or 60 Hz, and  $\phi$  represents the phase

shift of the waveform [43] - [46]. The phasor of the AC waveform in (2.1) is given by,

$$X = \frac{X_m}{\sqrt{2}} \angle \phi \quad (2.2)$$

PMU are aligned with GPS time signals which are referred as synchrophasors. Synchrophasors measure AC signals from frequency either 50 Hz or 60 Hz power grid at a standard sampling rate of 48 phasors per second, high up to 60 phasors per second, in the reference waveform [43] - [44]. The phasor quantities are measured by using a reference cosine function as shown in Figure 2.1. A Coordinated Universal Time (UTC) reference signal is then used to time-stamp the phasors measured throughout the power system for synchronous purpose. The UTC signal comes from a GPS clock which ensures same time reference for all phasor measurements and also ensure accuracy of the clock [42] - [43].

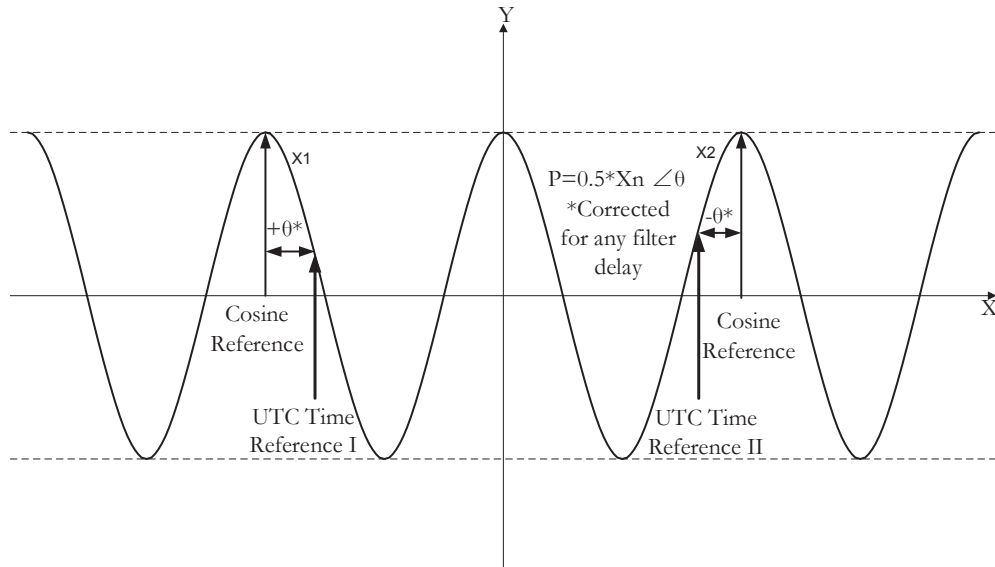


Figure 2.1 A Sinusoidal Waveform Illustrating Synchrophasors, adapted from [44].

A typical PMU functional block diagram is shown in Figure 2.2, which consists of five main components: Filter, Analog to Digital Converter, GPS Clock Receiver,

Phasor-locked Oscillator, Phasor Calculation, and Output Interface [43] - [44].

Power system AC waveforms are captured using current or voltage transformers, which are then processed through anti-aliasing filters. Analog signals are then digitized by the embedded Analog to Digital Converter. Phase-locked oscillator uses reference time signal from GPS receiver required for synchronized samples, which typically has an accuracy of 1 microsecond [42], [45]. The embedded microprocessor contains frequency estimation and phasor estimation algorithm (such as Fast Fourier Transform or Discrete Fourier Transform) which could send information to power system operators with a typical reporting rate of 1-2 phasor per second through Interface.

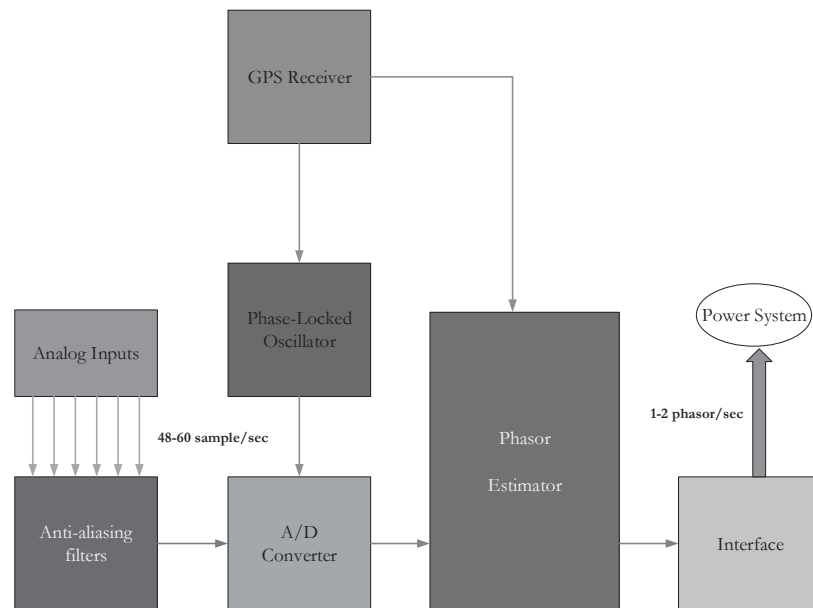


Figure 2.2 Block Diagram of Phasor Measurement Unit, adapted from [43].

A general phasor measurement unit data acquisition and transmission network is shown in Figure 2.3. The first communication level is between PMU devices and its closest phasor data concentrator (PDC). The phasor data available at this level is very high rate typically 10 to 30 phasors per second. These PMU measurements can be used

for real-time protection algorithm which need fast and large amount data from the system [46]. The next level is the communication between different local PDC layers. The third communication level eventually makes all local PDC layer connect to a master level. Based on these transmission procedures, the operating center could draw an entire detailed grid status picture quickly. Hence, this network could be suitable for wide-area controlling or protecting. However, due to the low transmitting rate of phasor data between the second communication level, which are typically not more than 10 phasors per second, and the third level, which is even lower down to 1 phasor per second, the PMU network is now mainly used for system-wide monitoring and after-fault event analyzing [44].

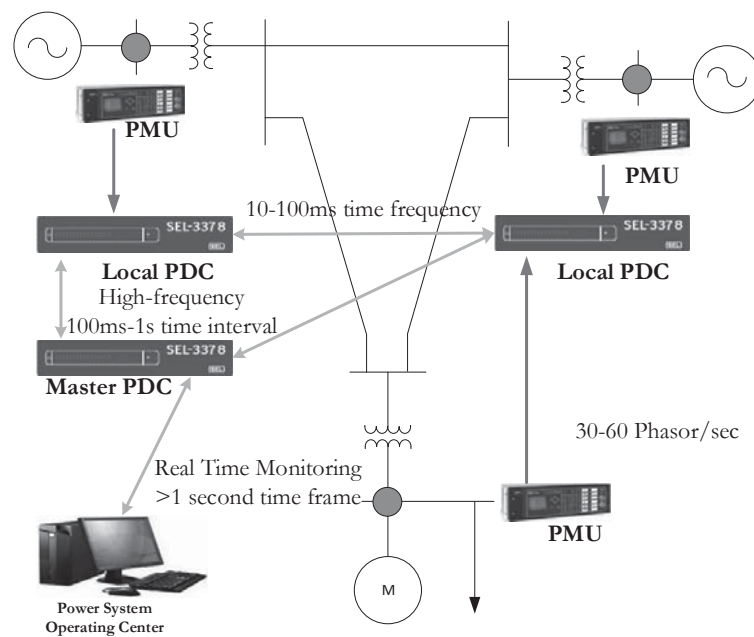


Figure 2.3 Power System Synchrophasor Network, adapted from [45].

## 2.3 Power Swing Fundamentals

From electro-mechanical viewpoint, steady state operation in power system means a balance between input mechanical power and output electrical power. Thus, the interconnected generators, for steady state conditions, are operating among their stable region of power angle, frequency, etc., making all electrical quantities keep stable throughout the power system [17], [47].

After disturbance, the input mechanical power and output electrical power are no longer the same, resulting in electro-mechanical oscillations called power swings. The disturbance could be severe that the oscillations do not damp out and system becomes out-of-step, as shown in Figure 2.4.

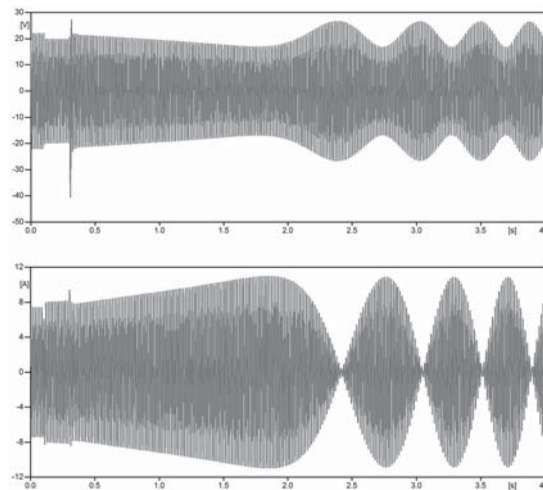


Figure 2.4 Current Waveform in Stable and Out-of-step Situation.

During power swing, generators rotate at different speeds and result change in relative rotor angle of the generators. The consequence is high fluctuation of voltages and currents at different nodes of the power system. The distance relays incorporated in a power system use these voltages and currents to calculate the impedance [47]. The nature of the impedance trajectory during a power swing is explained next.



Consider a two machine system as shown in Figure 2.5 . The motor voltage  $E_r$  is considered as the reference phasor. The generator  $E_g$  leads  $E_r$  by  $\theta$  phase angle, where  $\theta$  is referred to as the relative rotor angle (or the power angle) of the generator.

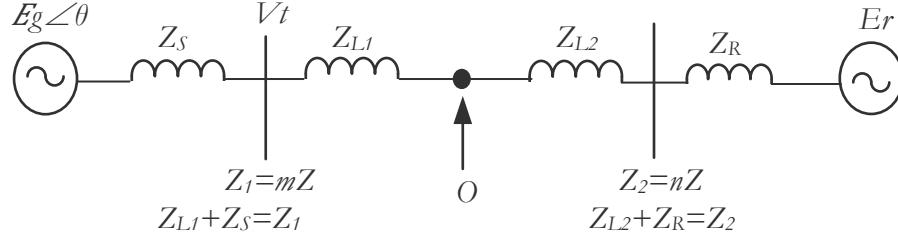


Figure 2.5 Two-machine Network to Illustrate Power Swing Loci.

The relay location at  $O$  divides the impedance in two sections with impedance  $mZ$  and  $nZ$  where  $m + n = 1$ . The current and voltage at relay location  $O$ ,

$$I_O = \frac{E_g \angle \theta - E_r}{Z_1 + Z_2} \quad (2.3)$$

$$V_O = n E_g \angle \theta + m E_r \quad (2.4)$$

Thus, the impedance seen by relay device at  $O$  is,

$$Z_O = \frac{V_O}{I_O} = \frac{n E_g \angle \theta + m E_r}{E_r \angle \theta - E_r} (Z_1 + Z_2) \quad (2.5)$$

Assuming  $E_g = E_r$ ,

$$\frac{Z_O}{Z} = \frac{n \angle \theta + m}{1 \angle \theta - 1} = -m + \frac{1 + \cos \theta + j \sin \theta}{2j \sin \theta} \quad (2.6)$$

where  $Z = Z_1 + Z_2$ ,

$$Z_O = \underbrace{\left(\frac{1}{2} - m\right)}_R - j \underbrace{\frac{1}{2} \cot \frac{\theta}{2}}_X Z \quad (2.7)$$

The impedance loci for different value of  $m$  and  $\theta$  from  $30^\circ$  to  $330^\circ$  are shown in Figure 2.6, where  $R$  and  $X$  are the resistance and impedance value at node  $O$  seen by

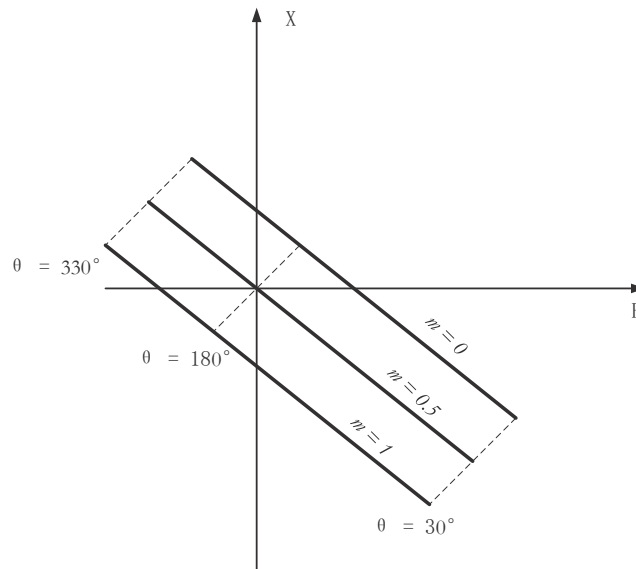


Figure 2.6 Impedance Loci at Relay Location O for  $E_g = E_m$ , adapted from [16].

relay device. Similarly, impedance loci for different ratio of  $E_g/E_m$  are shown in Figure 2.7.

A typical electrical protection system includes relays, circuit breakers, current and voltage transformers, advanced communication devices and digital event recorders. In modern power systems, or smart grids, the protection system also includes PMUs.

A Relay is an electric device embedded with pre-programmed protection algorithms and thresholds which outputs tripping signals for circuit breakers [42]. By using measurements through current and voltage transformers, relays could make tripping decisions and send output signals to circuit breakers to operate disconnections or to reclose the breakers. Different functional relays, for example overcurrent relay or differential relay, specifically focuses on their aspects. However, out-of-step relay, monitor the loss of synchronism in power systems and output necessary trip signals to isolate the impacted area from rest parts to help the system achieve a new steady-state status.

The relay evolution has gone through three generations from Electro-mechanical,

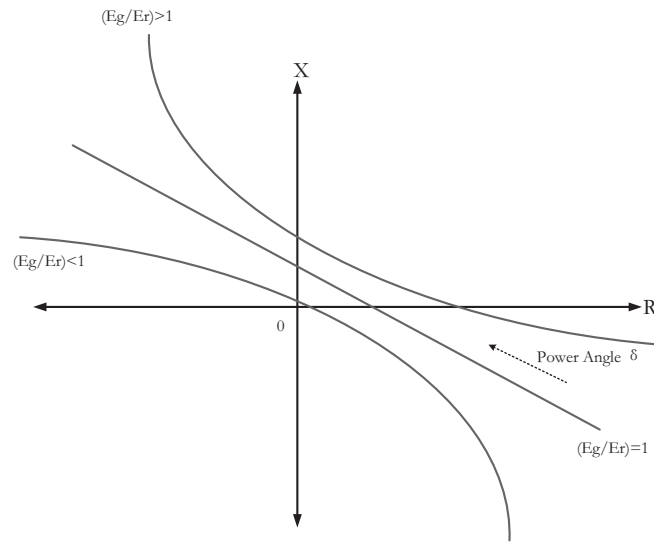


Figure 2.7 Impedance Loci at Relay Location O for  $E_g \neq E_m$ .

Static to the Modern Micro-processor based relays as shown in Figure 2.8 [48].

Electro-machanical relays are the first generation of protective device which generates signals by electromagnetic force of current going through coils [48]. Static relays or solid-state relays are based on the application of semiconductor devices which are smaller and lighter than the electro-machanical relays. Microprocessor based relays are developed by the advanced technology of very large scale integrated circuit and microprocessor in 1960's [29], [48]. In recent years, the microprocessor based relays are combined with the time-tagged PMU data acquired through wide-area system, as discussed in Chapter 1. The use of PMU based relays are increasing and are essential for out-of-step protection [29], [33], [48].

## 2.4 Out-of-Step Detection Techniques

A brief literature survey of 4 different out-of-step detection methods is discussed in Chapter 1. In this section, each method is explained in more details.

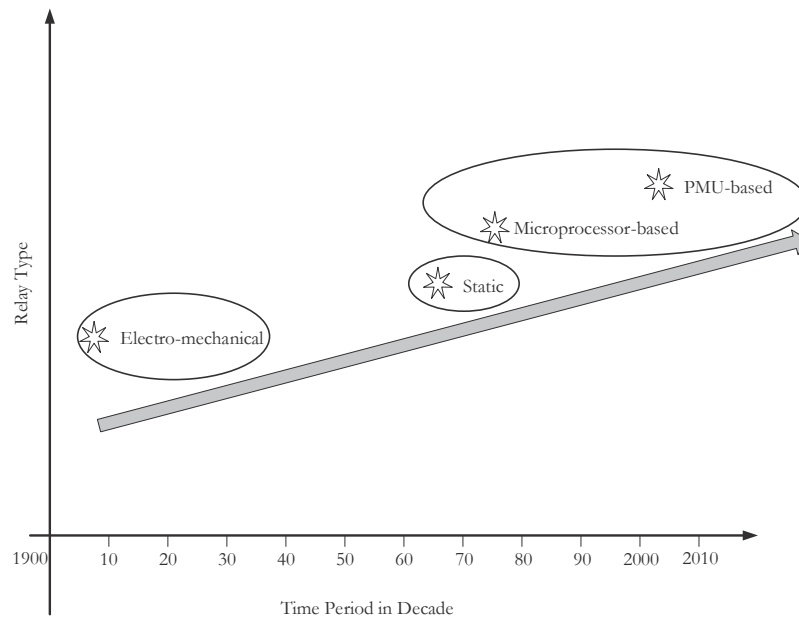


Figure 2.8 Relay Development Timeline, adapted from [48]

#### 2.4.1 Rate of Change of Impedance Based Method (Blinder Technique)

The most often used out-of-step protection method in commercial relays is the blinder method, which is based on the measurement of positive sequence impedance at the relay location. The out-of-step relay is normally a distance relay employing different protection algorithms in the impedance plane [17], [18].

Figure 2.9 shows a blinder scheme for out-of-step detection, with two rectangular regions (outer and inner blinder). The two-blinder method differentiates between faults and power swings by calculating the rate of change of the impedance ( $Z$ ). The measurements of the rate of change of  $Z$  is typically performed by measuring the time it takes the impedance to go through the two-blinders elements. The impedance seen by the relay during steady state conditions is the normal load impedance, which lies away from the relay's rectangular blinders, shown as the load region in Figure 2.9. A Relay continuously measures the rate of change of impedance when it penetrates into the

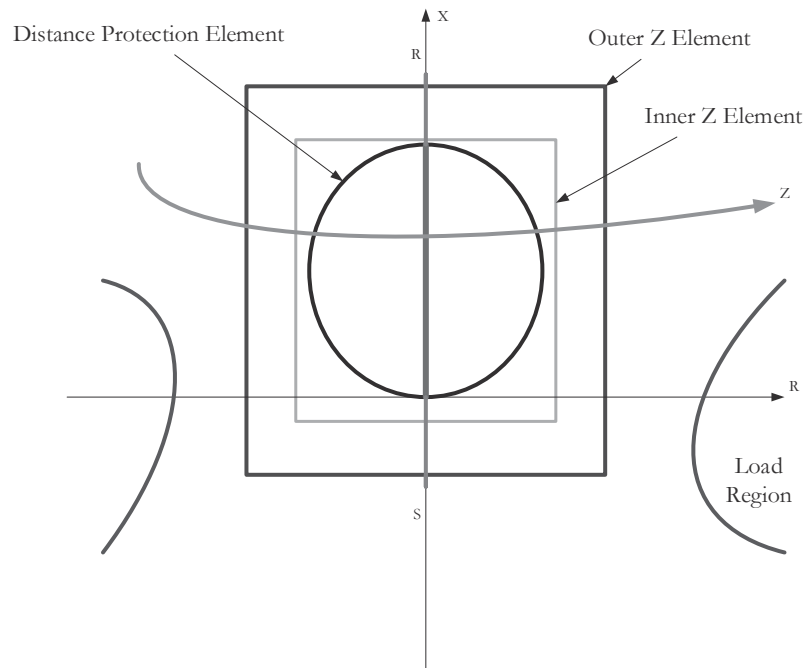


Figure 2.9 Blinder Scheme for Out-of-step Protection, adapted from [16].

protection regions of impedance relay, triggering the blinder detection part with a fixed time delay function called timer. Relay decides the case as fault if the impedance seen by the relay crosses the settings of outer and inner Z element before the timer expires. If the timer expires before the impedance crosses both two zones, the relay will decide it as a power swing. In this case, out of step relay blocking function triggers and blocks the distance protection function for a period of time. The outer blinder must be placed away from the load region to prevent relay blocking function from operation due to heavy loads.

## 2.4.2 Swing Center Voltage Technique

SCV computes voltage at a virtual center in the two-machine equivalent power system. During steady state conditions, the swing center is located on the system where the voltage magnitude is zero when the power angle is  $180^\circ$  apart between the two machines [20]. The equivalent two machine system of Figure 2.10 is used to illustrate the SCV method.

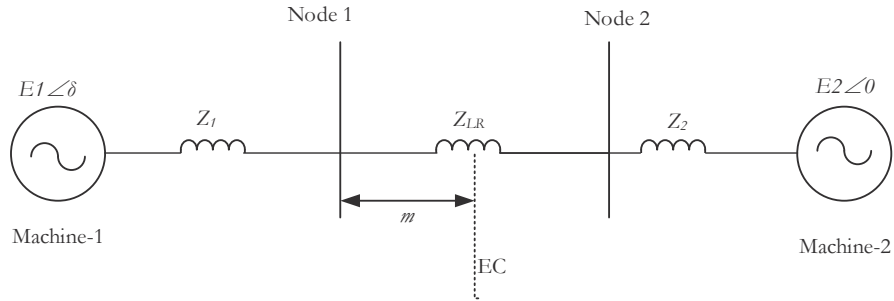


Figure 2.10 Two Machine Example for SCV.

If this system becomes out-of-step after a disturbance, the difference between two machine's angle,  $\delta(t)$  would fluctuate. In Figure 2.10,  $E_1$  and  $E_2$  respectively represent terminal voltage of two machines,  $m$  is the electrical distance from 1 to 2.

The voltage of two machines are :

$$V1 = E_1 \sin(\omega_1 t + \delta(t)) \quad (2.8)$$

$$V2 = E_2 \sin(\omega_1 t) \quad (2.9)$$

where,  $\delta$  is the initial power angle at Node-1.

$$\delta(t) = \delta_0 + \sin(\omega_1 t) \quad (2.10)$$

And the system impedance is:

$$Z = Z_1 + Z_2 + Z_{LR} \quad (2.11)$$

Voltage seen by distance relay at Node-1 is (assuming voltage at EC is zero):

$$V_{l1} = \frac{E_1 \sin(\omega_1 t + \delta(t))}{Z} [Z_2 + (1 - m) Z_{LR}] \quad (2.12)$$

Hence, the voltage at the Node-2 when voltage of EC is still zero,

$$V_{r2} = \frac{E_2 \sin(\omega_1 t + \delta(t))}{Z} [Z_1 + (m) Z_{LR}] \quad (2.13)$$

Based on the previous value, the impedance is this bracer required between Node-1 and Node-2:

$$Z_{12} = \frac{V}{I} = -Z_1 + Z_{sum} \frac{E_1 \angle \delta}{E_1 \angle \delta - E_2} \quad (2.14)$$

When  $|E_1| = |E_2| = 1$ ,

$$Z_{12} = \left[ \frac{Z_{sum}}{2} - Z_1 \right] - j \left[ \frac{Z_{sum}}{2} \cos \frac{\delta}{2} \right] \quad (2.15)$$

Thus, the swing center voltage is obtained as,

$$SCV = E_1 \sin \left[ \omega_1 t + \frac{\delta(t)}{2} \right] \cos \left[ \frac{\delta(t)}{2} \right] \quad (2.16)$$

The SCV could be simplified as,

$$SCV \approx E_1 \cos \left[ \frac{\delta(t)}{2} \right] \quad (2.17)$$

Based on (2.16) and (2.17), the maximum magnitude of the SCV occurs when the angle difference between two machines is zero. During a power swing, the rate of change of SCV is compared as,

$$\frac{dSCV}{dt} = -\frac{E_1}{2} \sin \left[ \frac{\delta(t)}{2} \right] \frac{d\delta}{dt} \quad (2.18)$$

Figure 2.11 shows the phasor diagram of the SCV in a two machine equivalent system, where the line  $OO'$  is the SCV.

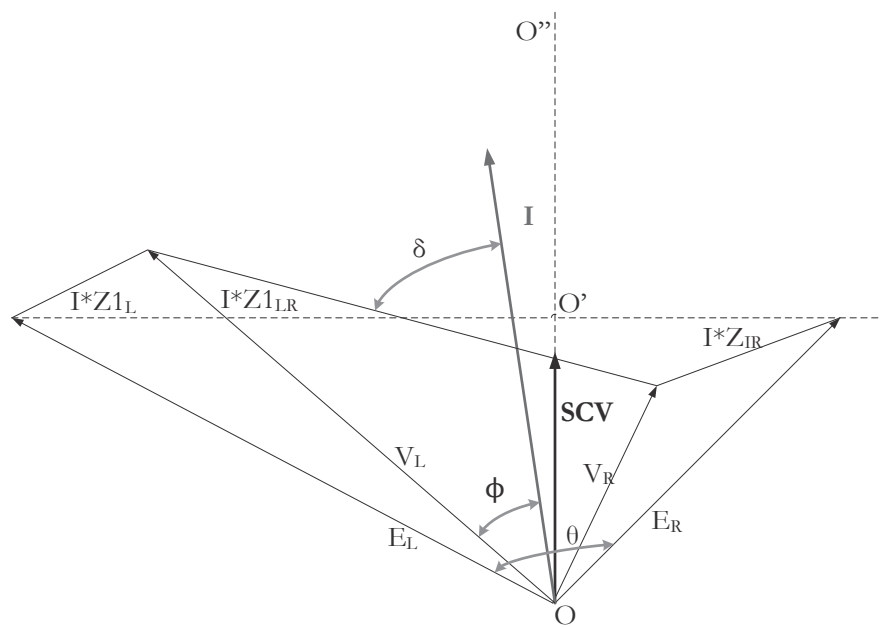


Figure 2.11 SCV in Phasor Diagram, adapted from [16].



### 2.4.3 Techniques Based on Fuzzy Logic and Neural Network

Computational Intelligence techniques applied to power systems are discussed in Chapter 1, details of which are discussed next [23]-[26].

The fuzzy logic algorithm can be summarized as finding a group of appropriate signal sets to train the programmed inference system, developing stable and swing criteria to discriminate system status, and making a correct decision based on this. A typical diagram of fuzzy block detection system is shown in Figure 2.12.

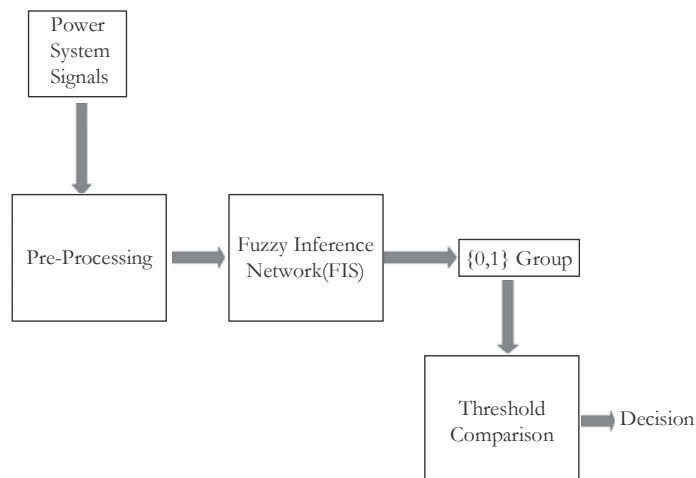


Figure 2.12 Fuzzy Algorithm for Out-of-Step Detection, adapted from [23].

In order to pick up the best inputs to fuzzy system, the statistical properties of different state variables are tested. Among them, machine's frequency deviation and machine's terminal impedance angle are the most useful measurements [23]. The most daunting part of this fuzzy logic algorithm is to have sufficient cases of out-of-step conditions before applying it. A power system has a large number of signals or measurements which could be applied for data analysis or pattern recognition, such as generators' terminal voltages, currents and rotor speeds. Reference [24], [25] proposed

an out-of-step detection based on back propagation trained neural networks. This schematic is shown in Figure 2.13. Besides the direct measurement data, other data like orthogonal values of phase voltages and currents could be calculated and used for deriving various composite information. Along with these derived data, other power system's energy measurements are also used such as machine's mechanical inputs, electrical outputs for pre-fault, and related load information.

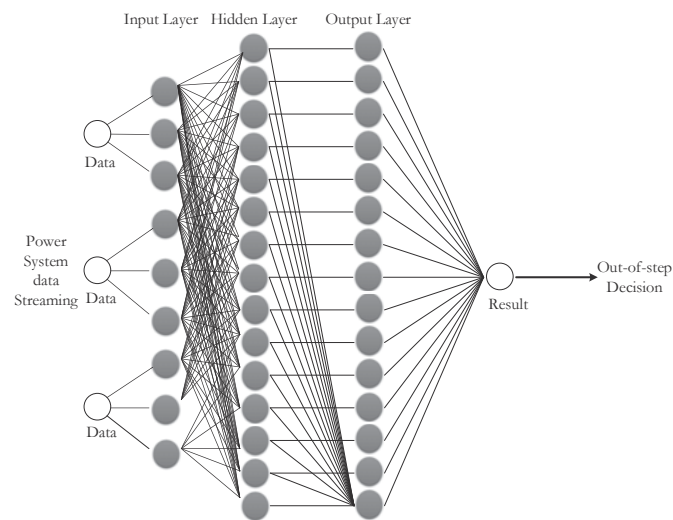


Figure 2.13 ANN Data Training Diagram for Out-of-step Detection.

#### 2.4.4 Techniques Based on EAC and Its Modification

EAC method is an energy based method for power system stability analysis, which could be applicable for out-of-step detection. Reference [30] proposed a method for out-of-step detection in  $\delta$  domain. In the original EAC method, two areas (acceleration and deceleration) are calculated under P-  $\delta$  curves, as Figure 2.14 shows. This EAC method consists of three  $P_e$ - $\delta$  curves for pre-fault, during-fault and post-fault conditions. The EAC method compares the area of  $ABCOA$  to  $DEOD$ . If these two areas are equal,

then the system is stable, otherwise the system becomes out-of-step.

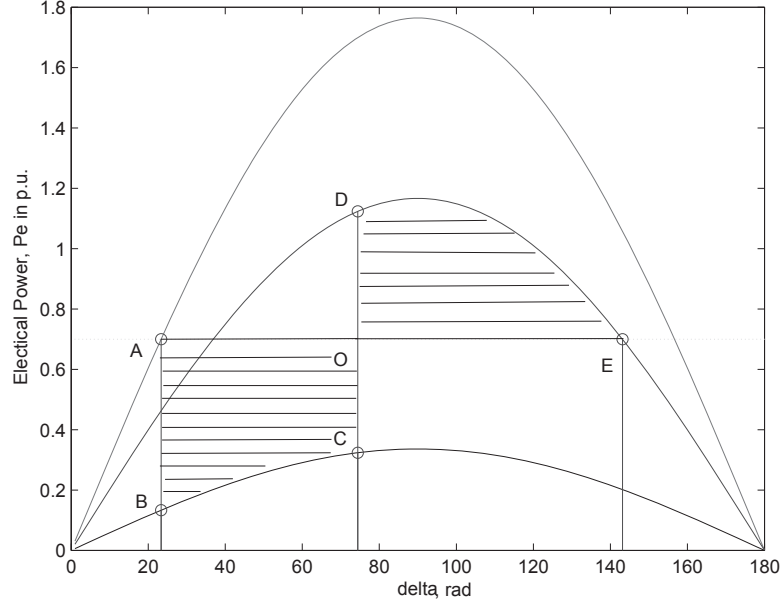


Figure 2.14 P- $\delta$  Curves for EAC Method, adapted from [30].

The modified EAC in time domain method transfers the power curves from P-  $\delta$  domain to P-  $t$  domain, as shown in Figure 2.15 [31], [49]. The out-of-step decision will be made by adding two areas,  $A_1$  and  $A_2$ , which represents the acceleration and deceleration energy, respectively. If the area add to zero, then the system becomes stable, otherwise, it becomes an out-of-step condition. The  $A_1$  could be calculated as:

$$A_1 = \int_{\delta_0}^{\delta_c} \frac{\omega_s}{H} (P_m - P_e) d\delta \quad (2.19)$$

Similarly, the  $A_2$  is calculated as:

$$A_2 = \int_{\delta_{max}}^{\delta_c} \frac{\omega_s}{H} (P_m - P_e) d\delta \quad (2.20)$$

where A, represents the total energy during transient condition.

For stable swing is,

$$A = A_1 + A_2 = 0 \quad (2.21)$$

For out-of-step condition,

$$A = A_1 + A_2 \geq 0 \quad (2.22)$$

In (2.19-2.22),  $H$  represents the machine inertia;  $\omega_s$  is synchronous speed,  $\omega_0$  represents the initial rotor angle at pre-fault,  $\delta_c$  is the post fault angle,  $\delta_{max}$  is the maximum rotor angle,  $P_m$  is the mechanical input power and  $P_e$  is the electrical input power [30].

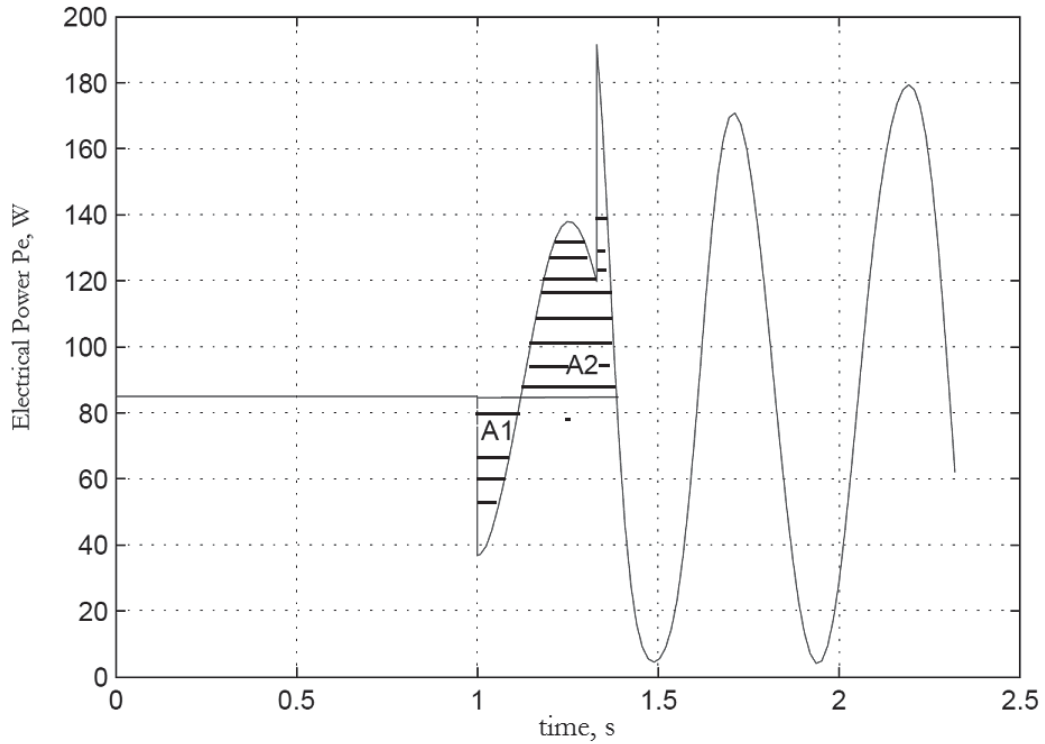


Figure 2.15 P-t Curve for Modified EAC Method in Time Domain, adapted from [49].

#### 2.4.5 Lyapunov's Theory Based Techniques

As discussed in Chapter 1.3, Lyapunov's second method for non-linear system stability analysis applied to power system applications has a vast number of research works. Different from the direct calculation of stability boundary, Zubov's method gives a

new approximate method for non-linear system stability boundaries, which is shown to be an efficient tool for power system stability analysis [34], [36], [38] - [40].

#### 2.4.5.1 Lyapunov's Second Method Based Energy Comparison Approach

Stability analyses are performed on the basis of Lyapunov Energy functions [17], [41]. The total energy of a generator that experiences a fault is evaluated as the sum of its kinetic and potential energy. The potential and kinetic energy of the generator can be calculated as:

$$E_{potential} = \int_{\delta_o}^{\delta_{pf}} [P_{epost}(\delta(t)) - P_m] d(\delta) \quad (2.23)$$

$$E_k = \frac{M\omega^2(t)}{2} \quad (2.24)$$

where the  $P_{epost}$  is the post-fault electrical power energy,  $\delta_o$  is the steady-state pre-fault power angle. For a fault clearing time  $t_c$ , if  $E_{total} < E_{max}$  then the system is stable, else it becomes unstable, where  $E_{max}$  is the maximum energy that a system can have before losing its synchronism [41]. Figure 2.16 shows pictorial representation of energy-based approach for stability studies.

#### 2.4.5.2 Zubov's Method for Stability Analysis

Zubov's stability method is to construct a Lyapunov construction of a partial differential equation by approximating the stability region as,

$$\sum_{i=1}^n \frac{\partial V}{\partial x_i} F_i = -\phi(1 - V) \quad (2.25)$$

where  $\phi$  is an arbitrary positive-definite function,  $V$  is assumed to be the sum of an infinite series of homogeneous polynomials [40].

For a general explanation, let an equation is respected by,

$$\dot{x} = Ax + g(x) \quad (2.26)$$

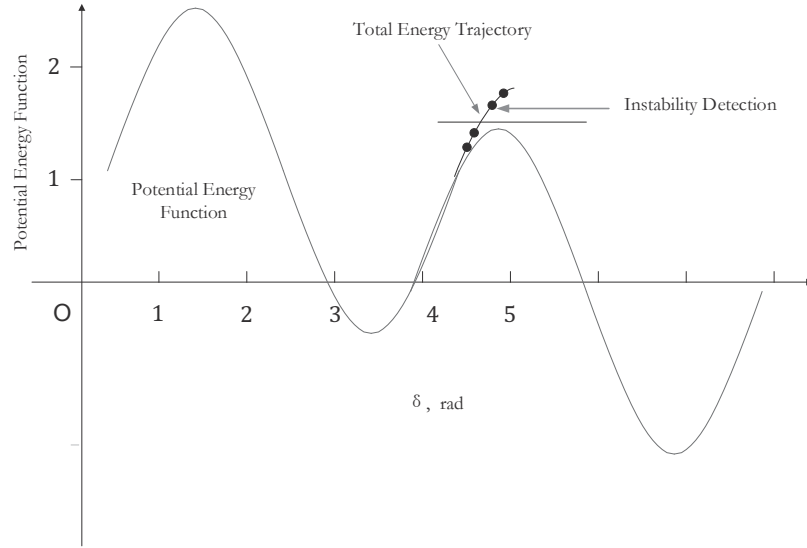


Figure 2.16 Energy Based Approach for Stability Detection, adapted from [41].

where  $g(x)$  consists of higher degree polynomials and  $A$  is the linear equation. Consider that  $A$  is stable, which has all eigenvalues with negative real parts,  $\phi$  is used for positive definite quadratic part [39] - [40]. Then the  $V$  in eqn.2.25 can be written as,

$$V = V^N = V_2(x) + V_3(x) + \dots + V_N(x) \quad (2.27)$$

where  $V_2(x)$  is quadratic in  $x$  and  $V_N(x)$ ,  $N = 3, 4, \dots$  are homogeneous equation in  $N$  degree. By substituting (2.27) in (2.25),  $V_N(x)$  could be calculated as,

$$\sum_{i=1}^n \frac{\partial V_N(x)}{\partial x_i} F_i(x) = -\phi V^{N-2} \quad (2.28)$$

Where the  $V^2$  is,

$$\sum_{i=1}^n \frac{\partial V_2(x)}{\partial x_i} F_i(x) = -\phi \quad (2.29)$$

Thus, the  $V$  is determined when  $V_N(x)$  and  $V_2(x)$  are known.

### 2.4.5.3 Examples for Zubov's Method

Consider the following p.d.f for illustration purpose [36], [39],

$$\dot{x} = -x + y + x(x^2 + y^2) \quad (2.30)$$

$$\dot{y} = -x - y + y(x^2 + y^2) \quad (2.31)$$

Assuming a function  $\phi(x, y) = 2(x^2 + y^2)$  and substituting in (2.25),

$$\frac{\partial V}{\partial x}(-x + y + x^3 + xy^2) + \frac{\partial V}{\partial y}(-x + y^3 - y + yx^2) = -2(x^2 + y^2)[1 - V] \quad (2.32)$$

Assuming  $V_2(x, y) = ax^2 + bxy + cy^2$  and substituting into (2.32), it shows that  $a = c = 1$ ,  $b = 0$  satisfies the (2.32). Therefore, the required  $V = V_2(x, y) = (x^2 + y^2)$  and the absolute stability boundary is given by equation,  $x^2 + y^2 = 1$ .

A Van Der Pol equation (2.33) is used to demonstrate another example of Zubov's boundaries [38], [39].

$$\ddot{x}_1 + \epsilon(1 - x_1^2)\dot{x}_1 + x_1 = 0 \quad (2.33)$$

Assuming  $\dot{x}_2 = -x_1$ , the Van Der Pol equation reduces to first-order equations as,

$$\dot{x}_1 = x_2 - \epsilon\left(x_1 - \frac{x_1^3}{3}\right) \quad (2.34)$$

$$\dot{x}_2 = -x_1 \quad (2.35)$$

The the recurrence items are calculated using this recursive equation from  $V_2(x_1, x_2)$ ,  $V_3(x_1, x_2)$  to  $V_N(x_1, x_2)$ . For  $N = 3$ , it is shown as,

$$V^3 = V_2 + V_3 \quad (2.36)$$

$$V_2 = d_{20}x_1^2 + d_{21}x_1x_2 + d_{22}x_2^2 \quad (2.37)$$

$$V_3 = d_{30}x_1^3 + d_{31}x_1^2x_2 + d_{32}x_1x_2^2 + d_{33}x_2^3 \quad (2.38)$$

Following the same construction procedures, For  $N = 6$ , it is shown as,

$$V^6 = V_2 + V_3 + V_4 + V_5 + V_6 \quad (2.39)$$

$$V_4 = d_{40}x_1^4 + d_{41}x_1^3x_2 + d_{42}x_1^2x_2^2 + d_{43}x_1x_2^3 + d_{44}x_2^4 \quad (2.40)$$

$$V_5 = d_{50}x_1^5 + d_{51}x_1^4x_2 + d_{52}x_1^3x_2^2 + d_{53}x_1^2x_2^3 + d_{54}x_1x_2^4 + d_{55}x_2^5 \quad (2.41)$$

$$V_6 = d_{60}x_1^6 + d_{61}x_1^5x_2 + d_{62}x_1^4x_2^2 + d_{63}x_1^3x_2^3 + d_{64}x_1^2x_2^4 + d_{65}x_1x_2^5 + d_{66}x_2^6 \quad (2.42)$$

Choosing  $\phi = x_1^2 + x_2^2$ , the partial derivative equation with  $V = V^3$  now could be rewritten as:

$$\frac{\partial V^3}{\partial x_1} \left[ x_2 - \epsilon \left( x_1 - \frac{x_1^3}{3} \right) \right] + \frac{\partial V^3}{\partial x_2} (-x_1) = -(x_1^2 + x_2^2)(1 - V^3) \quad (2.43)$$

Noticing the both sides variables keep the same degree, then get:

$$\frac{\partial V^2}{\partial x_1} (x_2 - \epsilon x_1) + \frac{\partial V^2}{\partial x_2} (-x_1) = -(x_1^2 + x_2^2) \quad (2.44)$$

$$\frac{\partial V^3}{\partial x_1} (x_2 - \epsilon x_1) + \frac{\partial V^3}{\partial x_2} (-x_1) = 0 \quad (2.45)$$

Choosing  $\epsilon = 0.3$ , provides the following results,

$$d_{20} = 1.42 \quad (2.46a)$$

$$d_{21} = -1 \quad (2.46b)$$

$$d_{22} = 1.92 \quad (2.46c)$$

The van der pol equation's time domain trajectory is plotted in Figure 2.17, and the absolute stability boundary is shown in Figure 2.18. The boundary of  $N = 2, 6$  is shown as Figure 2.19.



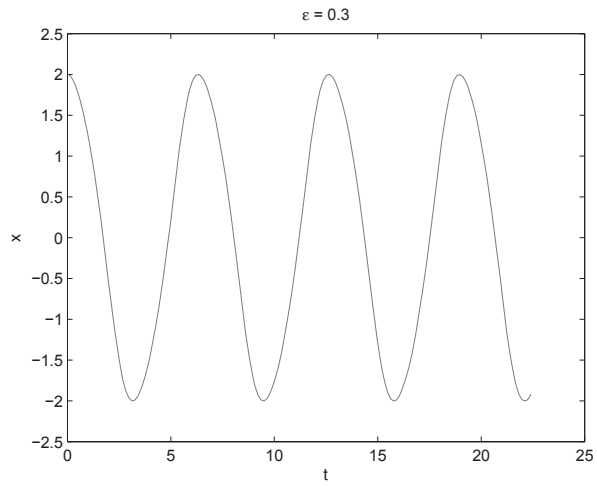


Figure 2.17 Solution of Van Der Pol's Equation in Time Domain.

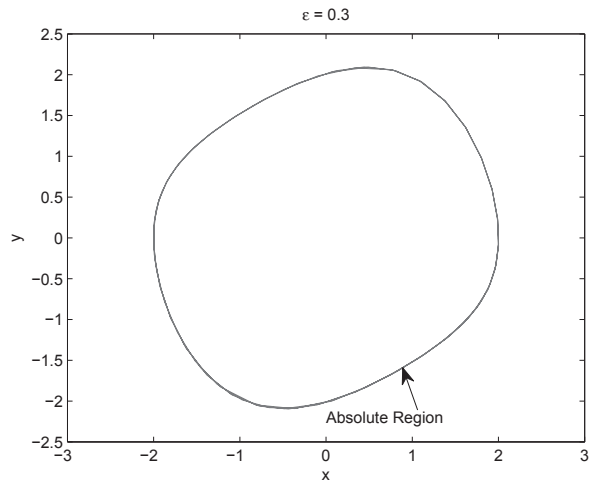


Figure 2.18 Van Der Pol Equation's Stability Boundary in State Plane.

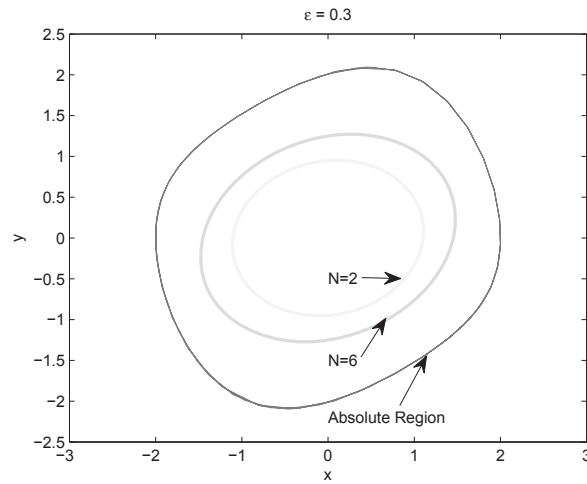


Figure 2.19 Approximation Boundary for Van Der Pol Equation.

## 2.5 Summary

In this Chapter, a brief overview of PMU technology, power system stability, out-of-step protection techniques, and examples on Zubov's boundary based stability studies are discussed, which are the background information needed for this work.

## **CHAPTER 3. Proposed Out-of-step Algorithm Applied to SMIB System**

### **3.1 Introduction**

In this chapter, Zubov's approximation boundary method is applied to power systems for out-of-step detection using numerical simulations. Mathematical formulation to compute the Zubov's stability boundaries for power system is first deduced. A novel out-of-step detection algorithm based on PMU data and Zubov's boundaries are explained. The proposed out-of-step algorithm is applied to Single Machine Infinite Bus system to demonstrate the effectiveness of the proposed algorithm.

### **3.2 Zubov's Stability Boundaries for Power Systems**

As discussed in Section 2.4.6, Zubov's method for stability analysis is based on creating approximate boundaries to differentiate between stable and unstable conditions. Instead of calculating one absolute stability boundary as in Lyapunov's method, Zubov's method uses multiple approximated boundaries. The decision regarding stability could be made faster if the inner boundaries of Zubov's method are used. This property of Zubov's boundaries are very suitable for out-of-step detection in power system, as the system operator needs to know out-of-step condition as fast as possible.

A SMIB system, as shown in Figure 3.1, is considered to explain Zubov's approximation boundary in power systems. The resistance and leakage conductance of transmission lines are neglected for convenience. In Figure 3.1, the equivalent reactance

of two parallel transmission lines is represented by  $x$  and their charging effect is represented by a lumped capacitor placed at machine's terminal with susceptance  $B$ . The machine is generating active power  $P$  and reactive power  $Q$ , with terminal voltage of  $V_t$  and infinite bus voltage of  $V_o$ . In the following mathematical formulations,  $E_q$  is the internal voltage of the generator,  $x'_d$ ,  $x_q$ ,  $T''_{do}$ ,  $T''_{qo}$  and  $x'_q$  are the machine's internal parameters. The machine rotor transient equation, which is referred as swing equation, is given by,

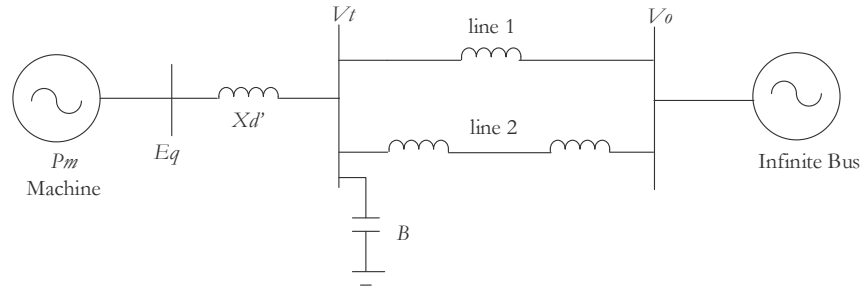


Figure 3.1 Single Machine Infinite Bus System.

$$M \frac{d^2 \delta}{dt^2} + D(\delta) \frac{d\delta}{dt} + P_m \sin \delta + P_s \sin 2\delta = P \quad (3.1)$$

where  $M$  is machine inertia constant,  $\delta$  is machine's power angle,  $D(\delta)$  is the damping factor,  $P_m$  is the mechanical input power, and  $P_s$  is the synchronizing power.

$$D(\delta) = \underbrace{\frac{V_o^2 (x'_d - x''_d) \tau''_{do}}{(x'_d + x)^2}}_a \sin \delta^2 + \underbrace{\frac{V_o^2 (x'_q - x''_q) \tau''_{qo}}{(x'_q + x)^2}}_b \cos \delta^2 \quad (3.2)$$

mechanical input power  $P_m$  is,

$$P_m = \frac{V_o E'_q}{(x'_d + x - x x'_d)} \quad (3.3)$$

similarly, synchronizing power coefficients  $P_s$  is,

$$P_s = \frac{V_o^2 (x'_d - x_q)}{2(x'_d + x - x x'_d B) (x_q + x - x x_q)} \quad (3.4)$$

The swing equation in (3.1) can be normalized by defining  $\tau = t\sqrt{\frac{P_m}{M}}$ ,

$$\frac{d^2\delta}{d\tau^2} + D'(\delta) \frac{d\delta}{d\tau} = P' - \sin \delta - P'_s \sin 2\delta \quad (3.5)$$

where,

$$D'(\delta) = D(\delta) \sqrt{\frac{1}{MP_m}}, \quad P'_s = \frac{P_s}{P'_m}, \quad P' = \frac{P}{P'_m}$$

At the system's stable equilibrium point (SEP) power angle and its derivatives are,

$$\delta = \delta_o \quad (3.6a)$$

$$\dot{\delta} = \ddot{\delta} = 0 \quad (3.6b)$$

where,  $\delta_o$  is the initial power angle. The system of equations are transferred to a new reference by assuming  $\delta = \delta_o + \delta'$ . Thus, equation (3.5) becomes,

$$\frac{d^2\delta'}{d\tau^2} + D'(\delta') \frac{d\delta'}{d\tau} + R(\delta') = 0 \quad (3.7)$$

where  $R(\delta') = P' - \sin(\delta_o + \delta') - P'_s \sin(2\delta_o + 2\delta')$ .

In equation (3.7),  $D'(\delta')$  could be simplified from (3.2),

$$D'(\delta') = D_o + \sum_{n=1}^{\infty} \left\{ \frac{2^n}{n!} \left( \frac{a-b}{2} \right) \cos \left( 2\delta_o + \frac{n\pi}{2} \right) \right\} \delta'^n \quad (3.8)$$

where  $D_o$  is calculated as,

$$D_o = \frac{a+b}{2} + \frac{a-b}{2} \cos(2\delta_o)$$

$R(\delta')$  could be simplified from (3.3) and (3.4) as,

$$R'(\delta') = \sum_{n=1}^{\infty} \left\{ \left\{ \cos \left( \delta_o + \frac{(n-1)\pi}{2} \right) + 2^n P'_s \cos \left( 2\delta_o + \frac{(n-1)\pi}{2} \right) \right\} / n! \right\} \delta'^n \quad (3.9)$$

Further,  $D'(\delta')$  could be written in power series as,

$$D(\delta') = D_o + D_1 \delta' + D_2 \delta'^2 + D_3 \delta'^3 + \dots \quad (3.10)$$

and similarly,  $R'(\delta')$  in power series is,

$$R(\delta') = R_1 \delta' + R_2 \delta'^2 + R_3 \delta'^3 + \dots \quad (3.11)$$

Let us define state variables as  $\dot{\delta}' = \omega'$ , where  $\omega'$  represents speed of the generator. Then (3.7) could be modified into two first order differential equations as,

$$\dot{\delta}' = \omega' \quad (3.12)$$

$$\dot{\omega}' = -D(\delta') \omega' - R(\delta') \quad (3.13)$$

The Zubov's method of solving the partial differential equation is discussed in Section 2.4.6, which in  $\delta$  domain can be written as,

$$\left\{ \nabla U(\delta', \omega') \right\}^T f_i(\delta', \omega') = -\phi(\delta', \omega') \left\{ 1 - U(\delta', \omega') \right\} \quad (3.14)$$

recurrence relation is modified with these two variables,

$$U = U^N = \sum_{i=2}^N v_i(\delta', \omega') = v_2(\delta', \omega') + v_3(\delta', \omega') + \dots + v_N(\delta', \omega') = \sum_{i=2}^N \sum_{k=2}^i d_{ik} \delta'^{i-k} \omega'^k \quad (3.15)$$

where  $v_i(\delta', \omega')$  is homogeneous polynomial of degree  $i$ . Expanding  $v_i(\delta', \omega')$  for  $i = 2, 3, 4, 5$ ,

$$v_2(\delta', \omega') : \nabla v_2 f_i(\delta', \omega') = -\phi \quad (3.16)$$

$$v_3(\delta', \omega') : \nabla v_2 f_i(\delta', \omega') + \nabla v_3 f_i(\delta', \omega') = 0 \quad (3.17)$$

$$v_4(\delta', \omega') : \nabla v_2 f_i(\delta', \omega') + \nabla v_3 f_i(\delta', \omega') + \nabla v_4 f_i(\delta', \omega') = -\phi U^2 \quad (3.18)$$

$$v_5(\delta', \omega') : \nabla v_2 f_i(\delta', \omega') + \nabla v_3 f_i(\delta', \omega') + \nabla v_4 f_i(\delta', \omega') + \nabla v_5 f_i(\delta', \omega') = -\phi U^3 \quad (3.19)$$

The polynomial  $U$  in (3.14) for  $N = 2$ ,

$$d_{20} \delta'^2 + d_{21} \delta' \omega' + d_{22} \omega'^2 = C_2 \quad (3.20)$$

For  $N = 3$ ,

$$d_{30} \delta'^3 + d_{31} \delta'^2 \omega' + d_{32} \delta' \omega'^2 + d_{33} \omega'^3 = C_3 \quad (3.21)$$

For  $N = 4$ ,

$$d_{40} \delta'^4 + d_{41} \delta'^3 \omega' + d_{42} \delta'^2 \omega'^2 + d_{43} \delta' \omega'^3 + d_{44} \omega'^4 = C_4 \quad (3.22)$$

For  $N = 5$ ,

$$d_{50} \delta'^5 + d_{51} \delta'^4 \omega' + d_{52} \delta'^3 \omega'^2 + d_{53} \delta'^2 \omega'^3 + d_{54} \delta' \omega'^4 + d_{55} \omega'^5 = C_5 \quad (3.23)$$

In Above equations,  $\phi$  is an arbitrary positive-definite function, which is defined as  $\phi(\delta', \omega') = \alpha \delta'^2 + \beta \omega'^2$ , where  $\alpha + \beta < 1$ .  $U(\delta', \omega') = C$  represents the Zubov's stability boundaries. The constants  $C$ , i. e.,  $C_2, C_3, C_4, C_5$ , are determined from system pre-fault  $\delta_o$  and  $\omega_o$  values. Equations from (3.1) to (3.15) provide overall construction of Zubov's method for power system stability studies.

### 3.3 Proposed Out-of-step Detection Algorithm

The proposed out-of-step detection method based on Zubov's boundaries and PMU data are explained with an example of SMIB system as shown in Figure 3.2. In this SMIB system, two PMU devices are assumed to be installed at generator bus and infinite buse for measurements. PMUs' data transmission error and delay are not considered as PMUs are treated as ideal devices. PMU sampling rate for this work is assumed at 60 samples per second.

Based on (3.20-3.23), different boundaries are created in  $\delta - \omega$  domain, with  $N = 2, 4, 6, 8, 10$ , and more boundaries if needed. The flowchart of the proposed algorithm is shown in Figure 3.3, with different boundaries referred as B1, B2, B3, B4, B5, and B6 respectively. Boundary B6 represents the out-of-step boundary, which covers the largest area of all the Zubov's boundaries B1-B5. After the boundaries are created, PMU data is used to obtain the initial operating condition of the power system, i. e.,  $\delta_o, \omega_o$ , then the boundaries are shifted from  $(0, 0)$  to  $(\delta_o, \omega_o)$  to account for the axis shift in reference in

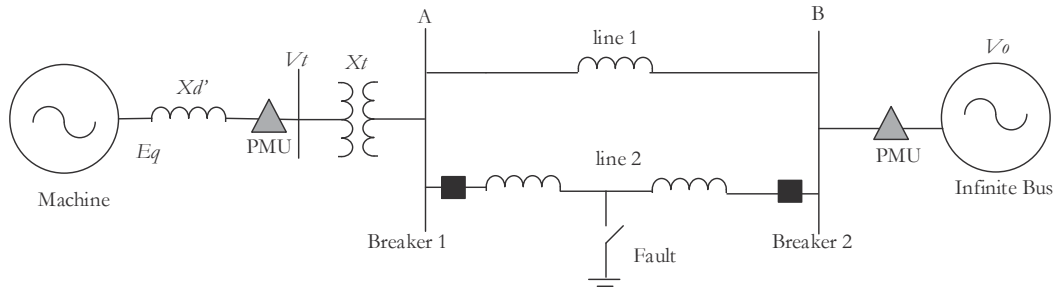


Figure 3.2 SMIB System Set-up for Out-of-step Detection.

(3.7). During the transients, continuous PMU data are obtained and used to plot trajectories on  $\delta$ - $\omega$  plane.

In this proposed method, detection is carried out into two steps: out-of-step detection and stable swing detection. For out-of-step detection, the judgment is straightforward as  $\delta$ - $\omega$  trajectory passes through the outermost boundary B6. For stable swing detection, the decision involves sequence of time delays (Delay 1-Delay 5) corresponding to each boundary the trajectory crosses. For stable swing cases, the trajectory will always settle at a new steady state condition. The separation of stable swing with different boundaries could provide benefits for the operators to think ahead for potential emergency control, which might prevent cascading failure that leads to blackout incidents. The decision time that the proposed method takes for stable swing depends on the delay parameters (Delay 1- Delay 5) shown in Figure 3.3.

### 3.4 SMIB Case Studies

The SMIB system as shown in Figure 3.2 is also used for the case studies. The parameters of SMIB system are listed in Appendix B [34]. The proposed algorithm for out-of-step detection needs three specific settings, which are discussed next.



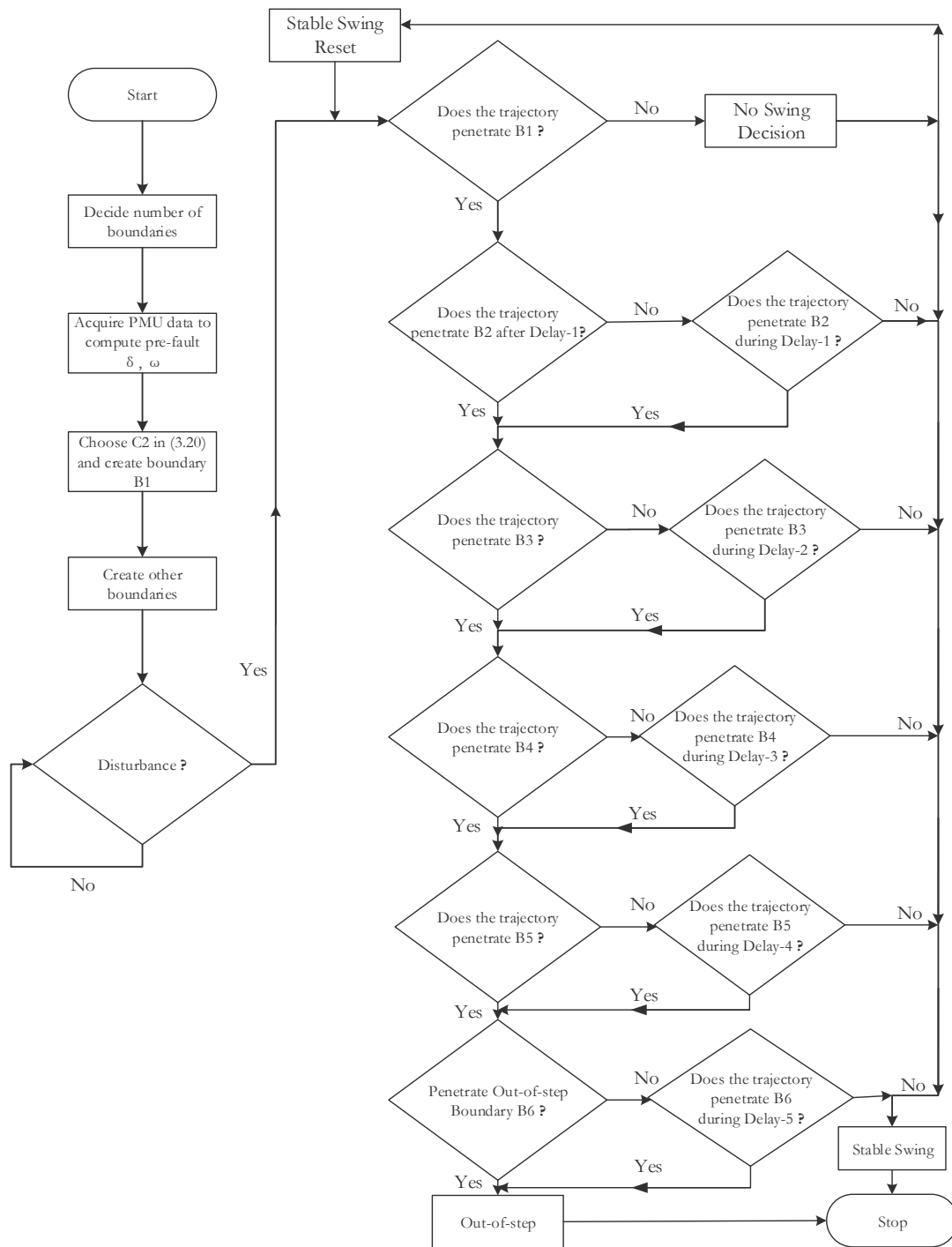


Figure 3.3 Flowchart of Zubov's Approximation Method for Out-of-step Detection.

First, the Zubov's boundaries should be increased gradually with the outermost out-of-step boundary having the largest area coverage. Thus, the constant values of  $C$  in (3.20)-(3.23) are set at 0.34, 1.57, 3.14, 6.28, 9.42, and 10 radian, respectively. The Zubov's boundaries thus created are shown in Figure 3.4.

Another settings are for boundary's time delay. If the time delay are set in decreasing orders, then severe swing (i. e., higher swing frequency) can be detected faster. In this simulation case studies, the delay values Delay 1-Delay 5 are chosen as 2, 1.5, 1.0, 0.5, 0.2 s, respectively. The first delay setting, i. e., 2 s is taken from commercial relay manual, and other five delays are decreased gradually [18]- [53].

The Zubov's boundaries, shown in Figure 3.5, is based on equation (3.20)-(3.23), where the reference is shifted to  $(0, 0)$  in equation (3.7). To account for this change in reference, the Zubov's boundary used in this work is shifted back to the original reference of  $(\delta_o, \omega_o)$ . The pre-fault  $\delta_o$  and  $\omega_o$  are obtained from the two PMU devices installed at the SMIB system. The case studies for SMIB system are carried out in MATLAB.

### 3.4.1 Stable Swing Simulations

Six different cases are listed next to demonstrate the performance of the proposed method in detecting stable swing for SMIB system. A three-phase to ground fault is applied at the middle of the transmission line 2. The fault duration time is first set at 0.048 s for pre-fault power angle  $\delta_o = 20^\circ$  and frequency  $\omega_o = 60$  Hz, which is referred here as Case-1. In this case, the proposed method makes decision as stable swing at 2.024 s. The trajectories on  $\delta$ - $\omega$  and  $\delta$ - $t$  domains are shown in Figure 3.6.

Figure 3.7 shows trajectories of another case, Case-2, where the fault duration time is increased to 0.096 s from Case-1. The pre-fault power angle is same as  $20^\circ$ . The proposed algorithm takes 1.508 s to detect the swing as stable swing. The swing trajectory only crossed boundary B1 and B2.

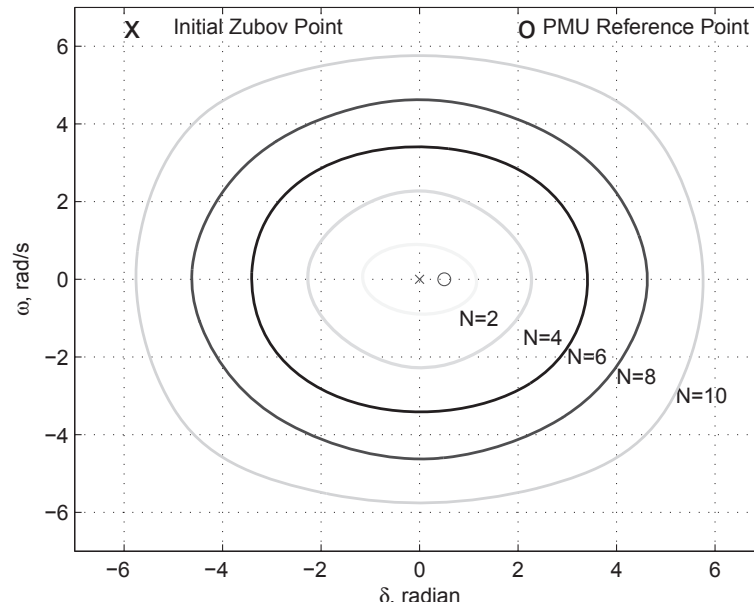


Figure 3.4 Zobov's Boundaries at Original Reference (0, 0).

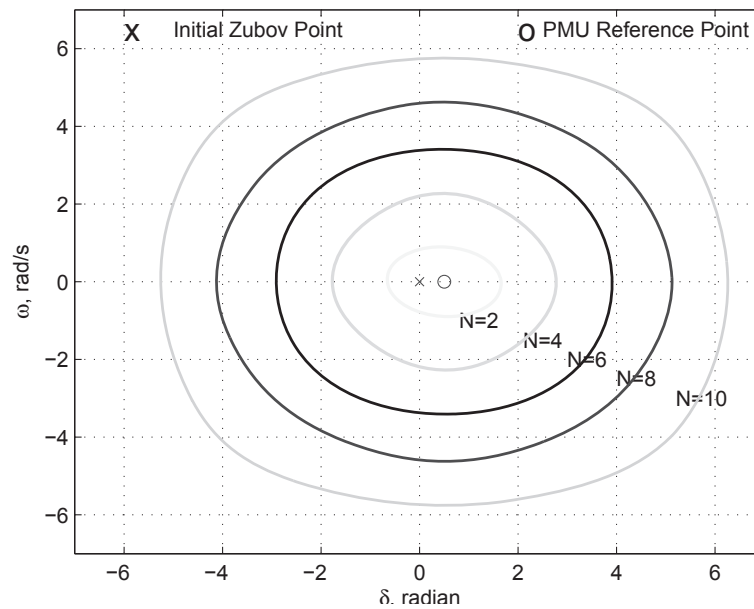


Figure 3.5 Zobov's Boundaries Shifted to a New Reference  $(\delta_o, \omega_o)$

In next simulation, the fault duration time is increased to 0.144 s, referred here as Case-3. The decision made by the proposed algorithm is stable swing and the decision is made at 1.212 s. The swing trajectory crosses boundaries B1 through B4, which is shown in Figure 3.8.

The fault time is further increased to 0.328 s (Case-4), the decision is made at 0.152 s as stable swing. The  $\delta-t$  and  $\delta-\omega$  trajectories for this case are shown in Figure 3.9.

In Case-5, the pre-fault power angle is increased to  $30^\circ$  and the fault duration time is set at 0.192 s. The proposed algorithm makes the decision at 0.68 s as a stable swing. The trajectory crosses all boundaries except out-of-step boundary. The trajectories in  $\delta-t$  and  $\delta-\omega$  domain are shown in Figure 3.10.

In Case-6, pre-fault power angle is kept at  $30^\circ$ , and fault duration time is increased to 0.288 s. The trajectories for this case are shown in Figure 3.11. The decision is made as stable swing at 0.208 s.

The summary of six case studies discussed above is presented in Table 3.1. Based on the case studies, it is clear that the swing is detected earlier if the swing is severe. Severe swings are obtained by increasing the fault duration time or increasing the pre-fault power angle. Thus, the fault duration for Case-2 is detected earlier compared to Case-1 as swing in Case-2 is more severe. Similarly for power angle of  $30^\circ$ , in Case 4 and 5, the swing is severe for Case-5 as the fault duration time is larger, thus the proposed algorithm takes less time to make the decision in Case-5 compared to Case-4.

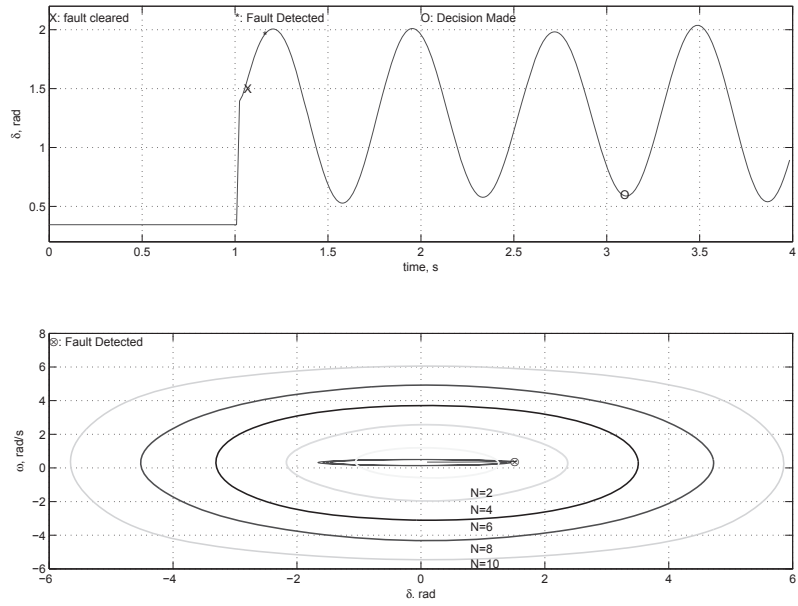


Figure 3.6 Stable Swing Case for Pre-fault Angle of  $20^\circ$ , Fault Duration Time 0.048 s.

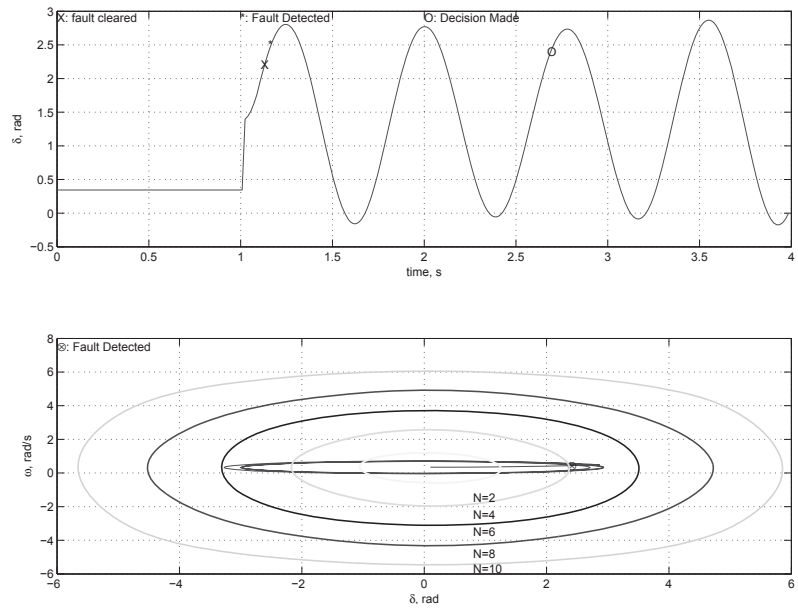


Figure 3.7 Stable Swing Case for Pre-fault Angle of  $20^\circ$ , Fault Duration Time 0.096 s.

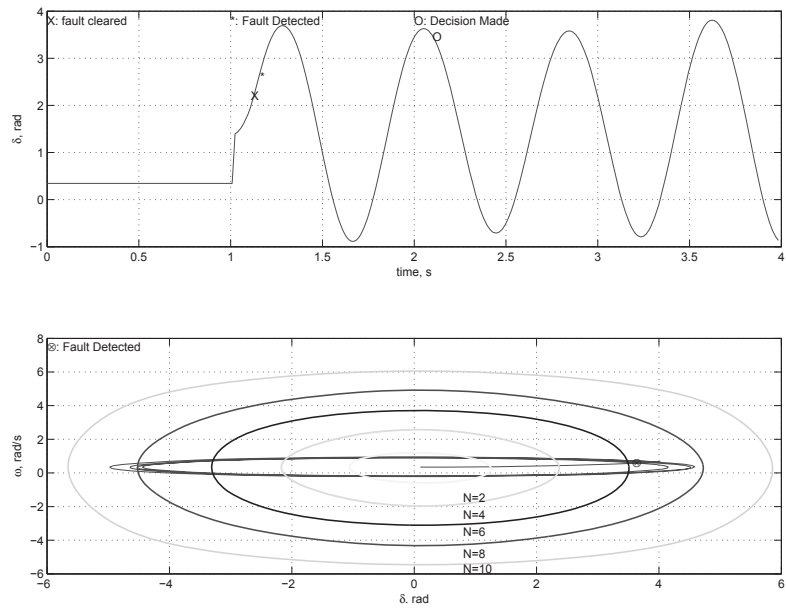


Figure 3.8 Stable Swing Case for Pre-fault Angle of  $20^\circ$ , Fault Duration Time 0.144 s.

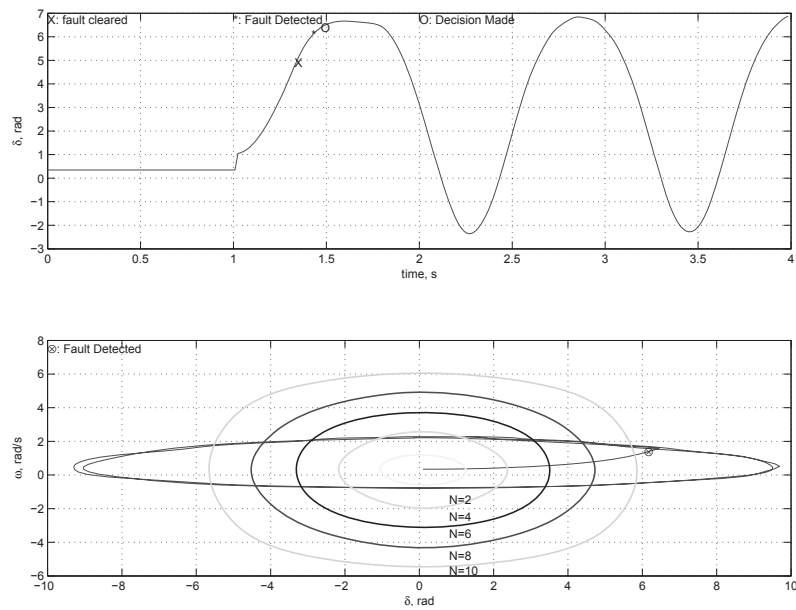


Figure 3.9 Stable Swing Case for Pre-fault Angle of  $20^\circ$ , Fault Duration Time 0.328 s.

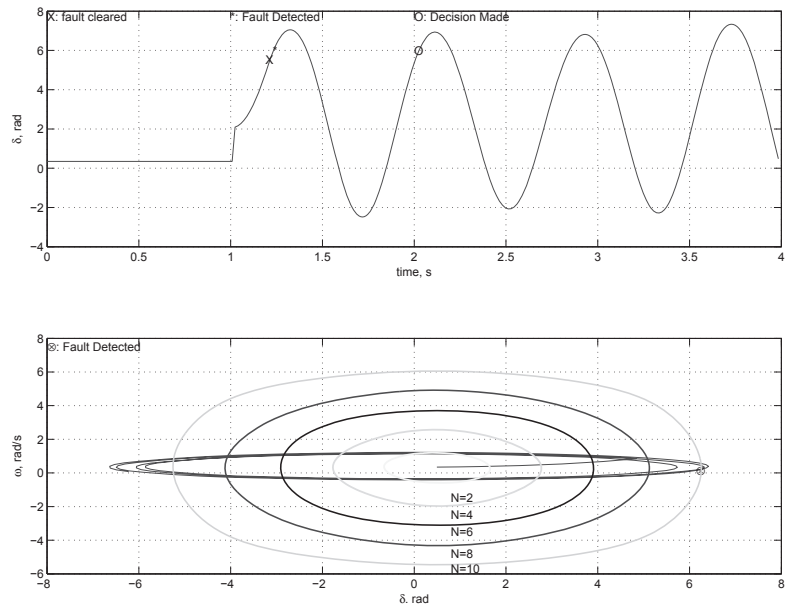


Figure 3.10 Stable Swing Case for Pre-fault Angle of  $30^\circ$ , Fault Duration Time 0.192 s.

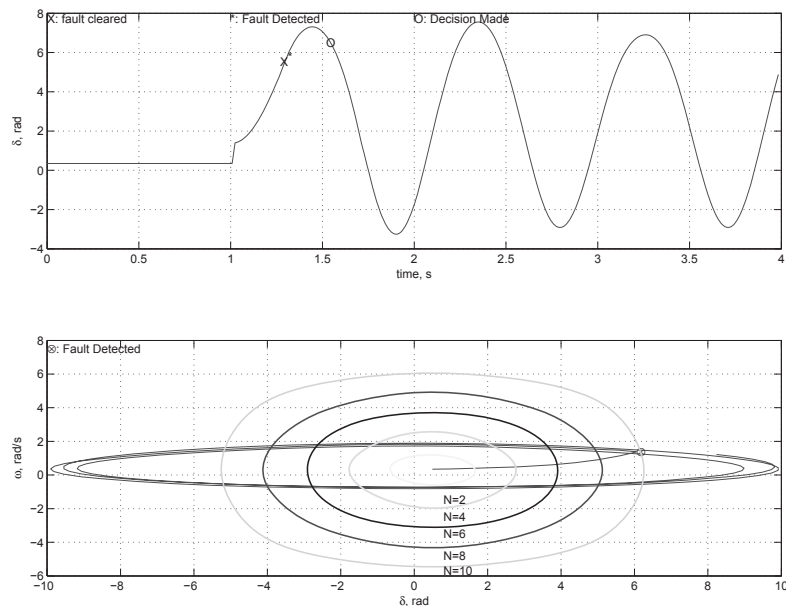


Figure 3.11 Stable Swing Case for Pre-fault Angle of  $30^\circ$ , Fault Duration Time 0.288 s.

Table 3.1 Performance of the Proposed Method in Stable Swing Detection in SMIB.

<b>case</b>	<b>1</b>	<b>2</b>	<b>3</b>	<b>4</b>	<b>5</b>	<b>6</b>
Pre-fault Power Angle	20°	20°	20°	20°	30°	30°
Fault Duration Cycles	3	6	9	20.5	12	18
Fault Duration Time (s)	0.048	0.096	0.144	0.328	0.192	0.288
Penetrated Boundaries	B1	B2	B4	B5	B5	B5
Decision Time, s	2.024	1.508	1.212	0.152	0.680	0.208
(After Fault Cleared)	After	After	After	After	After	After
Decision	Stable	Stable	Stable	Stable	Stable	Stable

### 3.4.2 Out-of-step Cases

Five out-of-step cases are simulated to demonstrate the effectiveness of the proposed algorithm. These out-of-step simulations are developed to verify the proposed method's robustness in severe situations. Starting from fault duration time of 0.384 s, it is then increased up to 0.576 s. Comparison is done based on the simulations carried out in the different fault duration time for pre-fault  $\delta = 20^0$  or  $\delta = 30^0$ . Notice that for out-of-step detection, there is no time delay like in stable swing simulations.

Case-7 represent first out-of-step case with fault duration time of 0.336 s, and pre-fault power angle of  $20^0$ . In fact, Case-7 is obtained by increasing the fault duration time from Case-4. The decision is made as out-of-step with 0.52 s after the fault is cleared. The trajectories  $(\delta-t, \delta-\omega)$  for this case are shown in Figure 3.12.

In case-8, fault duration time is increased to 0.352 s, keeping the power angle constant at  $20^0$ . Figure 3.13 shows the trajectories for this case. The proposed algorithm takes 0.344 s to make the decision as out-of-step, after the fault cleared time.

For Case-9, fault duration time is further increased to 0.384 s. The trajectories in



both  $\delta-t$  and  $\delta-\omega$  domain are shown in Figure 3.14. The decision is made as out-of-step with 0.232 s similarly like Case-7 and Case-8, after the fault cleared time.

In Case-10, the pre-fault power angle is increased to  $30^0$  and the fault duration time is set at 0.48 s. The proposed algorithm detects the power swing as out-of-step condition with 0.072 s just 4.5 cycles after the fault is cleared. Trajectories of  $\delta-t$  and  $\omega-\delta$  domain are shown in Figure 3.15.

The fault duration time increased to 0.576 s from Case-10, referred here as Case-11. The decision is made as out-of-step swing with 0.024 s earlier than the fault actually cleared. Note that the decision in this case is made before the fault is cleared due to the severest fault disturbance. The trajectories' plots are shown in Figure 3.16.

The summary of out-of-step case studies are shown in Table 3.2. Notice that the decision time for out-of-step is faster for sever swings, as similar observation was made in stable swing cases. The out-of-step condition is made more severe in the simulation by increasing the fault duration time. Thus, the decision time for Case-8 is faster compared to Case-7, since the out-of-step swing in Case-8 is more severe as it is created by applying a longer fault duration.

The out-of-step decision time lies on the out-of-step boundary setting, i. e., the Zubov's boundary constant  $C_6$ . For sensitive analysis studies, the out-of-step condition in case-11 is. Two new out-of-step boundaries are created by adjusting boundary radius by  $+ - 0.5$ , as shown in Figure 3.17. The decisions time based on three different out-of-step boundaries are 0.048 s (during fault), 0.024 s (during fault), and 0.016 (after fault cleared), respectively. Based on this study, it shows that out-of-step decision time depend on the settings of the boundaries.

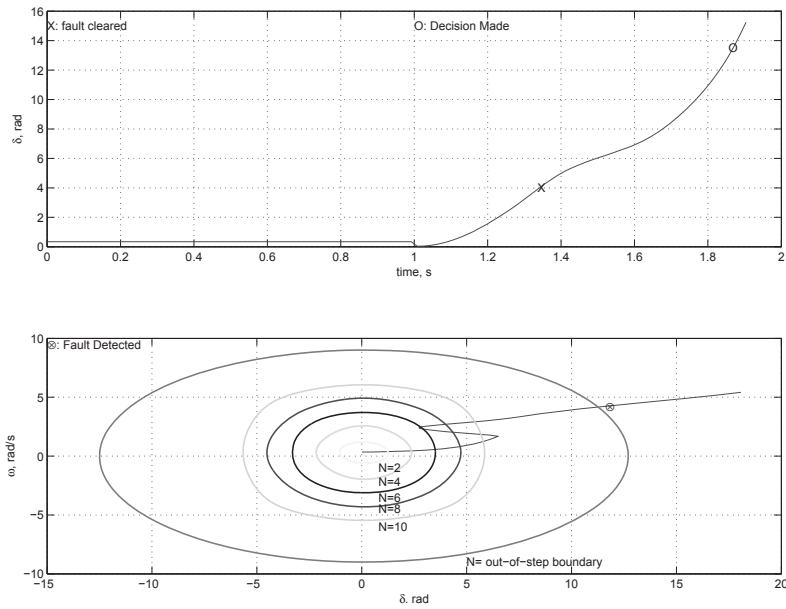


Figure 3.12 Out-of-step Case for Pre-fault Angle of  $20^{\circ}$ , Fault Duration Time of 0.336 s.

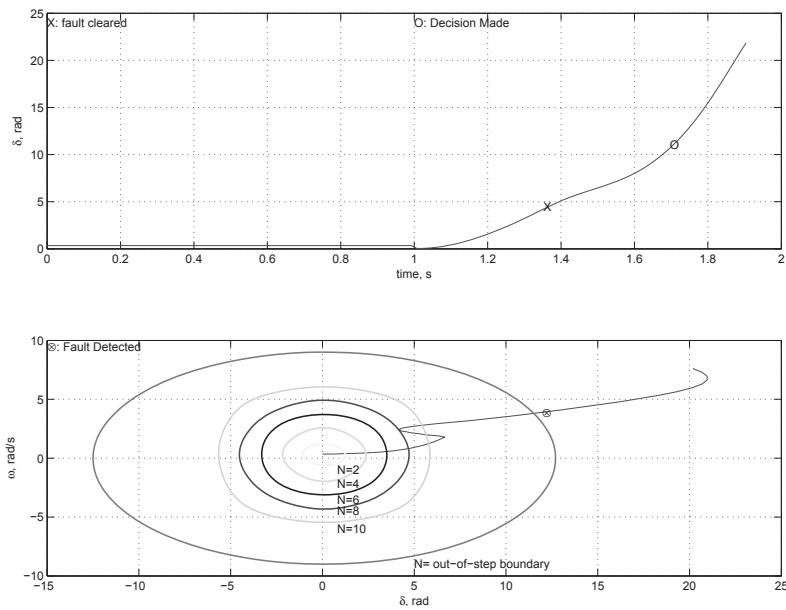


Figure 3.13 Out-of-step Case for Pre-fault Angle of  $20^{\circ}$ , Fault Duration Time of 0.352 s.

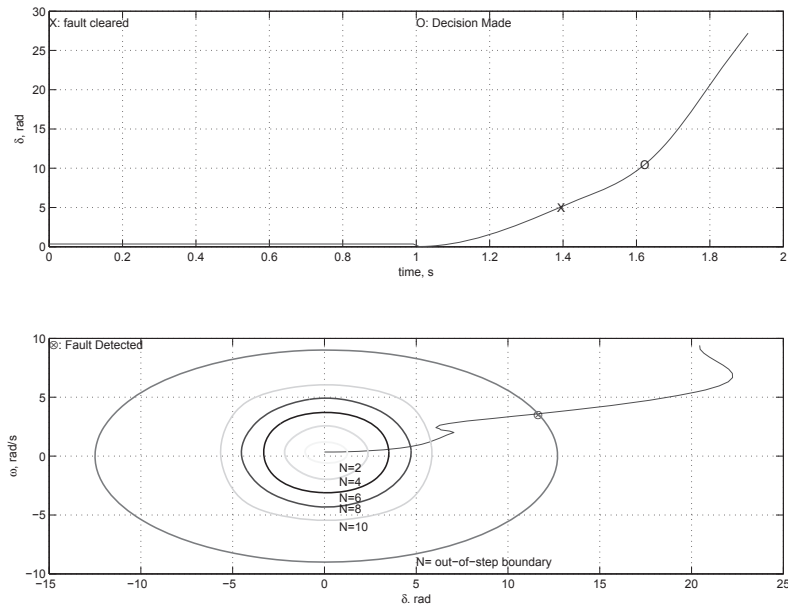


Figure 3.14 Out-of-step Case for Pre-fault Angle of  $20^0$ , Fault Duration Time of 0.384 s.

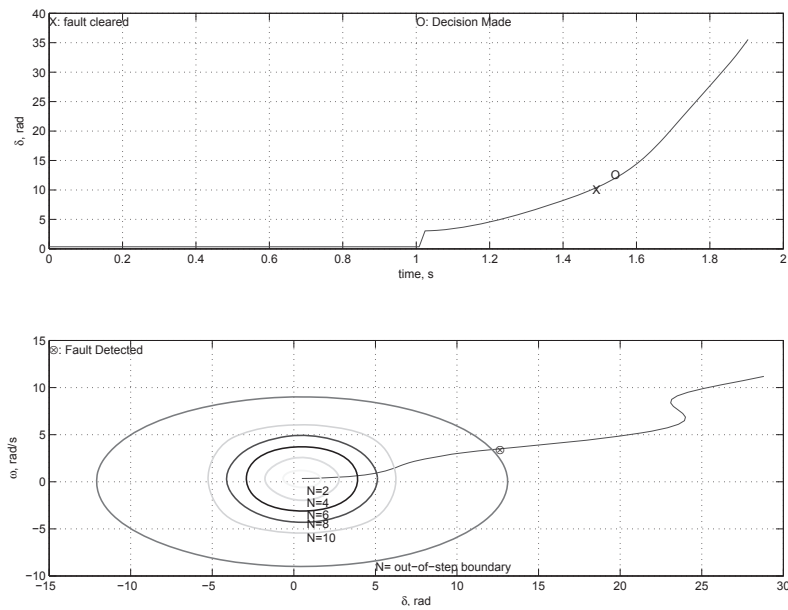


Figure 3.15 Out-of-step Case for Pre-fault Angle of  $30^0$ , Fault Duration Time of 0.480 s.

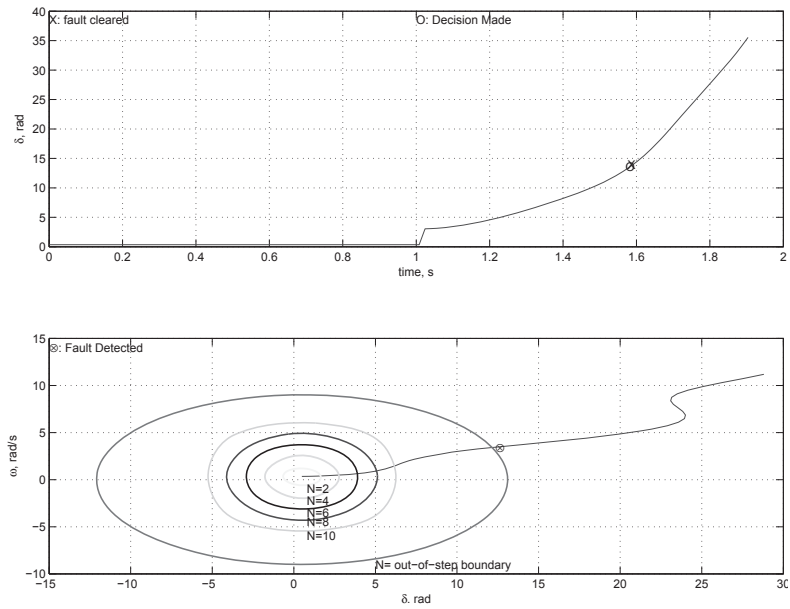


Figure 3.16 Out-of-step Case for Pre-fault Angle of  $30^0$ , Fault Duration Time of 0.576 s.

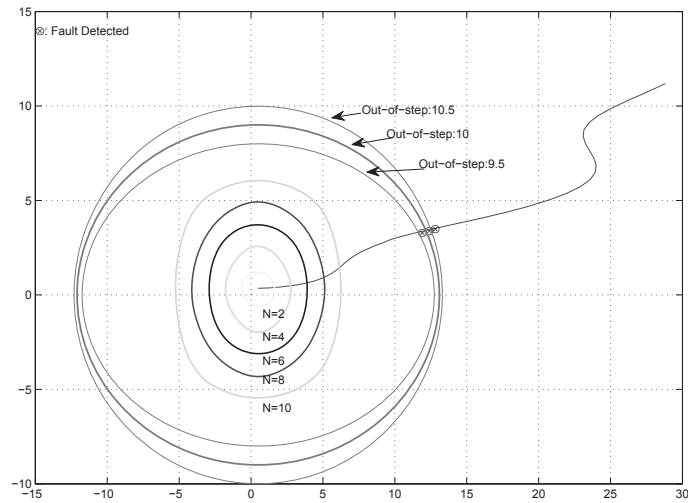


Figure 3.17 Out-of-step Case for Sensitivity Analysis with Fault Duration Time 0.576 s.

Table 3.2 Performance of the Proposed Method in Out-of-step Detection in SMIB.

<b>case</b>	<b>7</b>	<b>8</b>	<b>9</b>	<b>10</b>	<b>11</b>
Pre-fault Power Angle	20°	20°	20°	30°	30°
Fault Duration Cycle	21	22	24	30	36
Fault Duration Time,s	0.336	0.352	0.384	0.48	0.576
Penetrated Boundaries	B6	B6	B6	B6	B6
Decision Time,s	0.52	0.344	0.232	0.072	0.024
(After Fault Cleared)	After	After	After	After	<b>Before</b>
Decision	Out-of-step	Out-of-step	Out-of-step	Out-of-step	Out-of-step

### 3.5 Summary

In this chapter, a proposed out-of-step detection algorithm is introduced using general flowchart based on the Zubov's boundary method. The general boundary parameters and time delay settings are elaborated and PMU data are used to obtain the pre-fault operating condition and trajectory during boundaries. A specific SMIB model is simulated for stable swing and out-of-step cases to test the proposed algorithm. These case studies demonstrate that the proposed algorithm based on Zubov's method and PMU data is able to differentiate between out-of-step and stable swing. Based on the results, it is seen that the decision time is faster if the swing is severe.

## **CHAPTER 4. Proposed Out-of-step Algorithm Applied to Multi-machine Systems**

### **4.1 Introduction**

In this chapter, the proposed out-of-step detection algorithm based on Zubov's stability boundary method is applied to multi-machine power systems. First, a general procedure of out-of-step detection is explained with a flowchart. The proposed algorithm is applied to IEEE 3-machine 9-bus system and IEEE 10-machine 39-bus system to test the performance in multi-machine power systems. Various disturbances are created by changing the fault location and fault duration in each multi-machine system to generate stable and out-of-step swings. Cascading disturbances in both systems are also examined for the robustness of the proposed algorithm.

### **4.2 Proposed Out-of-step Detection Algorithm for Multi-machine Systems**

A general procedure to apply the proposed out-of-step algorithm in multi-machine power systems is shown in Figure 4.1. The procedure is similar to what discussed in Section 3.3 for SMIB system. Here, the Zubov's boundaries are created for all generators. Thus, the settings required are Zubov's boundaries for each generator, corresponding time delays, and the initial operating point of each generators ( $\delta_o$  and  $\omega_o$ ). The initial operating points are directly obtained from PMU devices installed in the multi-system.

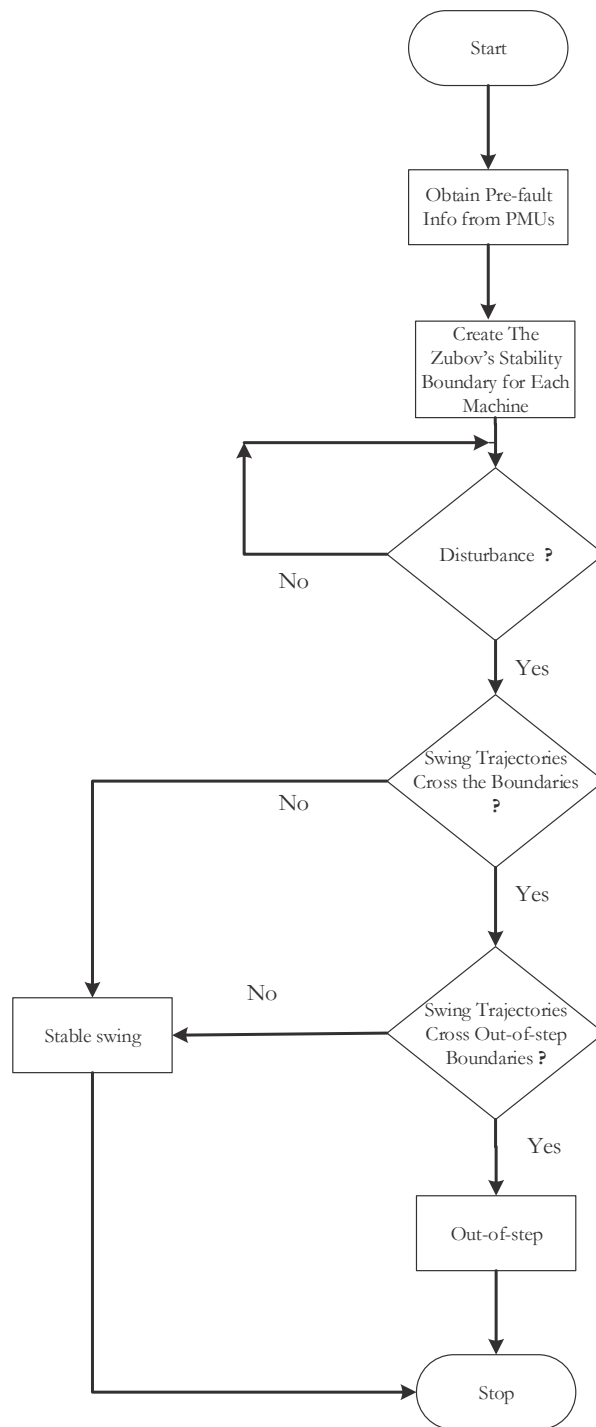


Figure 4.1 Flowchart of the Proposed Out-of-step Detection Algorithm in Multi-machine Power Systems.

### 4.3 IEEE 3-machine 9-bus System Case Studies

IEEE 3-machine 9-bus system is modeled in Powerworld [50]- [51]. The system configuration is shown in Figure 4.2 and its parameters are listed in Appendix C. It is assumed that each generator has a PMU to for measurements. The original system configuration of the IEEE 3-machine 9-bus system is modified by adding double transmission line between nodes 5-7 and 6-9. This modification is done to achieve simulation case studies considering multiple sequential disturbances.

The coefficient  $C_1$  required to obtain the boundary  $B_1$  for each generator is computed from corresponding pre-fault power angle. Larger the power angle of the generator, smaller the boundary was chosen. The remaining parameters  $C_2-C_5$  required to obtain other boundaries of  $B_2-B_5$  follow the same procedure as in SMIB case studies as discussed in Section 3.4. The boundaries of generators are shifted to new reference  $(\delta_o, \omega_o)$  corresponding to each generator's pre-fault operating condition.



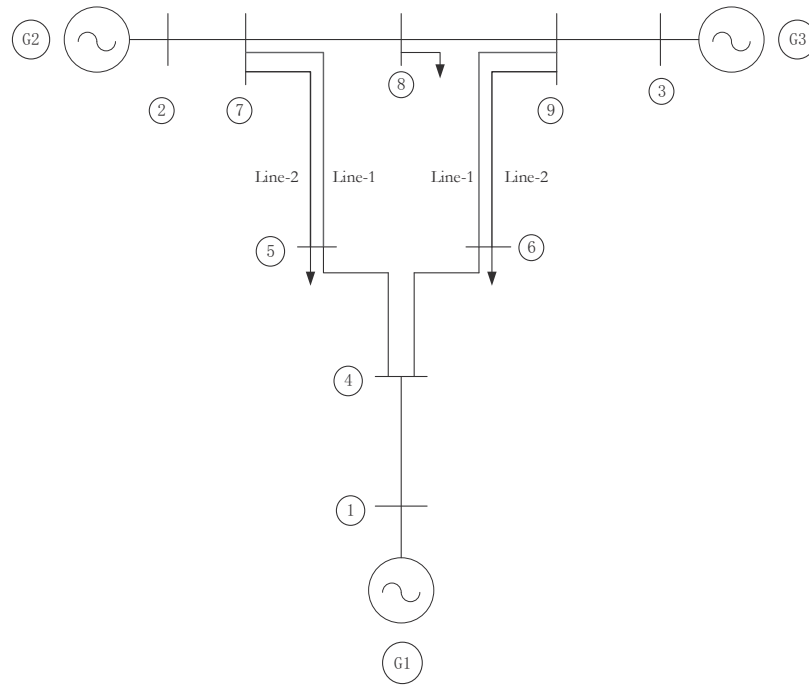


Figure 4.2 IEEE 3-machine 9-bus System.

For the IEEE 3-machine 9-bus system, total of 14 case studies are carried out. Two of the case studies include cascading disturbances. The pre-fault power angles of the three generators are set at  $3.58^\circ$  (for G1),  $63.54^\circ$  (for G2),  $64.68^\circ$  (for G3), respectively. The pre-fault frequency of the system is 60 Hz.

A three-phase fault is applied at the middle of the one of the transmission line between nodes 6-9 (Case-1). The fault duration time is set at 0.1 s. The decision is made as stable swing, with the decision time of G2 and G3 are 2.94 s and 2.052 s respectively. In this case the swing trajectory does not cross the boundaries for G1. The plot of  $\delta-t$  and  $\omega-t$  trajectories are shown in Figure 4.3, while the trajectories on  $\delta-\omega$  plane are shown in Figure 4.4. In Case-2, the fault duration time is increased to 0.45 s and the decision made is out-of-step. The decision time is 0.566 s (for G1), 0.502 s (for G2), and 0.438 s (for G3).

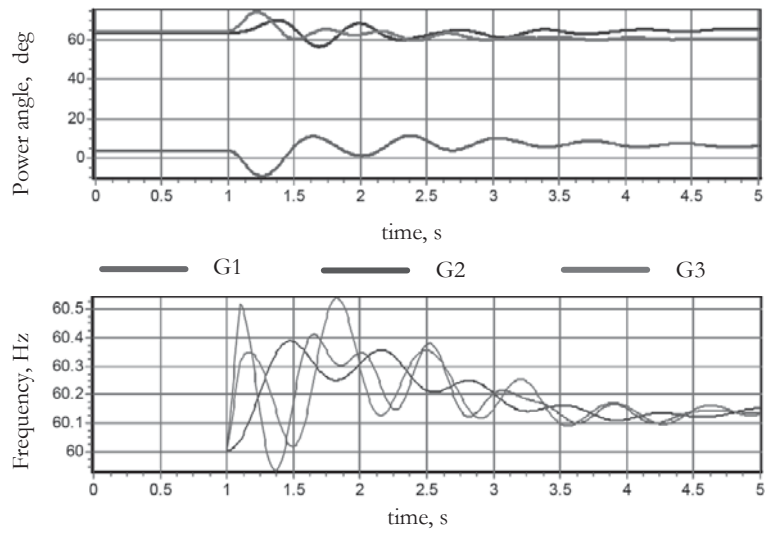


Figure 4.3  $\delta$ - $t$  and  $\omega$ - $t$  Curves for Stable Swing Fault Duration Time of 0.1 s Between Nodes 6-9.

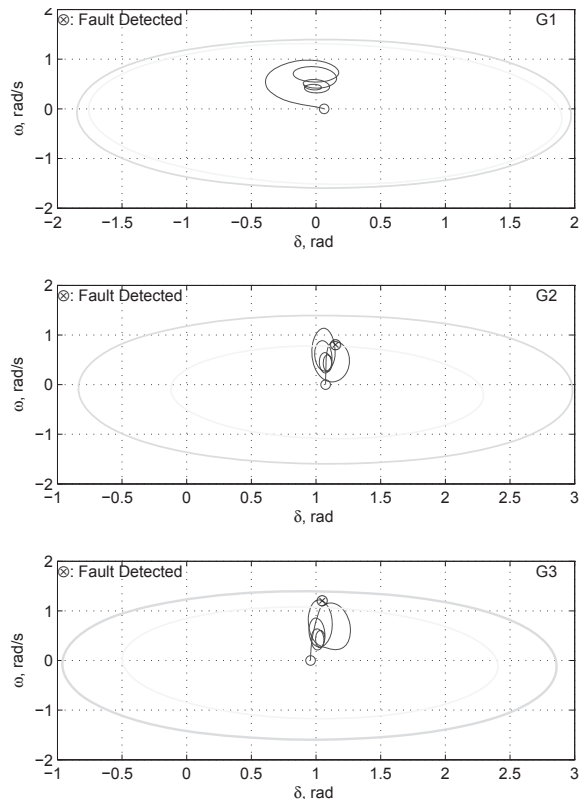


Figure 4.4  $\delta$ - $\omega$  Curves for Stable Swing Fault Duration Time of 0.1 s Between Nodes 6-9.

The plots corresponding to this case study are provided in Figure 4.5 and 4.6.

In Case-3 and Case-4, the fault location is changed to the middle of the transmission line between nodes 5-7. The fault duration time is set at 0.1 s and 0.45 s, respectively, to create stable and out-of-step swings. The swing trajectories of stable case are shown in Figure 4.7 and 4.8. The decision time for this case is 1.996 s and 2.092 s for G2 and G3, respectively. The swing trajectory in this case does not cross any boundary for G1. For the out-of-step case, the decision is made at 0.518 s for G1, 0.350 s for G2, and 0.510 s for G3, respectively. Figure 4.9 and 4.10 show the swing trajectories for this out-of-step case.

In other case studies (Case-5 to Case-12), the fault duration time is either kept at 0.1 s or 0.45 s to create stable or out-of-step condition. However, the fault location is changed as the fault is applied at the middle of nodes 7-8 for Case-5 and Case-6, nodes 8-9 for Case-7 and Case-8, nodes 4-5 for Case-9 and Case-10, and nodes 4-6 for Case-11 and Case-12, respectively.

The trajectory plots for Case-5, which is stable case are shown in the Figure 4.11 and 4.12. The trajectories for Case-6, which is out-of-step swing, are shown in Figure 4.13 and 4.14. Similarly, for other cases studies the trajectory plots are shown in Figure 4.15 to Figure 4.26. The decision time required by the proposed algorithm for above case studies are listed in Table 4.1.

Two cascading disturbances are also created to demonstrate the robustness of the proposed algorithm. In Case-13, first a three-phase line to ground fault is applied at the middle of the one of the transmission line between nodes 5-7, with fault duration of 0.1 s. After this disturbance, a second disturbance is created by applying a similar fault at the middle of the second transmission line between nodes 5-7 with fault duration of 0.1 s. This cascading disturbance leads to stable swing, and three generators' decision time are 0.988 s, 0.588 s, and 1.46 s respectively. These decisions demonstrate that the proposed

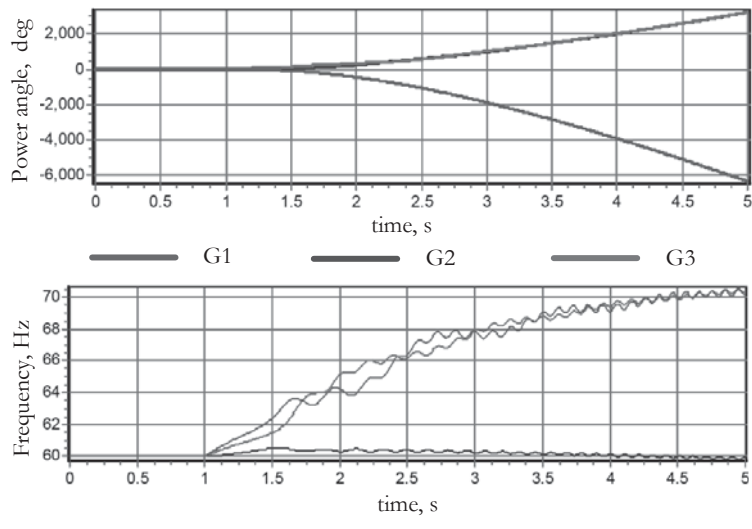


Figure 4.5  $\delta$ -t and  $\omega$ -t Curves for Out-of-step Fault Duration Time of 0.45 s Between Nodes 6-9.

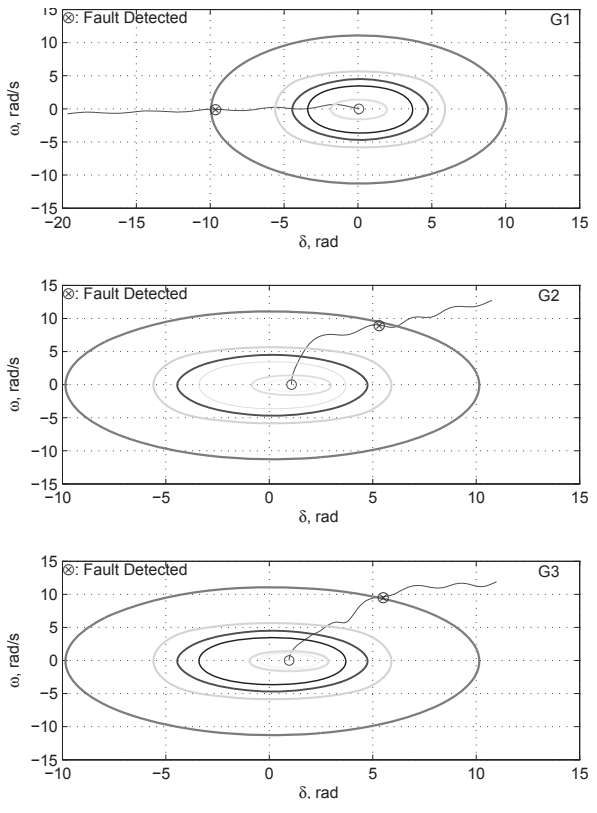


Figure 4.6  $\delta$ -  $\omega$  Curves for Out-of-step Fault Duration Time of 0.45 s Between Nodes 6-9.

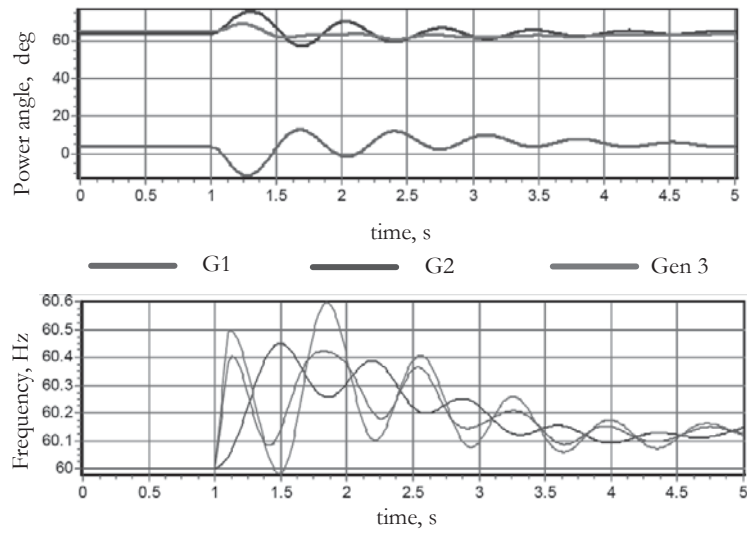


Figure 4.7  $\delta$ -t and  $\omega$ -t Curves for Stable Swing Fault Duration Time of 0.1 s Between Nodes 5-7.

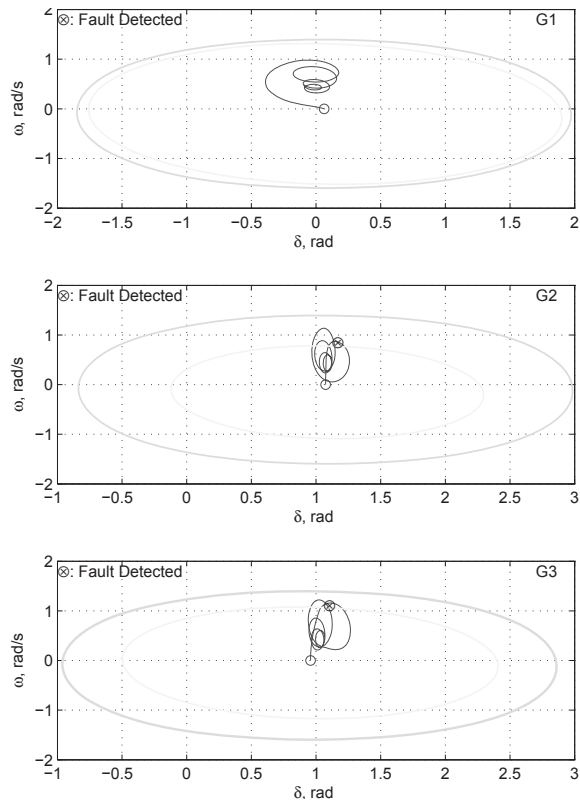


Figure 4.8  $\delta$ -  $\omega$  Curves for Stable Swing Fault Duration Time of 0.1 s Between Nodes 5-7.

algorithm is able to detect the swing for cascading disturbances as well. Next, in Case-14, another cascading disturbance is created for out-of-step condition. This case is created by applying a third disturbance, in addition to Case-13, at the middle of transmission line between nodes 6-9 for fault duration time of 0.45 s. The decision time for all three generators are 1.23 s for G1, 0.982 for G2, and 0.99 for G3, respectively. The summary of the results for cascading failures are listed in Table 4.2.

Table 4.1 Summary of Case Studies in IEEE 3-machine 9-bus System.

Case No.	Node No.	Fault (s)	Decision Time (s)			Decision
			G1	G2	G3	
1	6-9	0.10	N/A	2.940	2.052	Stable
2	6-9	0.45	0.566	0.502	0.438	Out-of-step
3	5-7	0.10	N/A	1.996	2.092	Stable
4	5-7	0.45	0.518	0.350	0.510	Out-of-step
5	7-8	0.10	N/A	1.956	2.428	Stable
6	7-8	0.45	0.470	0.310	0.366	Out-of-step
7	8-9	0.10	N/A	1.964	1.954	Stable
8	8-9	0.45	0.502	0.486	0.302	Out-of-step
9	4-5	0.10	N/A	1.965	2.76	Stable
10	4-5	0.45	0.598	0.638	0.654	Out-of-step
11	4-6	0.10	N/A	2.130	1.972	Stable
12	4-6	0.45	0.614	0.646	0.478	Out-of-step

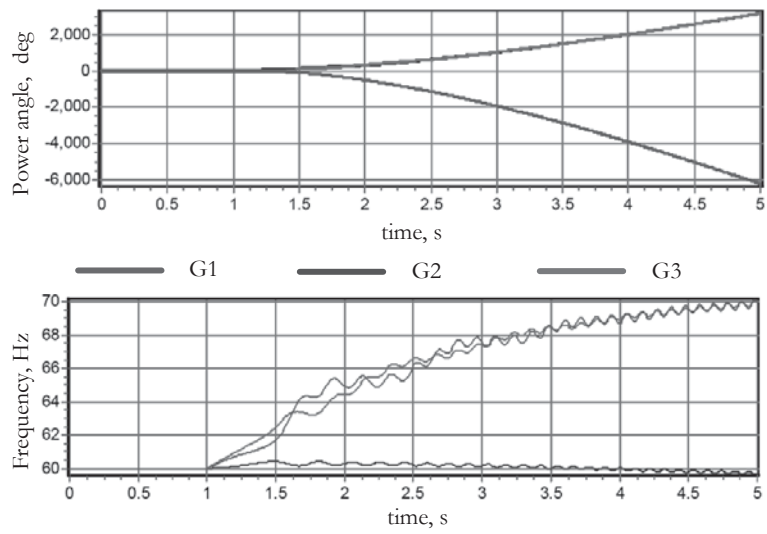


Figure 4.9  $\delta$ -t and  $\omega$ -t Curves for Out-of-step Fault Duration Time of 0.45 s Between Nodes 5-7.

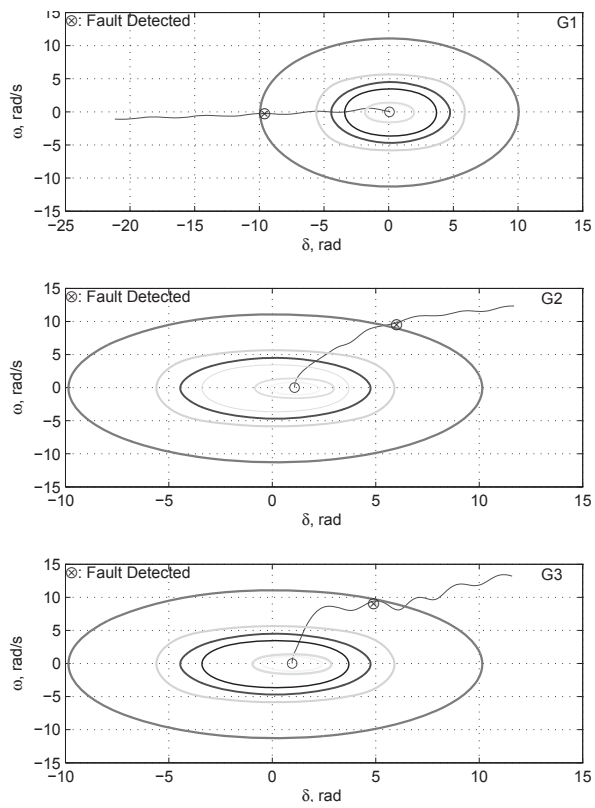


Figure 4.10  $\delta$ -  $\omega$  Curves for Out-of-step Fault Duration Time of 0.45 s Between Nodes 5-7.

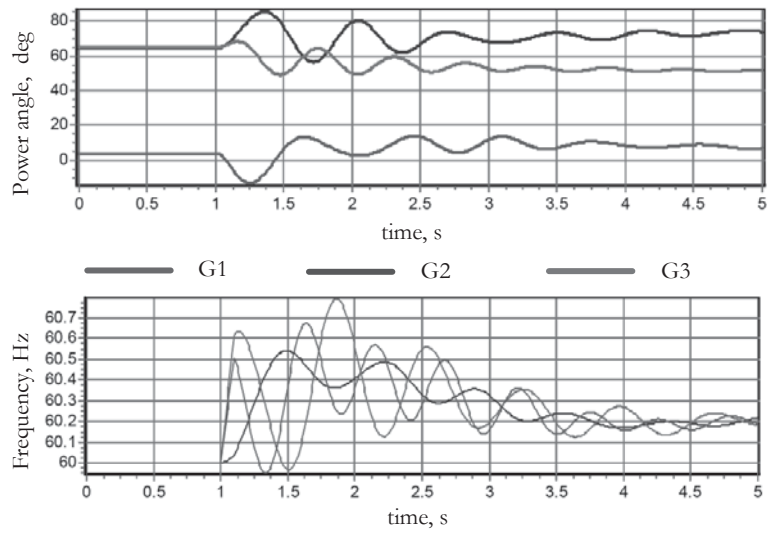


Figure 4.11  $\delta$ - $t$  and  $\omega$ - $t$  Curves for Stable Swing Fault Duration Time of 0.1 s Between Nodes 7-8.

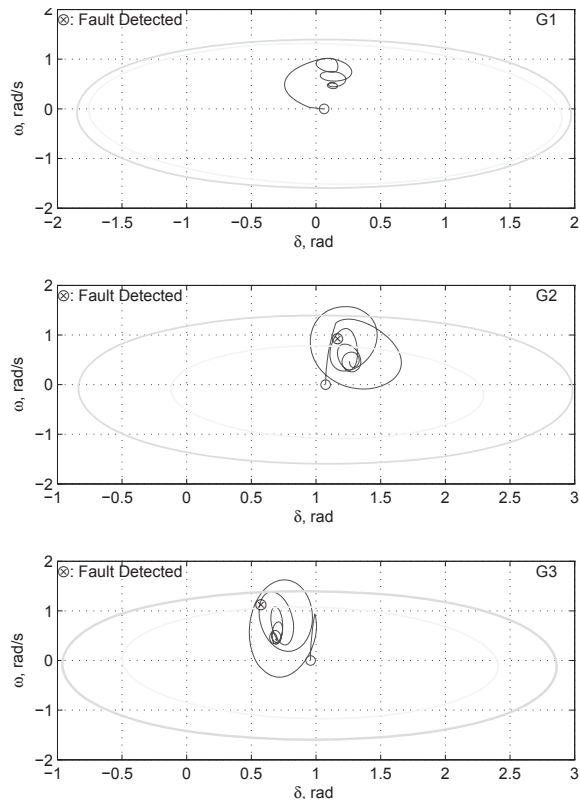


Figure 4.12  $\delta$ - $\omega$  Curves for Stable Swing Fault Duration Time of 0.1 s Between Nodes 7-8.



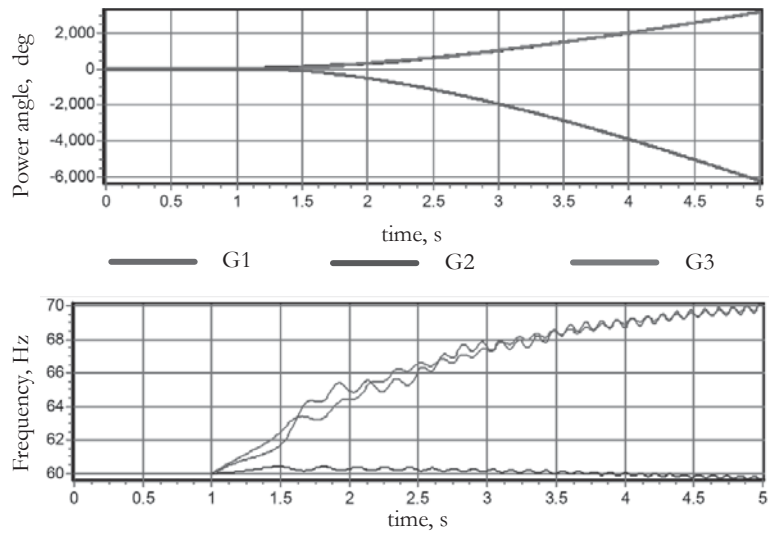


Figure 4.13  $\delta$ - $t$  and  $\omega$ - $t$  Curves for Out-of-step Fault Duration Time of 0.45 s Between Nodes 7-8.

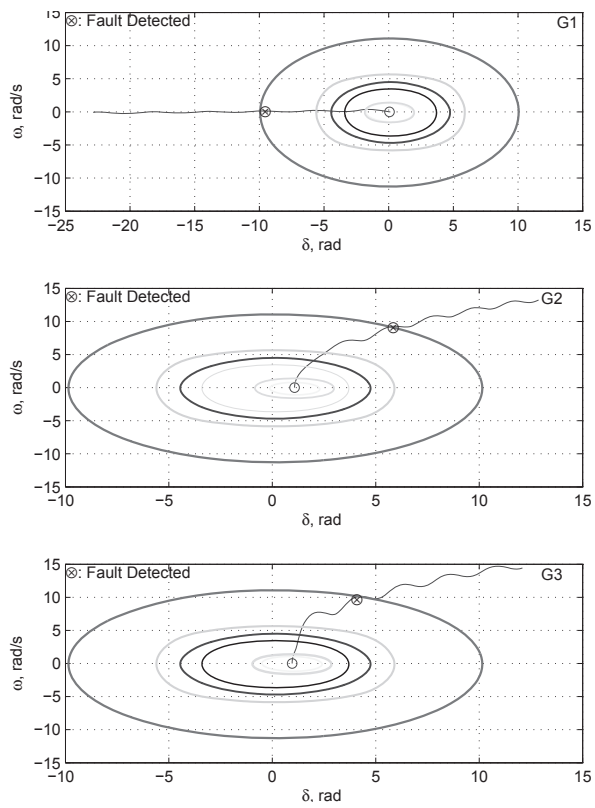


Figure 4.14  $\delta$ - $\omega$  Curves for Out-of-step Fault Duration Time of 0.45 s Between Nodes 7-8.

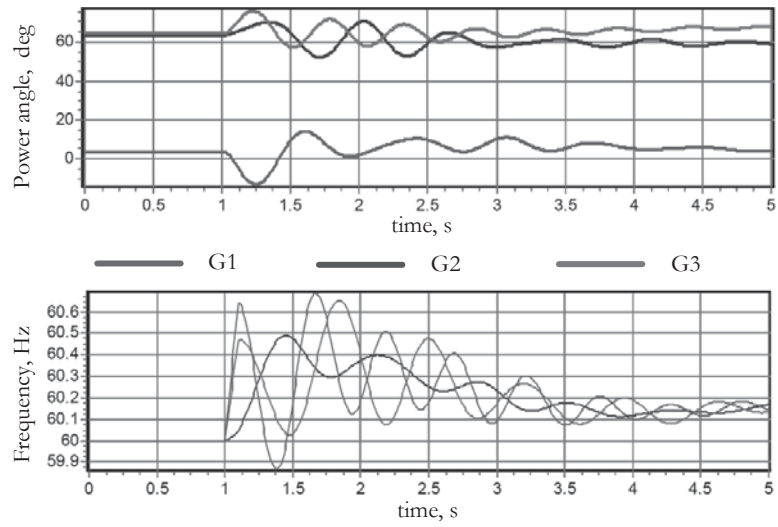


Figure 4.15  $\delta$ - $t$  and  $\omega$ - $t$  Curves for Stable Swing Fault Duration Time of 0.1 s Between Nodes 8-9.

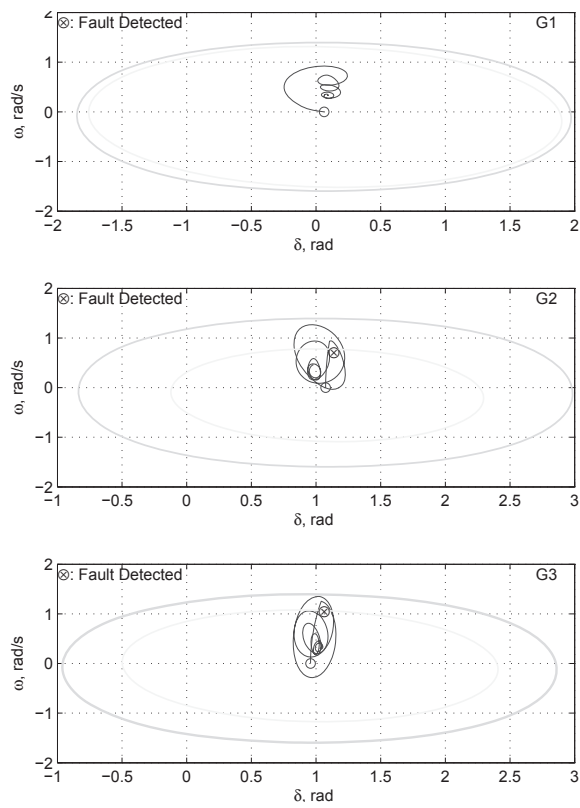


Figure 4.16  $\delta$ - $\omega$  Curves for Stable Swing Fault Duration Time of 0.1 s Between Nodes 8-9.

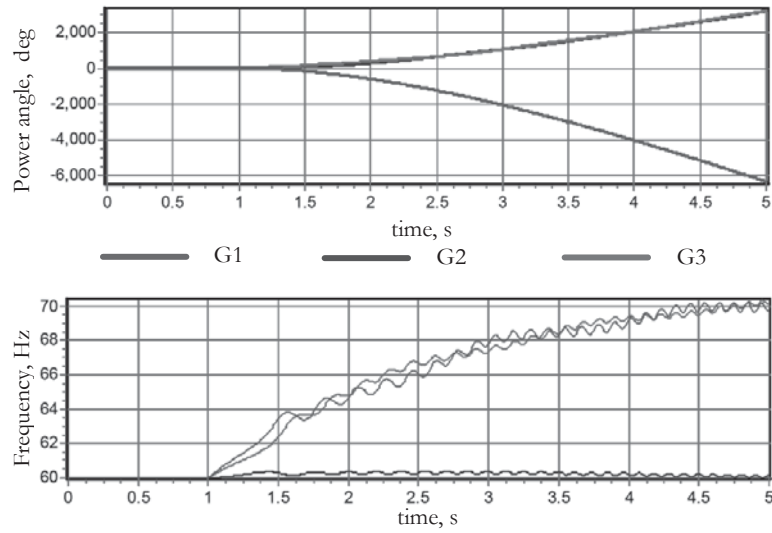


Figure 4.17  $\delta$ - $t$  and  $\omega$ - $t$  Curves for Out-of-step Fault Duration Time of 0.45 s Between Nodes 8-9.

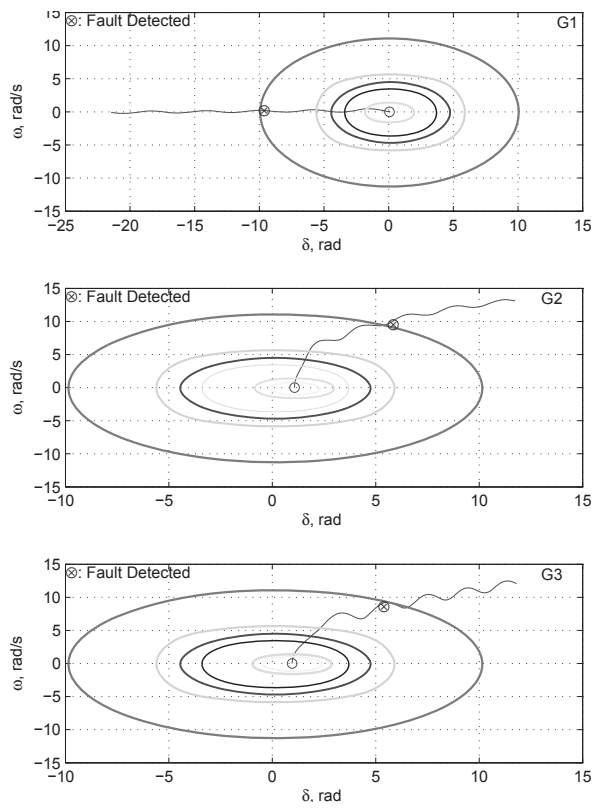


Figure 4.18  $\delta$ - $\omega$  Curves for Out-of-step Fault Duration Time of 0.45 s Between Nodes 8-9.

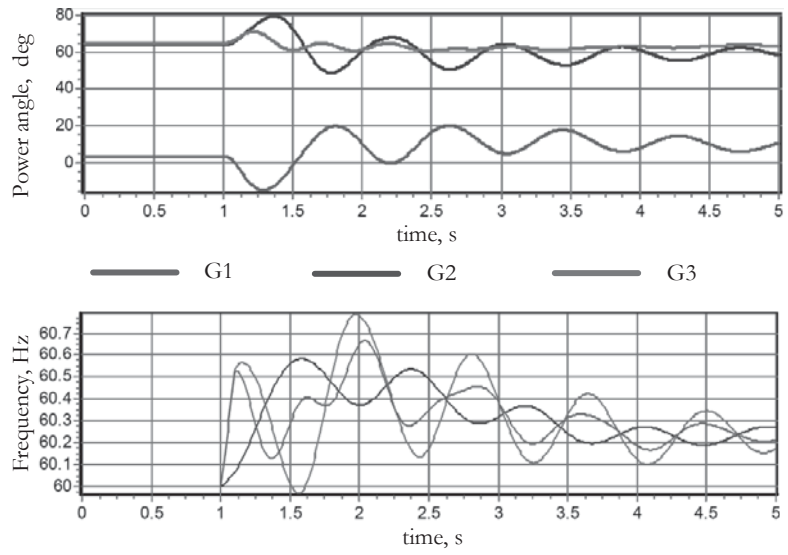


Figure 4.19  $\delta$ - $t$  and  $\omega$ - $t$  Curves for Stable Swing Fault Duration Time of 0.1 s Between Nodes 4-5.

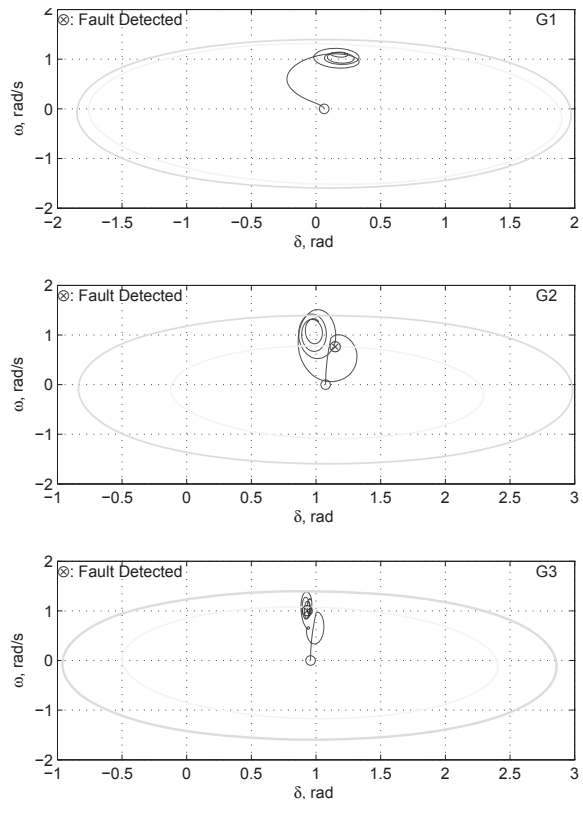


Figure 4.20  $\delta$ - $\omega$  Curves for Stable Swing Fault Duration Time of 0.1 s Between Nodes 4-5.

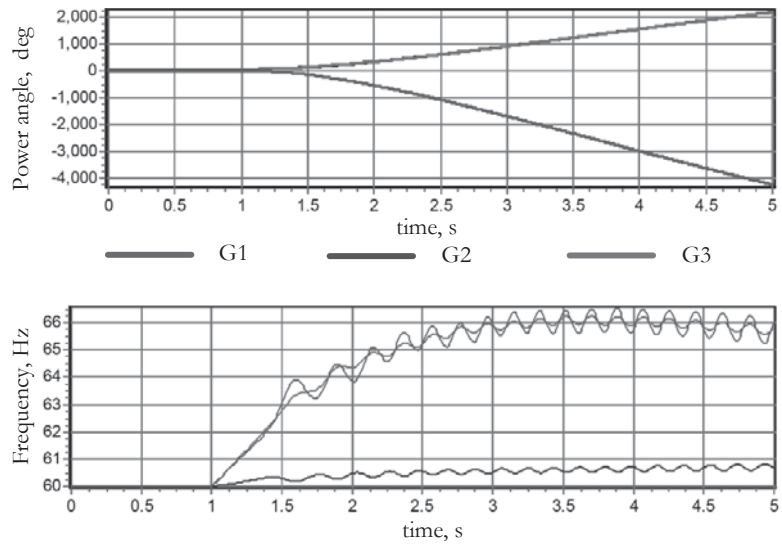


Figure 4.21  $\delta$ - $t$  and  $\omega$ - $t$  Curves for Out-of-step Fault Duration Time of 0.45 s Between Nodes 4-5.

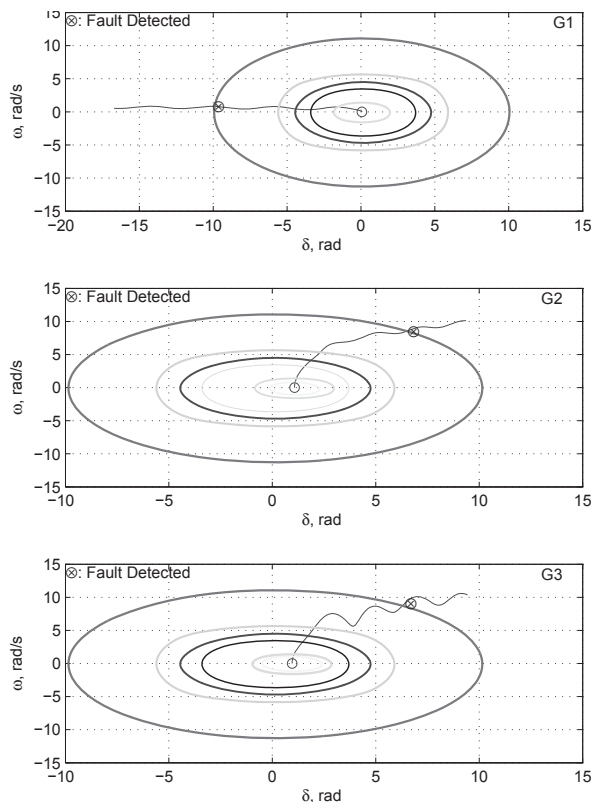


Figure 4.22  $\delta$ - $\omega$  Curves for Out-of-step Fault Duration Time of 0.45 s Between Nodes 4-5.

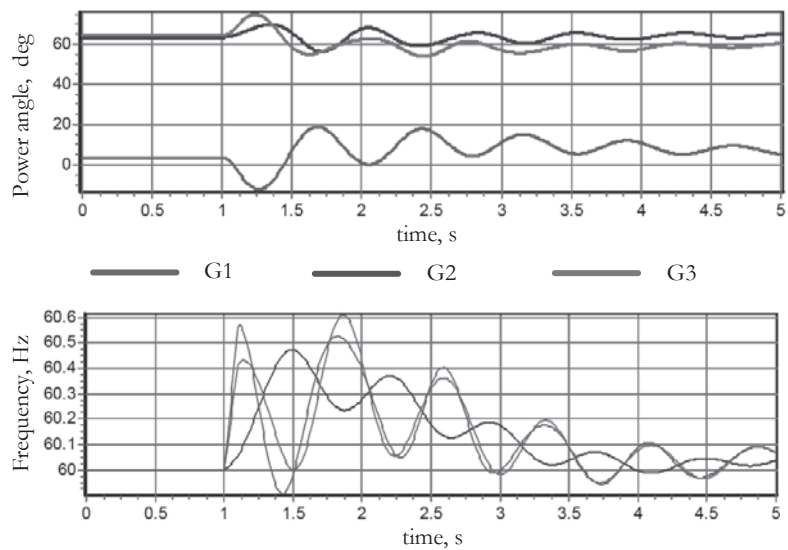


Figure 4.23  $\delta$ - $t$  and  $\omega$ - $t$  Curves for Stable Swing Fault Duration Time of 0.1 s Between Nodes 4-6.

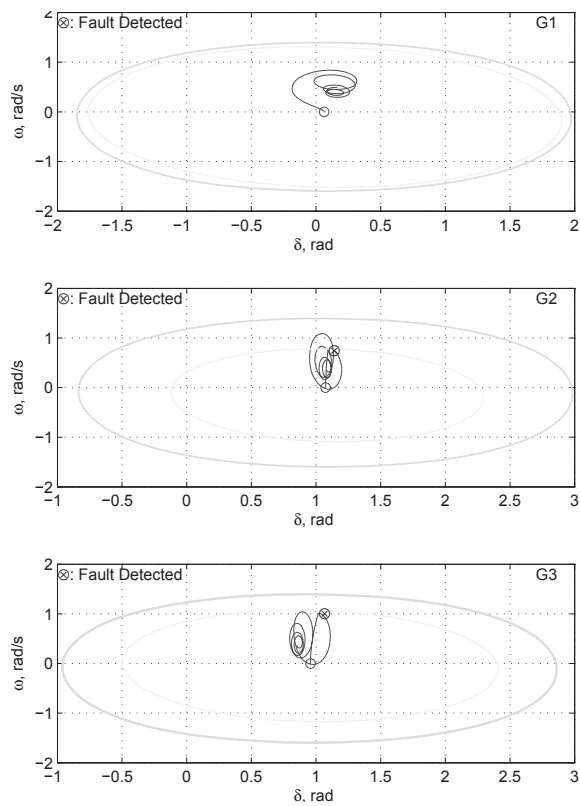


Figure 4.24  $\delta$ - $\omega$  Curves for Stable Swing Fault Duration Time of 0.1 s Between Nodes 4-6.

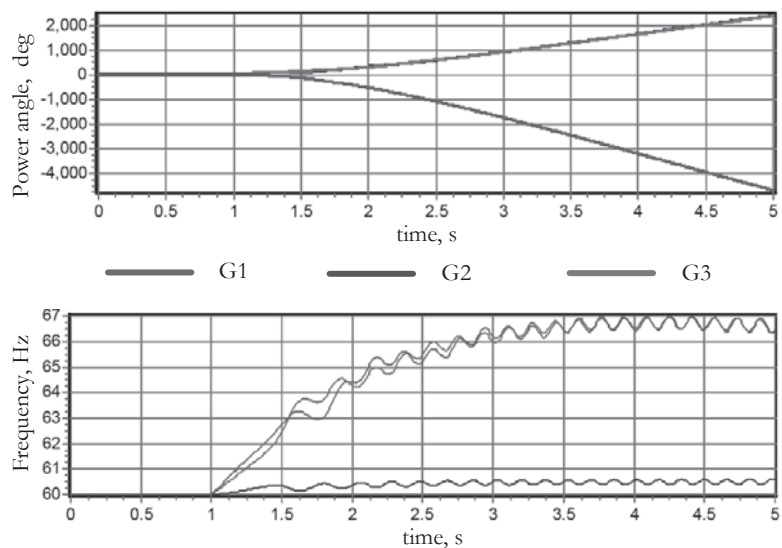


Figure 4.25  $\delta$ - $t$  and  $\omega$ - $t$  Curves for Out-of-step Fault Duration Time of 0.45 s Between Nodes 4-6.

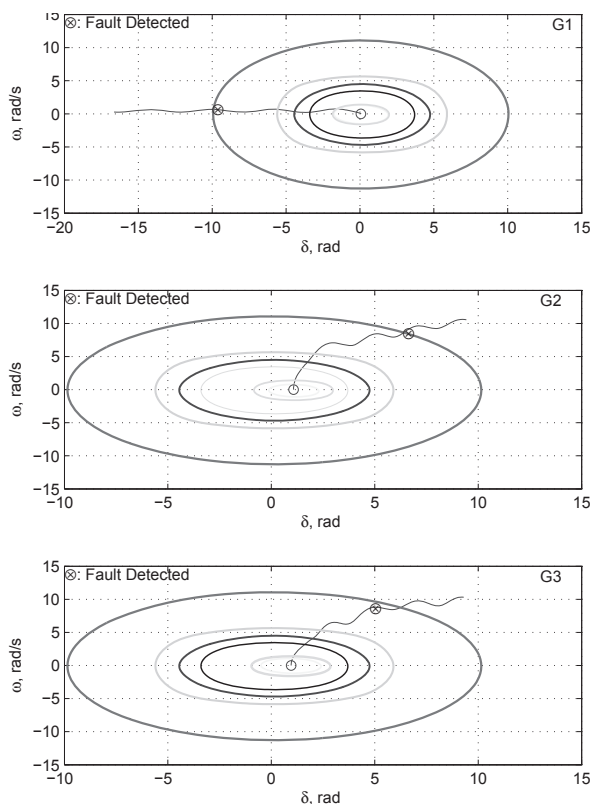


Figure 4.26  $\delta$ - $\omega$  Curves for Out-of-step Fault Duration Time of 0.45 s Between Nodes 4-6.

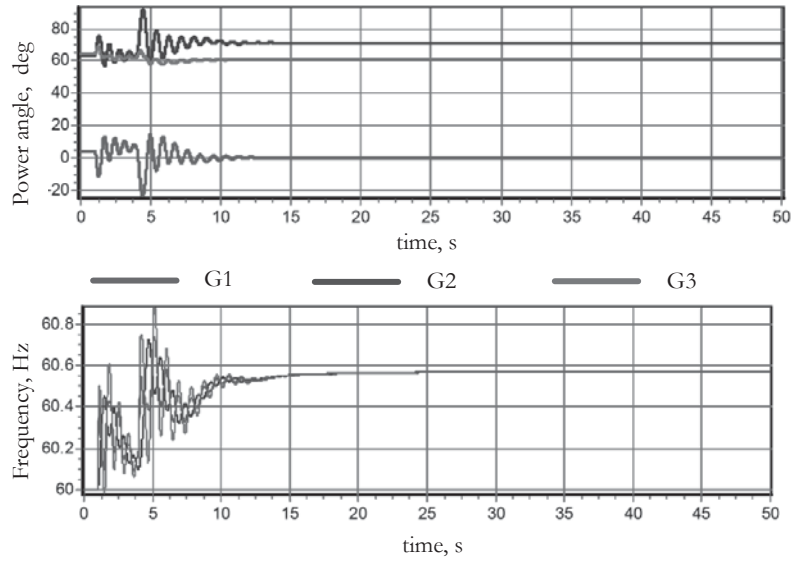


Figure 4.27  $\delta$ - $t$  and  $\omega$ - $t$  Curves for Stable Swing with Cascading Faults Between Nodes 5-7.

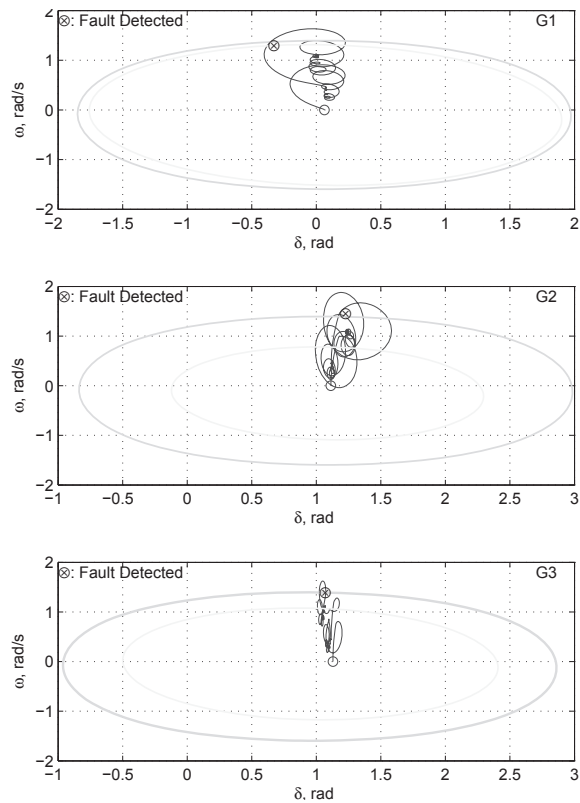


Figure 4.28  $\delta$ - $\omega$  Curves for Stable Swing with Cascading Faults Between Nodes 5-7.



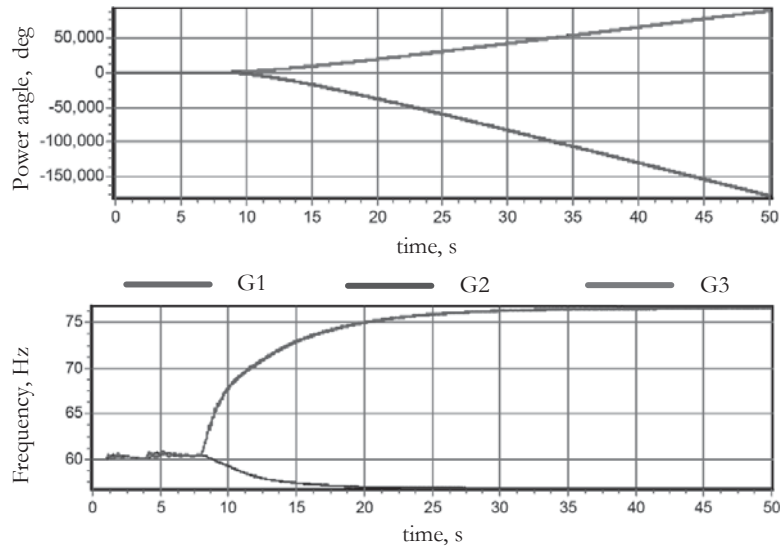


Figure 4.29  $\delta$ - $t$  and  $\omega$ - $t$  Curves for Out-of-step with Cascading Faults Between Nodes 5-7 and 6-9.

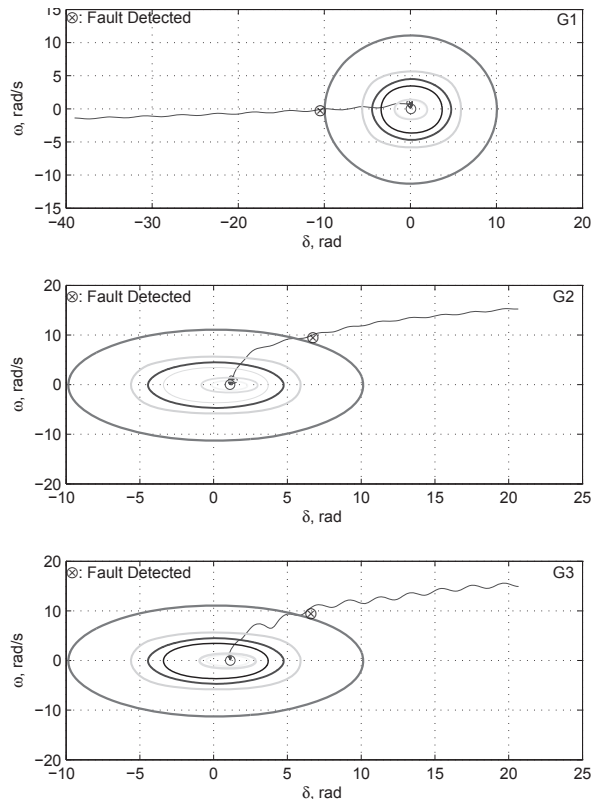


Figure 4.30  $\delta$ - $\omega$  Curves for Out-of-step with Cascading Faults Between Nodes 5-7 and 6-9.

Table 4.2 Summary of Case Studies for Cascading Failures in IEEE 3-machine 9-bus System .

<b>Case No.</b>	<b>Node No.</b>	<b>Fault (s)</b>	<b>Decision Time (s)</b>			<b>Decision</b>
			<b>G1</b>	<b>G2</b>	<b>G3</b>	
13	5-7	0.1-0.1	0.988	0.588	1.46	Stable
14	5-7 and 6-9	0.1-0.1-0.45	1.23	0.982	0.99	Out-of-step

#### 4.4 IEEE 10-machine 39-bus Case Studies

Another set of case studies are carried out in the IEEE 10-machine 39-bus system. The system is modeled in Powerworld and the system parameters are provided in the Appendix D.

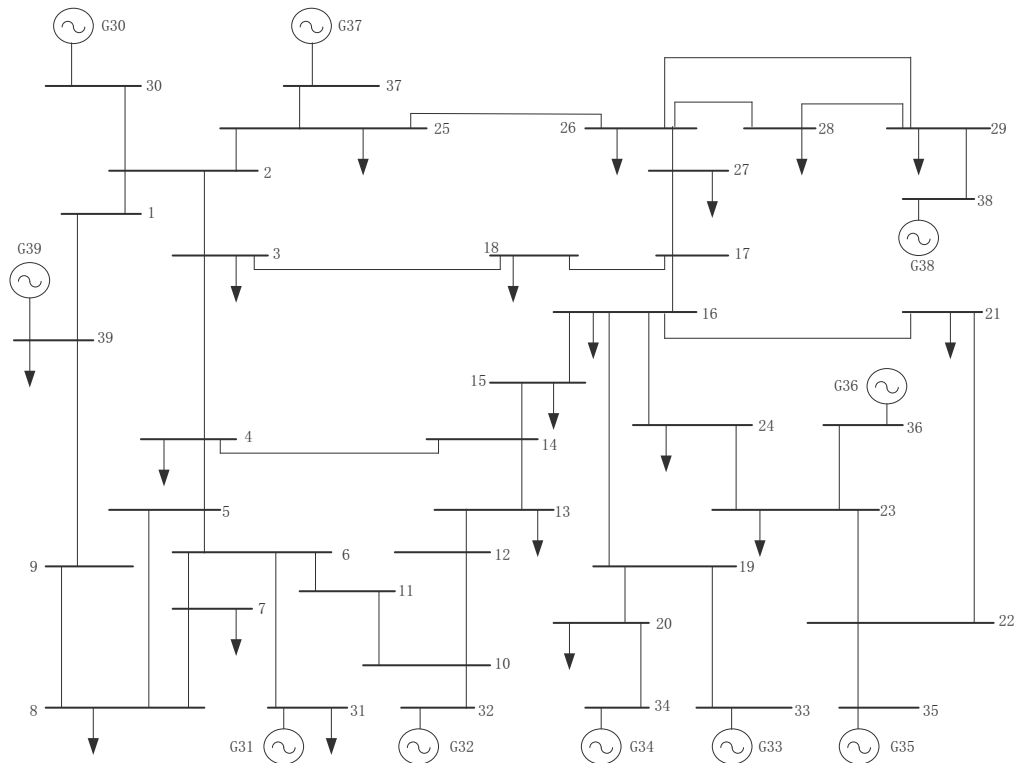


Figure 4.31 IEEE 10-machine 39-bus System.

Disturbances are created by applying three-phase fault at the middle of various transmission line to create stable and out-of-step swings. In total 35 case studies are carried by fixing with fault time at 0.3 s, the summary of the case studies are listed in Table 4.3. In the disturbance, the 10 generators would for different coherent groups in this case studies the performance of one representative generator from each coherent group

is discussed. The trajectories are shown in Figure 4.32 - Figure 4.36 .

The performance of the proposed method in detecting out-of-step condition for G38 is listed in Table 4.5 and 4.6. for stable and out-of-step conditions.

Cascading disturbances are also applied in this case studies. A three-phase line to ground fault is first applied at the middle of transmission line between nodes 25-26 with fault duration time of 0.1 s, a second similar disturbance is applied at the middle of transmission line 2-3 with fault duration 0.1 s. These disturbance leads to stable swing in the system. The proposed algorithm is able to detect the swing as stable. Then, a third disturbance is also applied at the middle of transmission line 10-11, with fault duration of 0.3 s. The propose algorithm is able to detect the swing as out-of-step condition, even in case of cascading disturbance. The trajectory of  $\delta-\omega$ ,  $\delta-t$ , and  $\omega-t$  in stable swing and out-of-step swing due to cascading failure are shown in Figure 4.35 to Figure 4.36.

Table 4.3 Out-of-step Condition for Line-between Cases Machine Coherent Results.

<b>Case</b>	<b>No.</b>	<b>Fault Duration Time (s)</b>	<b>Coherent Group Number</b>	<b>Decision</b>
1	1-2	0.3	1	out-of-step
2	2-3	0.3	4	out-of-step
3	2-25	0.3	3	out-of-step
4	3-4	0.3	1	out-of-step
5	3-18	0.3	1	out-of-step
6	4-5	0.3	1	out-of-step
7	4-14	0.3	1	out-of-step
8	5-6	0.3	2	out-of-step
9	5-8	0.3	1	out-of-step
10	6-7	0.3	1	out-of-step
11	6-11	0.3	1	out-of-step
12	7-8	0.3	1	out-of-step
13	8-9	0.3	2	out-of-step
14	10-11	0.3	3	out-of-step
15	10-13	0.3	2	out-of-step
16	11-12	0.3	2	out-of-step

Table 4.4 Out-of-step Condition for Line-between Cases Machine Coherent Results.

<b>Case</b>	<b>No.</b>	<b>Fault Duration Time (s)</b>	<b>Coherent Group Number</b>	<b>Decision</b>
17	12-13	0.3	1	out-of-step
18	13-14	0.3	2	out-of-step
19	14-15	0.3	1	out-of-step
20	15-16	0.3	2	out-of-step
21	16-17	0.3	2	out-of-step
22	16-19	0.3	3	out-of-step
23	16-21	0.3	1	out-of-step
24	16-24	0.3	1	out-of-step
25	17-18	0.3	1	out-of-step
26	17-27	0.3	2	out-of-step
27	19-20	0.3	2	out-of-step
28	21-22	0.3	3	out-of-step
29	22-23	0.3	3	out-of-step
30	23-24	0.3	1	out-of-step
31	25-26	0.3	4	out-of-step
32	26-27	0.3	2	out-of-step
33	26-28	0.3	2	out-of-step
34	26-29	0.3	2	out-of-step
35	28-29	0.3	2	out-of-step

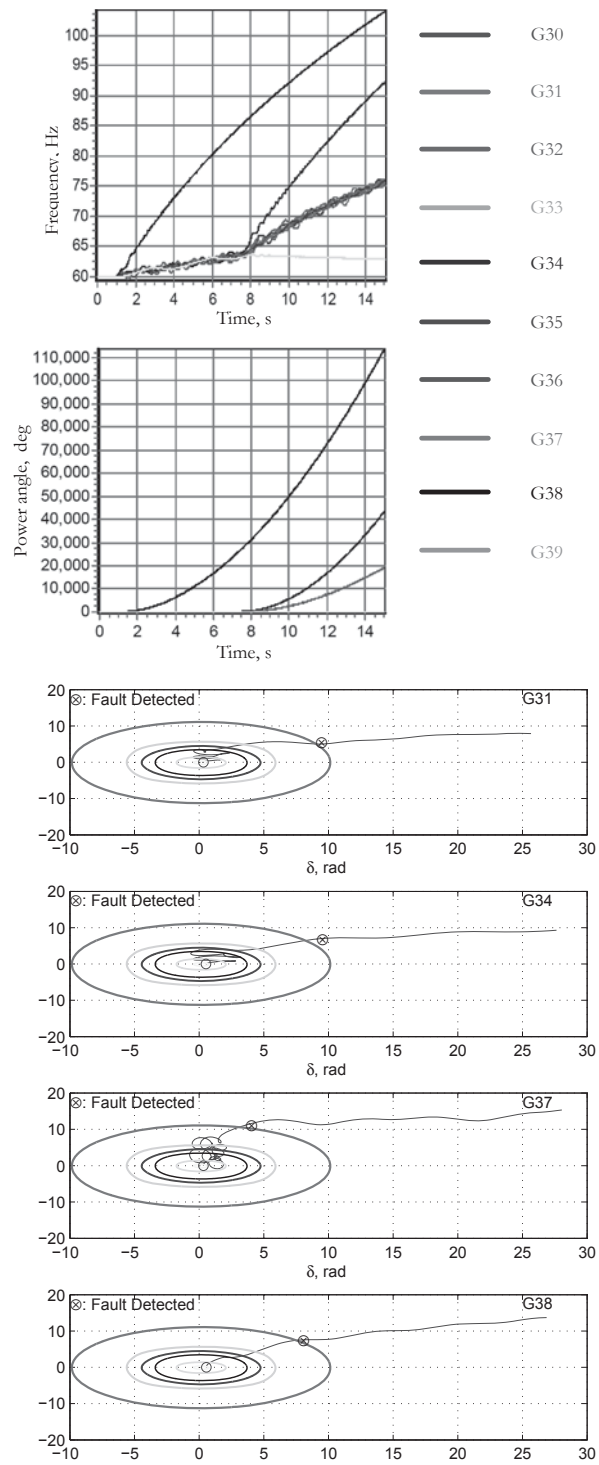


Figure 4.32  $\delta$ - $\omega$  Curve with Fault Duration 0.3 s, Fault at 25-26.

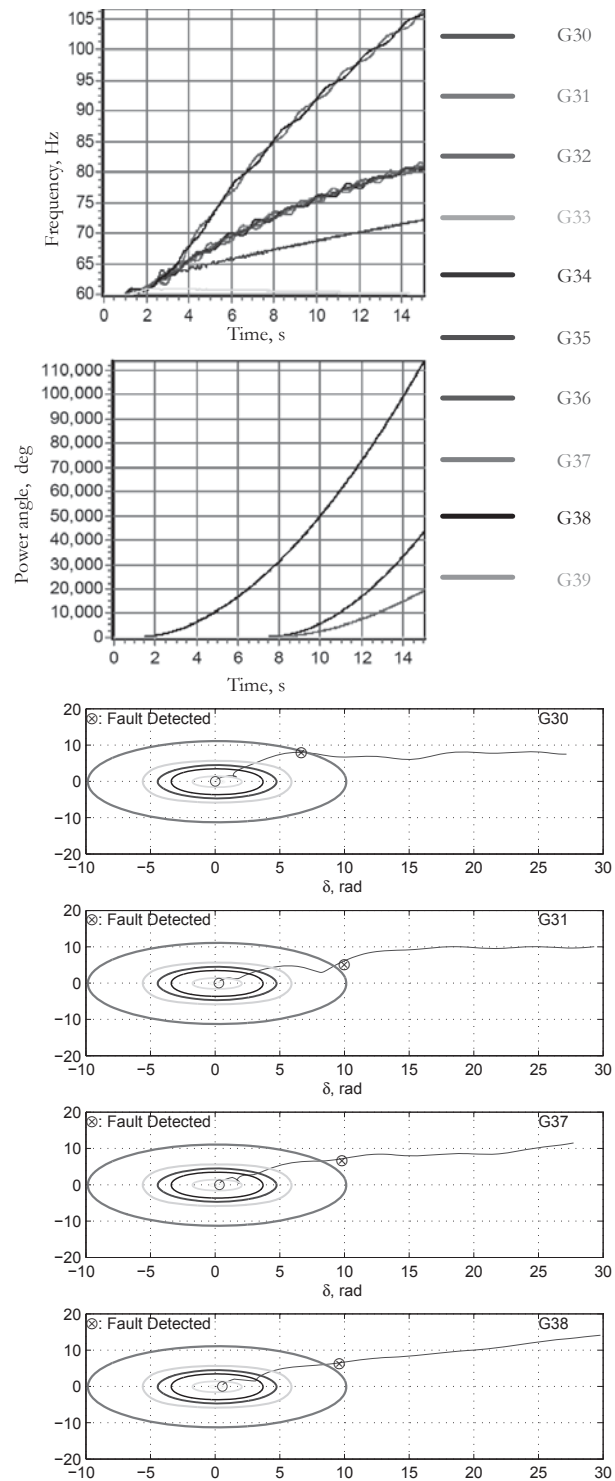


Figure 4.33  $\delta$ - $\omega$  Curve with Fault Duration 0.3 s, Fault at 2-3.



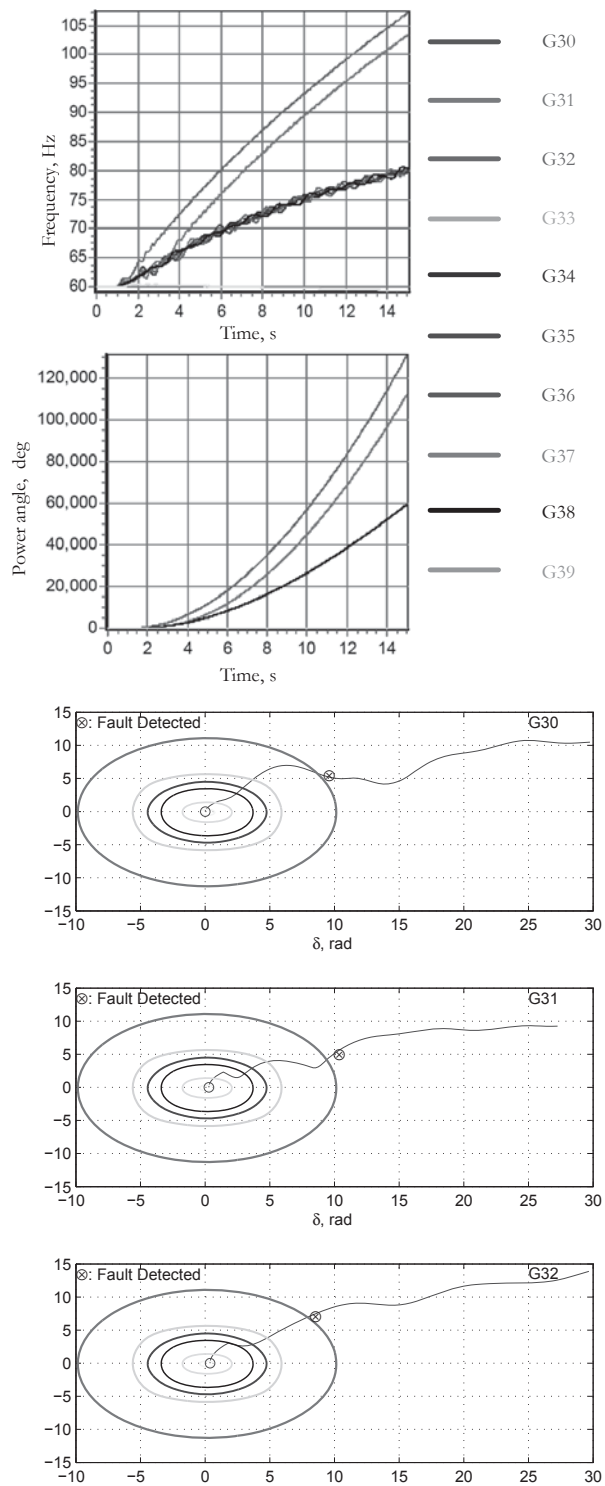


Figure 4.34  $\delta$ - $\omega$  Curve with Fault Duration 0.3 s, Fault at 10-11.

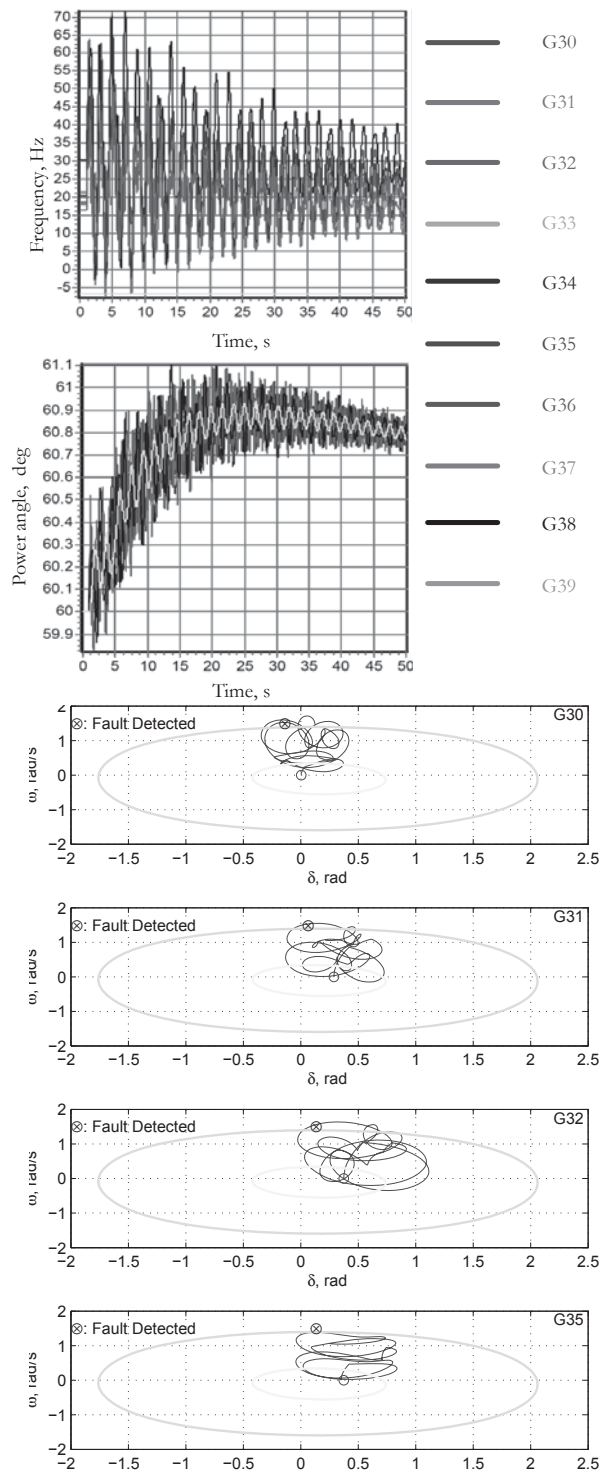


Figure 4.35 Stable Swing Trajectory for Cascading Faults.

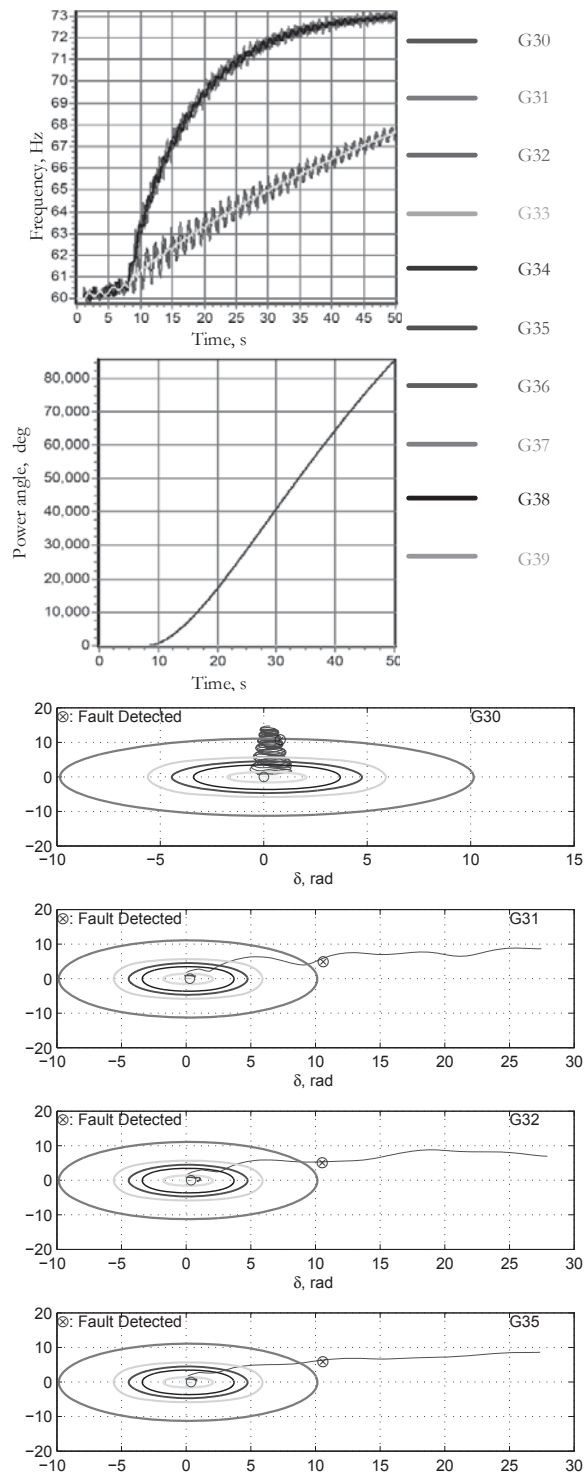


Figure 4.36 Out-of-step Trajectory for Cascading Faults.

Table 4.5 Performance of the Proposed Method in Stable Swing Cases Detection for G38 with Fault at Nodes 25-26.

<b>case</b>	<b>1</b>	<b>2</b>	<b>3</b>	<b>4</b>
Power Pre-fault Angle	7.3°	7.3°	7.3°	7.3°
Fault Duration Cycle	6	9	12	18
Fault Duration Time, s	0.048	0.096	0.144	0.192
Penetrated Boundaries	B5	B5	B5	B5
Decision Time, s	2.86	1.781	1.212	0.680
(After Fault cleared)	After	After	After	After
Decision	Stable	Stable	Stable	Stable

Table 4.6 Performance of the Proposed Method in Out-of-step Cases Detection for G38 with Fault at Nodes 25-26.

<b>case</b>	<b>1</b>	<b>2</b>	<b>3</b>	<b>4</b>
Pre-fault Power Angle	7.3°	7.3°	7.3°	7.3°
Fault Duration Cycle	19	25	28	36
Fault Duration Time,s	0.304	0.40	0.45	0.576
Penetrated Boundaries	B6	B6	B6	B6
Decision Time, s	2.174	0.431	0.356	0.223
(After Fault Cleared)	After	After	After	After
Decision	Out-of-step	Out-of-step	Out-of-step	Out-of-step

## 4.5 Summary

The proposed algorithm based on Zubov's boundary method is applied to two multi-machine test system, i. e., IEEE 3-machine 9-bus system and IEEE 10-machine 39-bus system. The case studies demonstrate that the proposed algorithm is robust and applicable to multi-machine systems as well. Please note that the proposed algorithm does not use any network reduction technique to detect out-of-step condition in multi-machine power systems.

## **CHAPTER 5. Hardware Implementation and Testing**

### **5.1 Introduction**

Chapter 3 and 4 discussed on the proposed algorithm and its settings on different cases through simulation software. This chapter discusses Schweitzer Engineering Laboratories (SEL) products to build a relay protection system and use of Doble's Power Simulator to compare the performance of the proposed algorithm with the blinder schemes. Due to limitation in the hardware, this work only shows open loop performance, but could be extended to closed loop if hardware like Real-time Digital Simulator (RTDS) or OPAL-RT become available.

### **5.2 Hardware/Software**

An overview of the hardware set-up is shown in Figure 5.1. Major components of this setup are discussed next.

#### **5.2.1 Phasor Measurement Unit**

The main hardware used are the SEL-421 and SEL-351S, PMU relay products, together with SEL-2407 GPS clock and SEL-3351S, the system computing platform [52] - [56]. The SEL-421 Relay is a microprocessor embedded relay for transmission line protection featuring different pole tripping and reclosing equipped with GPS [18], [52]. The SEL-421 features high-accuracy timekeeping when supplied with an IRIG-B signal [52].

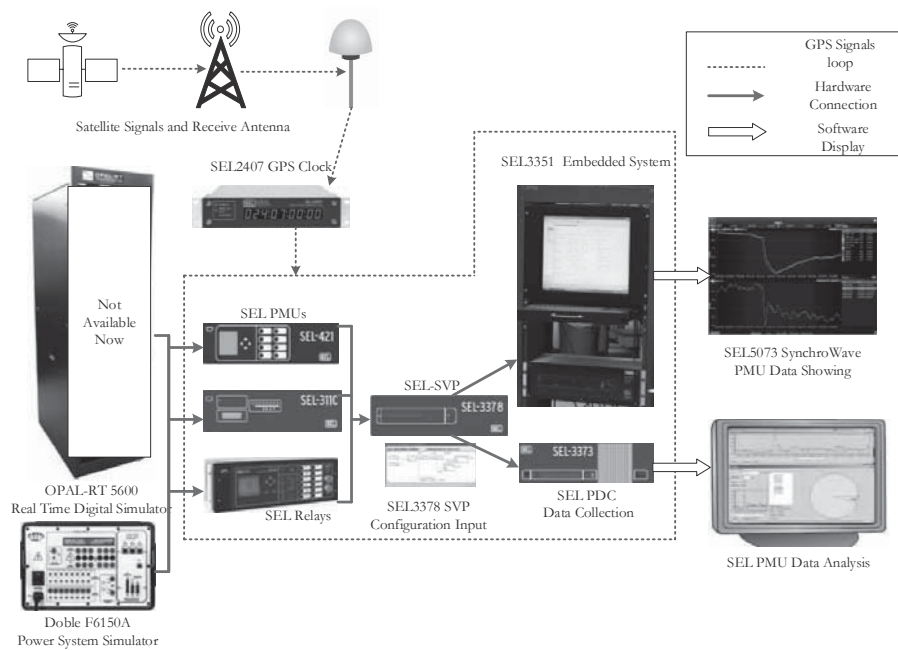


Figure 5.1 Michigan Tech Smart Grid Lab Relay Testbed.

When the supplied clock signal is sufficiently accurate, the SEL-421 can act as a PMU and transmit synchrophasor data representative of the power system at fixed time period to external systems [52] - [54]. The SEL-421 features Out-Of-Step logic [52] through the following two functions:

- Out-of-step blocking (OSB) logic blocks phase distance elements and Zone I ground distance elements during power swings [52].
- Out-of-step tripping (OST) logic trips the circuit breaker during unstable swings [52].

OSB logic blocks phase distance protection during a swing when the measured positive-sequence impedance enters the operating characteristics of the phase distance elements [53]. The OSB logic typically supervises forward-looking Zones 1 and 2 because

the operation time of these two zones is typically shorter than the time period during which the impedance of a power swing resides in these protection zones. During a power swing, the relay typically does not block overreaching zones of protection that provide time-delayed tripping [52]-[53]. The relay disables out-of-step blocking automatically when a fault occurs during a power swing. Therefore, the OST logic embedded in distance protection could detect all fault types and trip the circuit breakers during internal faults.

### **5.2.2 System Computing Platform**

SEL3351 is a robust device for data collection, which features alarm notifications, historical charts, one-line control, and user friendliness through Microsoft Windows-based system. Furthermore, the SEL-3351 accepts both modulated and demodulated IRIG-B signals (including GPS time stamped) thus it has the ability to record synchrophasors [56].

### **5.2.3 Doble Power Simulator**

Doble F6150 and its upgraded version F6150A are a very stable device to output voltages and currents with high power as a full power system simulator. The F6150 is the instrument with multiple simulation outputs, flexibility software to run full simulation tests on relays and protection schemes. The F6150A power system simulator, compared to previous version F6225, can provide more channels of voltage and current signals with using friendly interface and more ports. Moreover, it is capable for regenerating ATP-EMTP simulation result in pl4 format into AC waveforms for relay testing.

## **5.3 System Configuration**

The overview of Michigan Tech's relay test bed is shown in Figure 5.2. The components discussed in Section 5.2 are configured as PMU monitoring/protecting testbed, as shown in Figure 5.2. The three phase voltage and current cables are



connected from Doble simulator to SEL-421, which is on the top left in Figure 5.2. The closed view of SEL-421 and its GPS clock is shown in Figure 5.3. The SEL-421 has three different connections: the GPS time signal which comes from SEL-2407, the signal from Doble simulator, and signal that connects to the SEL-3351 control platform, as shown in the right side of Figure 5.2.



Figure 5.2 PMU Testbed-1.



Figure 5.3 PMU(SEL-421) and GPS Clock.

The SEL's PMU relay setting and monitor software for real-time synchrophasor

measurement window could be seen in reference [52]. The right top side of the data window provides the GPS calibrated time with three-phase voltages and current waveforms. The phasor angle information is at the center of the screen. Its sample parameter settings located at out-of-step tripping logic settings could also be modified based on [52]. The SEL device uses two blinder scheme for out-of-step detection.

A SMIB system, similar to one used in Chapter 3, is modeled in ATP-EMTP, with a three-phase line to ground fault at the middle of the transmission line with different fault duration time. The transmission line is modeled with  $\pi$ - equivalent model and the current transformer magnetizing inductance is not considered. This model is shown in Figure 5.4.

After creating the ATP model, the model is transferred to Doble simulator using a pl4 file generated by the ATP. The Doble simulator mimics this waveform and feeds to the SEL-421. The fault duration time is set at 0.328, 0.353, 0.384, and 0.480 s. These fault duration corresponds to the fault duration time used in Chapter 3 for comparison purpose. The relay report history for these 5 cases are shown in Figure 5.5.

The decision time required in SEL-421 for these case studies to detect power swing is summarized in Table 5.1. The decision times are higher based on the blinder scheme inside the SEL-421. The decision for critical stable case scenario was also detected as out-of-step condition by SEL-421. This could be attribute to a higher safety margin kept on the blinder based schemes.

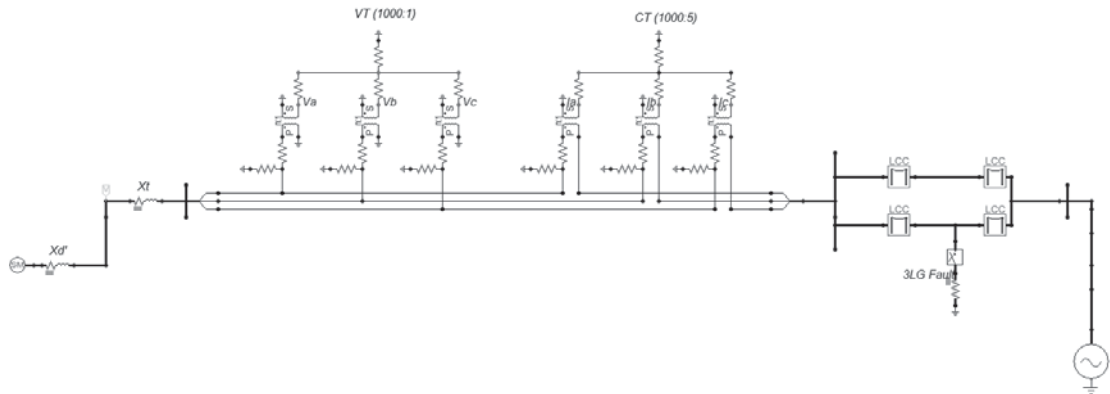


Figure 5.4 ATP-EMTP Model of SMIB System.

```

PMU                               Date: 06/18/2014   Time: 16:48:40.839
out-of-step test                  Serial Number: 2006305237

#      DATE      TIME      EVENT  LOCAT  CURR  GRP  TARGETS
10140 06/18/2014 16:47:13.156 ABC    $$$$ $$ 1451  1
10139 06/18/2014 16:45:48.427 ABC    $$$$ $$ 1451  1
10138 06/18/2014 16:44:44.498 ABC    $$$$ $$ 1451  1
10137 06/18/2014 16:42:35.194 ABC    $$$$ $$ 1451  1
10136 06/18/2014 16:39:55.369 ABC    $$$$ $$ 1452  1

```

Figure 5.5 SEL-421 Protection Event History Report.

Table 5.1 SMIB Comparisons for Different Fault Duration Time.

Fault Duration Time	Proposed Method Decision Time	Blinder Method Decision Time
0.480s	0.072s (out-of-step)	1.26 (out-of-step)
0.384s	0.232s (out-of-step)	1.33 (out-of-step)
0.352s	0.344s (out-of-step)	1.57 (out-of-step)
0.328s	0.152s (stable)	1.03 (out-of-step detected)

## 5.4 Summary

In this chapter, a hardware test bed is developed, where a blinder scheme is implemented and compared with the case studies discussed in Chapter 3 for SMIB system. The performance comparison shows that proposed algorithm is faster than the blinder schemes embedded in SEL-421.

## **CHAPTER 6. Summary and Conclusions**

### **6.1 Summary**

The motivation behind this work and impact of out-of-step impacts on power systems are discussed in Chapter 1. Literature review of different out-of-step techniques are also summarized in Chapter 1. PMU devices with wide-area measurement technique and detailed out-of-step methods are elaborated in Chapter 2. Also, the Lyapunov based method are discussed and modified Zubov's approximation method are presented in Chapter 2.

In Chapter 3, the modified Zubov's approximation method for out-of-step detection is proposed and developed for power system application. A SMIB model is simulated with 6 different stable swing and 5 out-of-step cases. The results show that the proposed method has a good performance for out-of-step detection, where the decision time is faster for severe swings.

In Chapter 4, the IEEE 3-machine 9-bus and the IEEE 10-machine 39-bus systems are simulated for stable swing and out-of-step cases. Performance of the proposed out-of-step detection method is also tested in cascading disturbances.

In Chapter 5, a hardware testbed is built to test the SMIB case using SEL-421. The comparison results show that the proposed method has a faster decision time than the blinder method embedded in the SEL-421 relay.

## 6.2 Conclusions

In this thesis, a new algorithm is proposed for power system out-of-step detection based on Zubov's stability boundary method. Based on the proposed algorithm, distinctions between power system stable swing and out-of-step are properly made in multi-machine power systems. The decision time varies based on settings of the boundaries and time delays. In the case study 88 stable swing is classified into 5 level of severity with distinct Zubov's boundaries. Due to the high speed and accurate PMU measurements, it is possible to differentiate the stable swing's severity compared to other methods, which provides benefits to operators by providing early warning. Besides, the sensitive analysis for out-of-step boundary shows that the decision time depend on the out-of-step boundary settings.

In the simulation studies of SMIB system, IEEE 3-machine 9-bus system, and 10-machine 39-bus system, the proposed algorithm shows a consistent performance for both the stable and out-of-step swings. Since the out-of-step trajectory is entirely different than the stable swing in  $\delta - \omega$  plane, the algorithm could balance the decision reliability with decision time. Longer the fault duration time is, quicker the decisions the proposed algorithm makes. This inverse relationship between fault duration and decision time gives benefit to system operators in emergency control.

The case studies demonstrate that the fault closest to generator in multi-machine systems is normally detected 5% faster in stable swing situation and 15% to 20% faster in out-of-step condition. The performance of the proposed algorithm is compared with a built in blinder scheme of SEL-421 and the results show that the proposed algorithm is faster than the blinder scheme. Based on the comparison results, the proposed algorithm shows decision time made are a 50% faster than the conventional blinder scheme.

### **6.3 Thesis Contributions**

The following are the contributions made through this thesis,

- Zubov's boundary based stability analysis method is developed for power system applications. The Zubov's boundary method, along with PMU data, is then used to propose a novel out-of-step algorithm.
- The proposed algorithm are tested in three systems: Single Machine Infinite Bus system, IEEE 3-machine 9-bus system, and IEEE 10-machine 39-bus system. The case studies show that the proposed method is suitable for out-of-step detection in large power systems, without using network reduction techniques.

### **6.4 Future Plans**

The following are the three main possible future directions of this work:

- Consideration of delay in data transmission from PMU to PDC and its impact on the decision time and the decision on out-of-step condition.
- Use of Bayesian Theorm based prediction algorithm to predict PMU measurements during disturbance to improve the decision time.
- Examine on the possibility of minimum number of boundaries to set in order to improve the decision time.

## APPENDIX A. SMIB System Parameters

The synchronous machine parameters are: The SMIB system's synchronous machine's parameters are,

$$x'_d = 0.27 \text{ p.u.}$$

$$x_d = 1.0 \text{ p.u.}$$

$$x_q = 0.6 \text{ p.u.}$$

$$x''_d = 0.22 \text{ p.u.}$$

$$x''_q = 0.29 \text{ p.u.}$$

$$\tau'_{do} = 9.0 \text{ s.}$$

$$\tau''_{do} = 0.04 \text{ s.}$$

$$\tau''_{qo} = 0.07 \text{ s.}$$

$$H = 4.0$$



## APPENDIX B. IEEE 3-machine 9-bus Parameters

Table B.1 Generators Parameters in p.u.

Gen No.	H	$X'_d$
1	23.64	0.0608
2	6.4	0.1198
3	3.01	0.1813

Table B.2 Transformer Parameter in p.u.

Gen No.	$X_d^T$
1	0.0576
2	0.0625
3	0.0586

Table B.3 Lines Parameters in p.u.

From Bus.	To Bus.	B	R	X
1	4	0.0	0.0576	0.0
4	6	0.079	0.092	0.017
3	9	0.0	0.0586	0.0
6	9	0.179	0.17	0.039
5	7	0.153	0.161	0.032
7	8	0.0745	0.072	0.0085
2	7	0.0	0.0625	0.0
8	9	0.1045	0.1008	0.0119

Table B.4 Load Parameters in p.u.

<b>Bus No.</b>	$P_g$	$Q_g$	$P_l$	$Q_l$	$V_{spc}$
1	0.0	N/A	0.0	0.0	1.04
2	1.63	0.0	0.0	0.00	1.025
3	0.85	0.0	0.0	0.00	1.025
4	0.0	0.0	0.0	0.0	N/A
5	0.0	0.0	1.25	0.5	N/A
6	0.0	0.0	0.9	0.3	N/A
7	0.0	0.0	0.0	0.0	N/A
8	0.0	0.0	1.0	0.35	N/A
9	0.0	0.0	0.0	0.0	N/A

## APPENDIX C. IEEE 10-machine 39-bus Parameters

Table C.1 Generators Parameters in p.u.

Unit No.	H	$X'_d$	$X'_q$	$X_d$	$X_q$
30	500	0.006	0.008	0.020	0.019
31	30.3	0.0697	0.170	0.295	0.282
32	35.8	0.0531	0.0876	0.245	0.237
33	28.6	0.0436	0.166	0.262	0.258
34	26	0.0697	0.170	0.295	0.282
35	34.8	0.0697	0.170	0.295	0.282
36	26.4	0.0697	0.170	0.295	0.282
37	24.3	0.0697	0.170	0.295	0.282
38	34.5	0.0697	0.170	0.295	0.282
39	42	0.0697	0.170	0.295	0.282

Table C.2 Lines Parameters in p.u.

<b>From Bus.</b>	<b>To Bus.</b>	<b>R</b>	<b>X</b>	<b>B</b>
1	2	0.0035	0.0411	0.6987
1	39	0.001	0.025	0.75
2	3	0.0013	0.0151	0.2572
2	25	0.007	0.0086	0.146
2	30	0	0.0181	0
3	4	0.0013	0.0213	0.2214
3	18	0.0011	0.0133	0.2138
4	5	0.0008	0.0128	0.1342
4	14	0.0008	0.0129	0.1382
5	6	0.0002	0.0026	0.0434
5	8	0.0008	0.0112	0.1476
6	7	0.0006	0.0092	0.113
6	11	0.0007	0.0082	0.1389
6	31	0	0.025	0
7	8	0.0004	0.0046	0.078
8	9	0.0023	0.0363	0.3804
9	39	0.001	0.025	1.2
10	11	0.0004	0.0043	0.0729
10	13	0.0004	0.0043	0.0729
10	32	0	0.02	0
12	11	0.0016	0.0435	0
12	13	0.0016	0.0435	0
13	14	0.0009	0.0101	0.1723
14	15	0.0018	0.0217	0.366
15	16	0.0009	0.0094	0.171
16	17	0.0007	0.0089	0.1342

Table C.3 Lines Parameters in p.u.

<b>From Bus.</b>	<b>To Bus.</b>	<b>R</b>	<b>X</b>	<b>B</b>
16	21	0.0008	0.0135	0.2548
16	24	0.0003	0.0059	0.068
17	18	0.0007	0.0082	0.1319
17	27	0.0013	0.0173	0.3216
19	20	0.0007	0.0138	0
19	33	0.0007	0.0142	0
20	34	0.0009	0.018	0
21	22	0.0008	0.014	0.2565
22	23	0.0006	0.0096	0.1846
22	35	0	0.0143	0
23	24	0.0022	0.035	0.361
23	36	0.0005	0.0272	0
25	26	0.0032	0.0323	0.531
25	37	0.0006	0.0232	0
26	27	0.0014	0.0147	0.2396
26	28	0.0043	0.0474	0.7802
26	29	0.0057	0.0625	1.029
28	29	0.0014	0.0151	0.249
29	38	0.0008	0.0156	0

Table C.4 Power Parameters

Bus	Type	Load		Generator		Voltage P.U.
		P(MW)	Q(MVar)	P(MW)	Q(MVar)	
1	PQ	97.6	44.2	0	0	1
2	PQ	0	0	0	0	1
3	PQ	322	2.4	0	0	1
4	PQ	500	184	0	0	1
5	PQ	0	0	0	0	1
6	PQ	0	0	0	0	1
7	PQ	233.8	84	0	0	1
8	PQ	522	176.6	0	0	1
9	PQ	6.5	-66.6	0	0	1
10	PQ	0	0	0	0	1
11	PQ	0	0	0	0	1
12	PQ	8.53	88	0	0	1
13	PQ	0	0	0	0	1
14	PQ	0	0	0	0	1
15	PQ	320	153	0	0	1
16	PQ	329	32.3	0	0	1
17	PQ	0	0	0	0	1
18	PQ	158	30	0	0	1
19	PQ	0	0	0	0	1
20	PQ	680	103	0	0	1
21	PQ	274	115	0	0	1
22	PQ	0	0	0	0	1
23	PQ	247.5	84.6	0	0	1
24	PQ	308.6	-92.2	0	0	1
25	PQ	224	47.2	0	0	1
26	PQ	139	17.0	0	2	1
27	PQ	281	75.5	0	0	1
28	PQ	206	27.6	0	0	1
29	PQ	283.5	26.9	0	0	1
30	PV	0	0	250	-	1.0475
31	PV	9.2	4.6	-	-	0.9820
32	PV	0	0	650	-	0.9831
33	PV	0	0	632	-	0.9972
34	PV	0	0	508	-	1.0123
35	PV	0	0	650	-	1.0493

## APPENDIX D. Zubov's Boundary Parameters for SMIB Case

The modified two first order differential equations are,

$$\dot{\delta}' = \omega' \quad (\text{D.1})$$

$$\dot{\omega}' = -D(\delta')\omega' - R(\delta') \quad (\text{D.2})$$

Use first boundary for calculation process illustration:

$$v_2(\delta', \omega') : \nabla v_2 f_i(\delta', \omega') = -\phi \quad (\text{D.3})$$

Based on the general definition, it could be rewritten as,

$$(2d_{20}\delta' + d_{21}\omega')\omega' + (2d_{22}\omega' + d_{21}\delta')(-D(\delta')\omega' - R(\delta')) = -\phi \quad (\text{D.4})$$

In this equation, the parameters are calculated by same degree variables equaling to each other,  $\phi = 0.01(\delta' + \omega')$ .  $D(\delta')$  and  $R(\delta')$  are power system parameters' power series as shown in Eqn 3.8 to Eqn 3.11. The results of  $d_{20}$ ,  $d_{21}$ , and  $d_{22}$  are shown in the following.

For  $N = 2$  the coefficients are,

$$d_{20} = 0.3; \quad d_{21} = 0.05; \quad d_{22} = 0.45; \quad r = 0.34 \text{ rad};$$

For  $N = 4$  the coefficients are,

$$d_{40} = 0.148; \quad d_{41} = 0.013; \quad d_{42} = 0.41; \quad d_{43} = 0.021; \quad d_{44} = 0.152; \quad r = 1.57 \text{ rad};$$

For  $N = 6$  the coefficients are,

$$d_{60} = 0.0022; \quad d_{61} = 0.00014; \quad d_{62} = 0.0052; \quad d_{64} = 0.0057;$$
$$d_{63} = 0.00017; \quad d_{65} = 0.00018; \quad d_{66} = 0.0024; \quad r = 3.14 \text{ rad};$$

For  $N = 8$  the coefficients are,

$$d_{80} = 3.1e - 5; \quad d_{81} = 1.15e - 6; \quad d_{82} = 2.12e - 4; \quad d_{83} = 1e - 6; \quad d_{84} = 1e - 6;$$
$$d_{85} = 1e - 6; \quad d_{86} = 1.47e - 4; \quad d_{87} = 1e - 6; \quad d_{88} = 2.82e - 5; \quad r = 6.28 \text{ rad};$$

For  $N = 10$  the coefficients are,

$$d_{100} = 1.3e - 5; \quad d_{101} = 1.03e - 6; \quad d_{102} = 2.73e - 5; \quad d_{103} = 4.2e - 5;$$
$$d_{104} = 3.93e - 5; \quad d_{105} = 1e - 7; \quad d_{106} = 4.47e - 5; \quad d_{107} = 1e - 7;$$
$$d_{108} = 4.53e - 5; \quad d_{109} = 1e - 7; \quad d_{110} = 0.93e - 5; \quad r = 9.42 \text{ rad};$$



## REFERENCES

- [1] "The SMART GRID: AN INTRODUCTION", U.S.Department Of Energy Report, 2004 [Online].  
Available: <http://energy.gov/oe/downloads/smart-grid-introduction-0>.
- [2] "Smart Grid: Enabler of the New Energy Economy", A Report by The Electricity Advisory Committee, 2008 [Online].  
Available: <http://energy.gov/sites/prod/files/oeprod/DocumentsandMedia>.
- [3] R. D. La and A. G. Phadke, "Catastrophic Failures in Power Systems: Causes, Analyses, and Countermeasures," *Proceedings of the IEEE*, Vol.93(5), pp. 956-964, May, 2005.
- [4] P. Kundur, *Power System Stability and Control*. New York: McGraw-Hill, 1994.
- [5] T. Overbye, *Power System Analysis and Design* ,5th ed., Toronto, CA: Thomson Learning, 2012.
- [6] J. L. Blackburn, *Protective Relaying Principles and Applications* ,3rd ed., Boca Raton: CRC Press, 2006.
- [7] Y. Yao-nan, *Electric Power System Dynamics*. London: ACADEMIC PRESS, 1983.
- [8] J. S. Thorp and A. G. Phadke, "Protecting power systems in the post-restructuring era," *IEEE Comput. Appl. Power*, Vol.12(1), pp. 33-37, Jan, 1999.

- [9] "Synchrophasor Technologies and Their Deployment in the Recovery Act Smart Grid Programs", U.S. Department of Energy Electricity Delivery and Energy Reliability, 2013 [Online].  
Available: <https://www.smartgrid.gov/document/synchrophasor-technologies>.
- [10] "Final Report on the August 14,2003 Blackout in the United States and Canada:Causes and Recommendations", 2004 [Online]. Available:  
<http://www.nerc.com>.
- [11] "Accommodating High Levels of Variable Generation", A Special Report by NERC, 2009 [Online].  
Available: <http://www.nerc.com/files/ivgtf-report-041609.pdf>.
- [12] "Real-Time Application of Synchrophasors for Improving Reliability" A Special Report by NERC, 2008 [Online].  
Available:  
<http://www.nerc.com/docs/oc/rapirtf/RAPIR%20final%20101710.pdf>.
- [13] B. Tianshu, "The PMU Dynamic Performance Evaluation and The Comparison of PMU Standards," *Power and Energy Society General Meeting, 2011 IEEE*, pp. 1-5, July, 2012.
- [14] B. Tianshu, "The PMU Dynamic Performance Evaluation and The Comparison of PMU Standards," *2013 IEEE Grenoble Power Tech*, pp. 1-5, June, 2013.
- [15] T. Hashiguchi, "Power System Dynamic Performance Measured by Phasor Measurement Unit," *2007 IEEE Lausanne Power Tech*, pp. 1694-1699, July, 2007.
- [16] IEEE Power System Relaying Committee Working Group D6. "Power Swing and Out-of-step Considerations on Transmission Lines," *presented at the 59th Annual Conference Protection Relay Engineering*, 2006, College Station,TX.

- [17] W. A. Elmore, *Protective Relaying Theory and Applications*, 2nd ed., New York:Marcel Dekker, 2004.
- [18] “SEL421-4,-5 Relay Protection and Automation System, Instruction Manual User’s Guide”, SEL,INC., Vol-20130222, 2013.
- [19] C. Taylor, J. Haner, L. Hill, W. Mittelstadt, and R. Cresap, “A New Out-of-step Relay with Rate of Change of Apparent Resistance Augmentation,” *IEEE Trans. Power Syst.*, Vol. PAS-102(3), pp. 631-639, June, 1983.
- [20] D. A. Tziouvaras, “Out-of-step protection fundamentals and advancements,” *2004 57th Annual Conference for Protective Relay Engineers*, pp. 282-307, 2004.
- [21] H. Ruhai, “Power Swing And System Separation Based on Phasor-domain Simulations,” MS Thesis,Michigan Technological University, 2007 [ Online ].  
Available: <http://services.lib.mtu.edu/etd/THESIS/2006/> .
- [22] N. Fischer and G. Benmouyal, “Do System Impedances Really Affect Power Swings – Applying Power Swing Protection Elements without Complex System Studies,” *Protective Relay Engineers, 2012 65th Annual Conference for*, pp. 108-119, April, 2012.
- [23] W. Rebizant and K. Feser, “Fuzzy Logic Application to Out-of-step Protection of Generators,” *Power Engineering Society Summer Meeting, 2001* pp.927-932, 2001.
- [24] A. Y. Abdelaziz, “Adaptive Protection Strategies for Detecting Power System Out-of-step Conditions using Neural Networks,” *Generation, Transmission and Distribution,IEE Proceedings* Vol. 145, pp. 387-394, 1998.

- [25] A. Bahbah and A. A. Girgis “New Method for Generators’ Angles and Angular Velocities Prediction for Transient Stability Assessment of Multimachine Power Systems Using Recurrent Artificial Neural Network,” *IEEE Trans. Power Syst.*, Vol. 19(2), pp. 1015-1022, 2004.
- [26] F. Hashiesh, “A wide area synchrophasor based ANN transient stability predictor for the Egyptian Power System,” *IEEE PES Innovative Smart Grid Technologies Conference Europe*, pp. 1-7, 2010.
- [27] P. C. Krause, *Analysis of Electric Machinery and Drive Systems* ,2nd ed., New York: Wiley, 2002.
- [28] A. E. Fitzgerald, *Electric Machinery* ,6th ed., New York: McGraw-Hill, 2003.
- [29] Q. H. Wu, *Protective Relaying of Power Systems Using Mathematical Morphology* , New York: Springer, 2009.
- [30] V. Centeno, “An Adaptive Out-of-step Relay for Power System Protection,” *IEEE Trans. Power Delivery*, Vol. 12(1), pp. 61-71, Jan, 1997.
- [31] S. Paudyal, G. Ramakrishna, and M. S. Sachdev, “Application of Equal Area Criterion Conditions in the Time Domain for Out-of-step Protection,” *IEEE Trans. Power Delivery*, Vol. 25(2), pp. 600-609, 2010.
- [32] M. Pavella and D. Ernst, “Transient Stability of Power systems,” MA:Kluwer, 2000.
- [33] A. G Phadke and J.S Thorp, *Synchronized Phasor Measurements and Their Applications*, New York: Springer, 2008.
- [34] Y. Yannan and K. Vongsuriya, “Nonlinear Power System Stability Study by Liapunov Function and Zubov’s Method,” *IEEE Trans. Power App. Syst.*, Vol. PAS-86(12),pp. 1480-1485, April, 1967.

- [35] L. J. Eugene, "A Guide of the Application of the Liapunov Direct Method to Flight Control Systems", NASA Contractor Report: NASA CR-209, April, 1965.
- [36] S. G. Margolis, "Computation of Regions of Asymptotic Stability for Closed-loop Systems by Liapunov's Second Method," PhD Disertation, University of Pittsburgh, 1962.
- [37] T. L. Saaty, *Modern Nonlinear Equations* , New York: Dover, 1983.
- [38] M. A. Pai, *Power System Stability Analysis by the Direct Method of Lyapunov* , New York: North-Holland, 1981.
- [39] S. G. Margolis and W.G. Vogt., "Control Engineering Applications of V.I.Zubov's Construction Procedure for Lyapunov Functions," *IEEE Trans. Automat. Contr.*, Vol. 8(2),pp. 104-113, 1962.
- [40] V. I. Zubov, "Voprosy teorii vtorogo metoda Lyapunova, postroenie obshchego resheniya v oblasti asimptoticheskoi ustoichivosti,(Problems in the theory of the second method of Lyapunov, construction of the general solution in the domain of asymptotic stability)" *Prikladnaya Matematika i Mekhanika*, Vol. 19, pp. 179-210, 1955.
- [41] F. Evangelos, H. Renke, J. C. George, and A. P. Meliopoulos, "A Predictive Out of Step Protection Scheme based on PMU Enabled Dynamic State Estimation," *Power and Energy Society General Meeting, 2011 IEEE*, pp. 1-8, 2011.
- [42] IEEE Std *C37.90<sup>TM</sup>* – 2005, IEEE Standard for Relays and Relay Systems Associated With Electric Power Apparatus.
- [43] IEEE Std *C37.118.2<sup>TM</sup>* – 2011, IEEE Standard for Synchrophasors for Power Systems.

- [44] J. D. Weber and T. J. Overbye,, "Synchrophasors: Definition,Measurement, and application," *IEEE Trans. Power Syst.*, Vol. 17(3), pp. 590-596, July, 2002.
- [45] A. Mark, "Synchrophasors: Definition,Measurement, and Application," *Ninth Annual Carnegie Mellon Conference on the Electricity Industry 2006* [ Online ].  
Available: <http://www.gedigitalenergy.com/SmartGrid/Sep06>.
- [46] A. Muhammad, "Development of System Separation Strategy Using Synchrophasor Data," PhD Disertation,Michigan Technological University, 2011 [ Online ].  
Available: <http://digitalcommons.mtu.edu/etd-restricted/17>
- [47] R. Arunachalam, "Time-domain Models for Power System Stability and Unbalance," MS Thesis,Michigan Technological University, 2006 [ Online ].  
Available: <http://digitalcommons.mtu.edu/etds/42>.
- [48] B. Lundqvist, "100 Years of Relay Protection, the Swedish ABB Relay History," 2001. [ Online ].  
Available: <http://www05.abb.com/>
- [49] S. Paudyal, "Out-of-Step Protection Using Energy Equilibrium Criterion in the Time Domain," MS Thesis,University of Saskatchewan, 2008 [ Online ].  
Available: <http://hdl.handle.net/10388/etd-06272008-100122>.
- [50] T. J. Overbye, R. P. Klump, and J. D. Weber, "Development and Application of A Power System Simulation Environment," *IEEE 39th Midwest symposium on Circuits and Systems*, Vol.3, pp.1097-1100, 1996.
- [51] J. D. Weber and T. J. Overbye, "Voltage Contours for Power System Visualization," *IEEE Trans. Power Syst.*, Vol.15(1), pp.404-409, March, 2000.

- [52] “SEL421-4,-5 Relay Protection and Automation System, Instruction Manual Reference Manual”, SEL,INC., Vol-20130222, 2013.
- [53] “SEL421-4,-5 Relay Protection and Automation System,Instruction Manual Applications Handbook”, SEL,INC., Vol-20130222, 2013.
- [54] “SEL-2407 Satellite-Synchronized Clock Instruction Manual”, SEL,INC., Vol-20130828, 2013.
- [55] “SEL-3378 Synchrophasor Vector Processor Instruction Manual”, SEL,INC., Vol-20140307, 2014.
- [56] “SEL-3354 Embedded Automation Computing Platform Instruction Manual”, SEL,INC., Vol-20110309, 2011.